A Seasonal Perspective on Regional Air Quality in Central California – Phase 1

Final Report

Prepared for:

San Joaquin Valleywide Air Pollution Study Agency

California Air Resources Board

Contract 04-1CCOS

With support from:

California Energy Commission

U.S. Department of Energy

by

Robert A. Harley

Department of Civil and Environmental Engineering
University of California, Berkeley, CA

Nancy J. Brown, Shaheen R. Tonse, and Ling Jin

Atmospheric Science Department
Lawrence Berkeley National Laboratory, Berkeley, CA

December 2006

Disclaimer

The statements and conclusions in this report are those of the contractor and not necessarily those of the California Air Resources Board, the San Joaquin Valleywide Air Pollution Study Agency, its Policy or Technical Committees, their employees or their members. The mention of commercial products, their source, or their use in connection with material reported herein is not to be construed as actual or implied endorsement of such products.

Acknowledgments

The authors wish to thank the following people for their help and advice: Jim Wilczak, Jian-Wen Bao and Sara Michelson (NOAA), Allison Steiner (UC Berkeley), Bruce Jackson, Ajith Kaduwela, Jin-You Liang, Klaus Scott, Patricia Velasco, Eugene Yang (California Air Resources Board), Daniel Cohan (Georgia Environmental Protection Division), Philip Martien (Bay Area Air Quality Management District), Stephen Ziman (Chevron), Steven Reynolds (Envair), Xiaoling Mao and Claire Agnoux (LBNL).

Abstract

Central California spans a wide variety of urban, agricultural, and natural terrain, including the San Francisco Bay area, the Central Valley, and the Sierra Nevada Mountains. Population within this region is growing rapidly, and there are persistent, serious air pollution problems including fine particulate matter ($PM_{2.5}$) and ozone. Summertime photochemical air pollution is the focus of the present study, which represents a first phase in the development and application of a modeling capability to assess formation and transport of ozone and its precursors within Central California over an entire summer season. This contrasts with past studies that have examined pollutant dynamics for a few selected high-ozone episodes each lasting 3-5 days.

The Community Multiscale Air Quality model (CMAQ) has been applied to predict air pollutant formation and transport in Central California for a 15-day period beginning on July 24, 2000. This period includes a 5-day intensive operating period (July 29 to August 2) from the Central California Ozone Study (CCOS). Day-specific meteorological conditions were modeled by research collaborators at NOAA using a mesoscale meteorological model (MM5). Pollutant emissions within the study domain were based on CARB emission inventory estimates, with additional efforts conducted as part of this research to capture relevant emissions variability including (1) temperature and sunlight-driven changes in biogenic VOC, (2) weekday/weekend and diurnal differences in light-duty (LD) and heavy-duty (HD) motor vehicle emissions, (3) effects of day-specific meteorological conditions on plume rise from point sources such as power plants. We also studied the effects of using cleaner pollutant inflow boundary conditions, lower than indicated during CCOS aircraft flights over the Pacific Ocean, but supported by other surface, ship-based, balloon and aircraft sampling studies along the west coast.

Model predictions were compared with measured concentrations for O_3, NO_x, NO_y, and CO at about 100 ground observation stations within the CCOS domain. Comparisons were made both for time series and for statistically aggregated metrics, to assess model performance over the whole modeling domain and for the individual air basins within the domain. The model tends to over-predict ozone levels along the coast where observed levels are generally low. Inland performance in the San Joaquin Valley is generally better. Model-measurement agreement for night-time ozone is improved by evaluating the sum of predicted O_3+NO_2 against observations; this removes from the comparison the effect of any ozone titration that may occur.

A variety of diagnostic simulations were conducted to investigate the causes for differences between predictions and observations. These included (1) enhanced deposition of O_3 to the ocean, (2) reduced vertical mixing over the ocean, (3) attenuation of sunlight by coastal stratus, (4) the influence of surface albedo on photochemistry, and (5) the effects of observation nudging on wind fields.

Use of advanced model probing tools such as process analysis and sensitivity analysis is demonstrated by diagnosing model sensitivity to boundary conditions and to weekday-weekend emission changes.

Table of Contents

List of Tables

List of Figures

List of Acronyms

BAAQMD	Bay Area Air Quality Management District
BC	Boundary Conditions
BEIGIS	Biogenic Emission Inventory Geographical Information System
CARB	California Air Resources Board
CB	Carbon Bond
CCOS	Central California Ozone Study (summer 2000)
CCTM	CMAQ Chemical Transport Modeling System
CIMIS	California Irrigation Management Information System
CMAQ	Community Multi-Scale Air Quality Model
DDM	Direct Decoupled Method (sensitivity analysis tool)
DOE	U.S. Department of Energy
EBI	Euler Backward Iterative (numerical solver for chemical kinetics)
EF	Emission Factor
EPA	U.S. Environmental Protection Agency
FDDA	Four dimensional data assimilation (observation nudging tool)
GAP	Gap Analysis Project (California vegetation/land cover mapping)
GMT	Greenwich Mean Time (GMT is 8 hours ahead of PST)
HD	Heavy Duty (vehicle weight category)
IC	Initial Condition (values at start of simulation)
IOP	Intensive Operation Period (CCOS days with special/extra measurements)
JPROC	Photolysis Rate (J value) processor
LBNL	Lawrence Berkeley National Laboratory
LD	Light Duty (vehicle weight category)
LT	Lake Tahoe air basin
MC	Mountain Counties (air basin east/uphill from California's Central Valley)
MCIP	Meteorology to Chemistry Interface Processor (processes MM5 output)
MM5	Mesoscale Meteorological Model version 5
MPI	Message Passing Interface (enables communication in parallel computer)
NC	North Coast air basin
NCC	North Central Coast air basin

NMHC	Non-methane Hydrocarbon
NMOC	Non-methane Organic Compound (NMHC + oxygenated compounds)
NOAA	U.S. National Oceanic and Atmospheric Administration
NOx	Nitrogen Oxides
PAVE	Package for Analysis and Visualization of Environment
PAW	Physics Analysis Workstation
PDT	Pacific Daylight Time
PE	Processor Element (1 processor in parallel computing cluster)
PST	Pacific Standard Time
RADM	Regional Acid Deposition Model
RMSE	Root Mean Squared Error
SARMAP	San Joaquin Valley Air Quality Study Regional Model Adaptation Project
SCC	South Central Coast air basin
SFB	San Francisco Bay area (air basin)
SIP	State Implementation Plan
SJV	San Joaquin Valley air basin
SMOKE	Sparse Matrix Operator Kernel Emissions (emission inventory software)
SMVGEAR	Sparse Matrix Vectorized Gear (numerical solver for chemical kinetics)
SV	Sacramento Valley
TOMS	Total Ozone Mapping Spectrometer (satellite-borne instrument)
UCB	University of California, Berkeley
VOC	Volatile Organic Compound

1. Introduction

California has serious air pollution problems, a rapidly growing population, and significant potential for transport of ozone and its precursors. More than half of California's 58 counties are designated non-attainment areas for the federal 8-hour ozone standard, with the vast majority of these areas being populated or agricultural regions. Approximately 1 out of 7 US residents live in California and its population is forecast to increase by approximately 60% between 2000 and 2050. Its agricultural regions are some of the most productive in the nation. Some crops show declines in yield when exposed to ozone. As a consequence, we should be vigilant of the consequences of poor air quality on human health and agriculture.

During the Central California Ozone Study (CCOS), in the summer of 2000, detailed and intensive measurements of ozone, its precursors, and other pollutants were made throughout the study area, both on the ground and aloft. The CCOS study region is shown in Figure 1. The metropolitan areas of Sacramento and the San Francisco Bay Area, the San Joaquin Valley, the Sacramento Valley, and peaks of the Sierra Nevada mountain range to the east are all within it. Under typical summer conditions, Central California experiences the inflow of westerly winds bringing clean marine air into the region. Typically several times over the summer, a large high-pressure region forms over the Great Basin (Nevada-Utah) and persists for several days, creating an offshore pressure gradient that reduces incoming westerly flow and creates the stagnant conditions favorable to ozone production [Lehrman, 2001]. During summer 2000, several of these high-ozone episodes were designated as IOP's (Intensive Observation Periods), and were studied heavily using an augmented program of surface and aloft measurements on the affected days. Phase 1 of this study focuses on IOP2, in late July/early August, and the 5-day periods preceding and following it. The overall objective of this research is to develop and demonstrate air quality modeling capabilities, and to study formation, transport and control of ozone and its precursors, for the entire summer 2000 season in Central California. A more detailed discussion of research objectives is provided as part of a separate modeling protocol document that accompanies this report.

Study Domain

The CCOS modeling domain is a 760 km x 760 km area. Phase 1 uses a subset of this, actually the original San Joaquin Valley Air Quality Study Regional Model Adaptation Project (SARMAP) domain. Both domains are shown in Figure 1. The SARMAP grid has a horizontal resolution of 4 km, with 96 grid cells in the east-west direction and 117 grid cells in the north-south direction covering approximately 34.5^{o}N to 39^{o}N and 118.5^{o}W to 123^{o}W. The vertical upper bound is at pressure 100 mbars, about 16 km above sea level. The basic grid parameters are listed in Table 1.

Figure 1: The outer red rectangle shows the CCOS domain, modelled on a 190 x 190 grid. The inner purple rectangle shows the extent of the 96 x 117 SARMAP domain. Labeled air basins include Sacramento Valley (SV), San Joaquin Valley (SJV), South Central Coast (SCC), North Central Coast (NCC), San Fransico Bay Area (SFB), Mountain Counties (MC), and Lake Tahoe (LT).

Table 1: A summary of SARMAP grid parameters

Parameter name	Parameter Value	Parameter Description
P_ALP	30 degrees	Lambert Cone Center Alpha
P_BET	60 degrees	LCC Beta
P_GAM	–120.5 degrees	LCC Gamma
XCENT	–120.5 degrees	LCC reference point X
YCENT	+37 degrees	LCC reference point Y
XORIG	–204000 m	Grid origin offset from LCC
YORIG	–252000 m	Grid origin offset from LCC
XCELL	4000 m	Cell size in X
YCELL	4000 m	Cell size in Y
NCOLS	96	Number of columns
NROWS	117	Number of rows
NLAYS	27	Number of vertical layers

2. Model Input Data

2.1 Meteorology

Gridded hourly meteorological fields were developed using the mesoscale meteorological model, version 5 [MM5; Grell, 1994]. Wilczak and coworkers at NOAA conducted the MM5 simulations for the 15 day period from July 24 to August 8, 2000, using three nested grids (Figure 2): an outer 36 km resolution grid, within which is nested a 12 km grid, within which is nested the 4 km CCOS grid with 190 cells in each horizontal direction and 50 vertical layers. We acquired 190×190 4 km resolution MM5 output from NOAA. The MM5 simulations were conducted with and without observational nudging, and with various time-averaging schemes. Observational nudging was conducted with respect to a network of surface wind observations, and radar wind profilers for readings at higher altitudes, operated during CCOS.

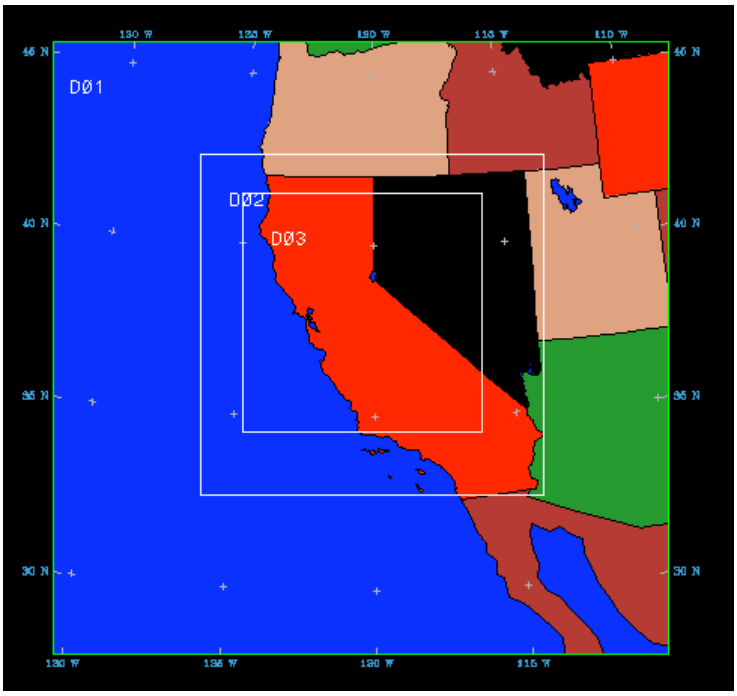

Figure 2: Depiction of the outer D01 (36 km, occupies full figure), middle D02 (12 km) and inner D03 (4 km) nested grids used in the MM5 simulations.

The Meteorology to Chemistry Interface Processor (MCIP) is used to construct air quality model-ready input files from the MM5 output. MCIP allows for consolidation of MM5 layers; we used 27 layers in the community multiscale air quality (CMAQ) model from the original 50 MM5 layers (see Table 2 and Appendix B for MM5→CMAQ layer mapping). MCIP has been revised several times during the course of this study. Each time we upgraded to a new MCIP version, we re-processed the CMAQ input files and conducted tests to ensure that the results were reasonable. Drs. Jian-Wen Bao of NOAA and Shaheen Tonse of LBNL made contributions to the upgraded MCIP 3.0 for which they were acknowledged in EPA's release document.

Table 2: Vertical layer structure used for CMAQ simulations

Layer	Pressure (mbars)	Height of bottom (m)
1	1012.0	0.0
2	1009.7	20.1
3	1006.6	42.3
4	1003.3	65.8
5	999.8	90.8
6	996.2	117.1
7	992.2	146.2
8	988.0	176.7
9	983.5	209.4
10	973.6	282.5
11	956.1	412.6
12	943.1	510.9
13	929.3	617.5
14	914.4	733.7
15	898.6	859.1
16	873.0	1067.5
17	842.9	1320.3
18	817.5	1540.3
19	787.2	1812.2
20	751.1	2150.5
21	658.7	3095.0
22	561.7	4242.0
23	433.6	6105.8
24	333.4	7997.6
25	222.2	10920.0
26	173.4	12706.0
27	133.0	14613.0
28	100.0	16668.1

Figures 3-5 illustrate temperatures and wind fields during one day of the simulation. Northwesterly winds over the Pacific tend to flow parallel to the coastline, with air moving inland through breaks in the mountains. During daytime, marine air enters through the Golden Gate and flows south through the San Joaquin Valley. The wind vectors also show the influence of topography on air flow. The coastal mountain chain extending from San Francisco southward to Santa Barbara tends to block incoming air, while the Sierras induce a daytime upslope flow as illustrated by the vectors which reverses to downslope flow during the night (not shown). This indicates that air reaching the inland portions of the state tends to originate from marine air entering through breaks in the coastal mountain chain. Figure 5 shows that wind patterns vary strongly with altitude; note the two panels of this figure and the center panel of Figure 4 all display wind fields from the same time step.

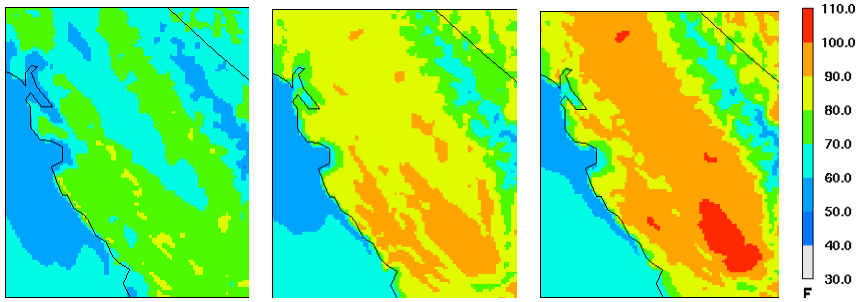

Figure 3: Surface temperatures from MM5/MCIP on July 30, 2000 at 8 am (left), 12 pm (middle) and 4 pm (right), PDT.

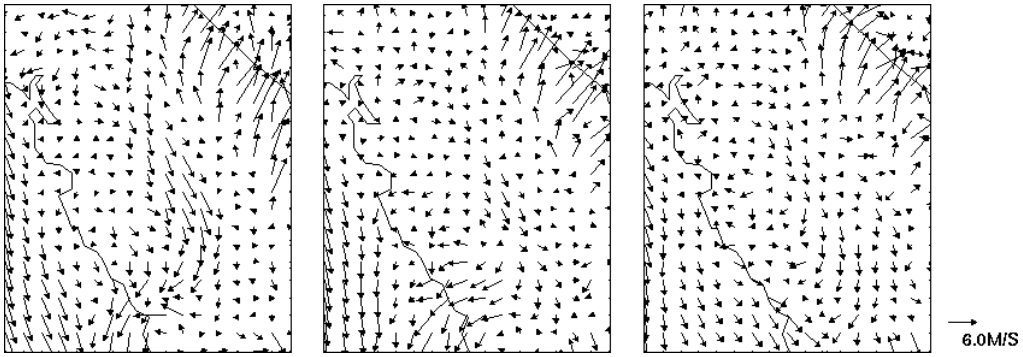

Figure 4: Wind fields at 500 m altitude for 8 am (left), 12 pm (middle), and 4 pm (right) PDT on July 30, 2000.

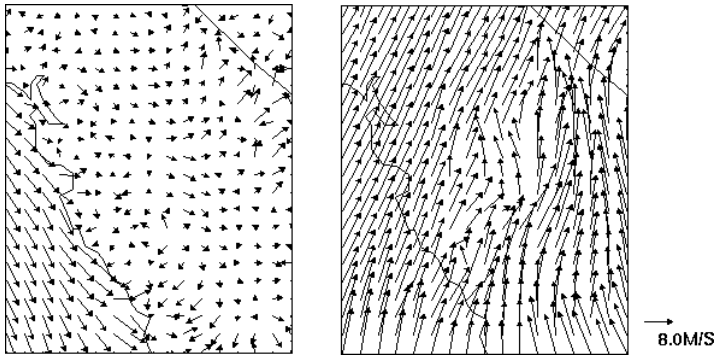

Figure 5: Wind fields at the surface (left panel), and at 3 km altitude (right) at 12 pm PDT July 30, 2000.

With a few exceptions, the meteorological output from MM5/MCIP was used unchanged as input for the air quality model. Two exceptions to this (described in the Diagnostic Simulations section) in which the meteorological data were altered inside CMAQ are:

1. The attenuation of incoming solar radiation by low-altitude coastal stratus clouds was perturbed, since we think this is being under-estimated in CMAQ.
2. The minimum value of eddy diffusivity over the ocean was changed and its effect on vertical mixing of ozone was studied. We think that this is currently set to a value that is too high in CMAQ.

2.2 Emissions

Emission inputs fall into five major source categories: area, biogenic, motor vehicle, point and forest fires. Note that off-road mobile sources were inventoried along with area sources rather than on-road motor vehicle emissions. The general procedure for processing these files into model-ready form is to translate and re-format the acquired files, and produce gridded output files with hourly emissions of each species in moles/sec. The processing for point sources includes plume rise calculations done on a day-by-day basis to account for variations in meteorological variables. CARB speciation profiles were used to define the chemical composition of volatile organic compound (VOC) emissions.

Area Source Emissions: Area source emission estimates were obtained from CARB (RF934 V04/21/04 R003). Emissions had been assigned to the CCOS 190 × 190 4 km resolution grid, with hourly time resolution and speciation appropriate for the SAPRC99 chemical mechanism. Estimates are day-of-week specific, with differences between weekdays (Monday-Friday) and weekends (Saturday, Sunday).

Biogenic Emissions: With assistance from Klaus Scott of CARB and Allison Steiner of UC Berkeley, we estimated date-specific biogenic VOC emissions of isoprene, monoterpenes, and methylbutenol. The flux of biogenic VOC to the atmosphere is determined by the amount and type of biomass present, as well as the impact of environmental factors such as light and temperature. Emissions are estimated hourly over the model domain using the biogenic emissions inventory (BEIGIS) modeling system [Scott, 2003], which utilizes detailed land cover data and an extensive emission factor database for California. The majority of biogenic VOC emissions occur in the forested regions of the model domain, particularly in the foothills of the Sierra Nevada and coastal mountains. Isoprene emissions are the dominant daytime biogenic VOC, with large fluxes arising from oak trees in the Sierra Nevada foothills. Additionally, certain crops are emitters of monoterpenes, leading to sources in the Central Valley. Isoprene emissions occur only in the presence of light, and increase with solar radiation until a saturation point is reached. The emissions increase exponentially with temperature up to approximately 35-40°C, after which they decrease. In our model, monoterpene emissions increase exponentially with temperature and are not dependent on light. These light and temperature effects are represented in the model using parameterizations developed in [Guenther, 1995].

The BEIGIS model provides a greater level of detail than other regional-scale modeling efforts in the United States [Geron, 1994; Guenther, 2006]. Fluxes of biogenic emissions are estimated as:

$$\textbf{Flux } [\mu g\ C\ m^{-2}\ hr^{-1}] = EF \times D \times c_L \times c_T$$

where EF represents the emission factor (μg C emitted g^{-1} dry weight biomass hr^{-1}), D is the foliar density (gram dry weight biomass m^{-2}), and c_L and c_T are environmental factors

to account for the impact of light and temperature. This equation is applied hourly to each model grid cell in the CMAQ model domain.

There are two important inputs into the model to estimate biogenic emissions: (1) land cover data, providing emission factors (EF) and foliar density (D) based on the vegetation type, and (2) meteorological data to determine the environmental effects of light and temperature (c_L and c_T).

Land cover data is compiled for natural, agricultural, and urban areas. The naturally occurring vegetation is represented by the Gap Analysis Project (GAP), provided by the US Geological Survey-Biological Resources Division. This dataset is generated from a combination of satellite images, color infrared imagery, and ground-based vegetation maps and surveys [Scott, 2003]. Agricultural data are derived from county-level data by the California Department of Water Resources, and urban areas are outlined within the GAP database.

Emission factors (EF) for isoprene and monoterpenes have been developed for the California natural vegetation species in previous CARB studies [Benjamin, 1996]. Crop species can emit isoprene and/or monoterpenes and CARB has developed emission factors specifically for California crop species. Emission factors from various urban areas within the model domain (Fresno, Oakland and Sacramento) are included to model biogenic VOC emissions from these urban regions.

The foliar density term (D) is estimated by multiplying the specific leaf weight (g dry biomass m^{-2} leaf area) by the leaf area index (m^2 leaf area m^{-2} ground area). Specific leaf weight factors for the GAP and crop categories have been developed [Nowak, 2000], and leaf area index for the summer month of July have been derived from a remotely sensed 1.0 km^2 leaf area index [Nikolov, 1999].

The second input, meteorological data, is used to determine the impacts of light and temperature on the emissions. Mesoscale modeling simulations show positive temperature biases of several degrees over the Central Valley of California [Umeda, 2002], and could result in over prediction of the amount of biogenic VOC emitted. Therefore, we use ground based radiation and temperature measurements in order to determine the environmental factors c_L and c_T for the present study.

Ground based observations of temperature and radiation are available from the California Irrigation Management Information System (CIMIS) with good coverage of the coastal and Central Valley regions. This data is supplemented with temperature data from CARB sites in the mountain counties and observations at the Blodgett Forest Research Station. We interpolate these observations to the same model grid as CMAQ, to produce gridded hourly radiation and temperature information. This yields meteorological data at the same horizontal resolution as the CMAQ simulations and therefore can provide easy and direct input of biogenic VOC emissions into CMAQ. Based on the land cover data and observed meteorological data we generate hourly biogenic emissions of isoprene and monoterpenes.

Motor Vehicle Emissions: The motor vehicle emission inventory estimates for summer 2000 used in this research describe light-duty gasoline and heavy-duty diesel vehicle activity patterns and emissions separately by time of day and day of week. Separate activity patterns are specified for normal weekdays (Monday-Thursday), Friday, Saturday, and Sunday. Within a diurnal cycle on weekdays, diesel truck activity peaks during the middle of the day whereas passenger vehicles show a bimodal distribution with peaks associated with morning and afternoon commute periods. Compared to weekdays, there are large (60-80%) reductions in diesel truck traffic and the accompanying NO_x emissions on weekends. Overall light-duty vehicle traffic decreases only slightly on weekends, but is shifted in time with a single broad peak in the afternoon hours. These temporal patterns in motor vehicle emissions, as well as the increasingly important role of diesel engines as a source of NO_x, are described in further detail elsewhere [Harley et al., 2005]. Motor vehicle emission inventories and underlying estimation methodologies are described elsewhere [Harley et al., 2004]. Briefly, fuel sales at the county level were combined with emission factors expressed per unit of fuel burned to estimate CO and NO_x emissions. NMOC emissions were estimated from CO using NMOC/CO ratios derived from ambient air measurements.

Point Source Emissions: Emission estimates were obtained from CARB (RF934 V04/21/04 R002). Each source is described by location, stack parameters (diameter, height, exit temperature, exit velocity), and hourly emissions of pollutants speciated into SAPRC99. Emissions are day-of-week specific, with differences between weekdays (Monday-Friday), Saturdays and Sundays. EPA's emissions preprocessor (SMOKE 2.1) was installed at LBNL. We extracted the plume-rise algorithm from SMOKE, and wrote input and output modules for it. Our processor checks for (1) missing point sources, (2) correct time ordering of entries, (3) missing chemical species, and (4) reasonable daily total emission values. Plume rise is then estimated for each point source using time and location-specific meteorological variables from MM5.

Forest Fire Emissions: These emission estimates were obtained from CARB (V10/02/03 R002) for the 5-day IOP2, July 29 to August 2, 2000. We received the fire emissions in an already vertically distributed form. Each fire is represented by a number of individual point sources, each point source representing the emissions at a particular height, after a buoyancy calculation has been applied. The processing procedure for estimating fire parameters and plume rise is described in [Loomis, 2003 and FEJF, 1996]. The NO_x and CO emission profiles associated with area. motor vehicle, point, and fires for Days 211 through 216 are illustrated in Figures 6 and 7. Since fire emissions are only available for a 5-day period, for the purpose of consistency they are not included in any 15-day simulations.

Emissions files from the various categories were processed and merged to produce an input file for 15-day CMAQ simulations, stretching from July 24 to August 8, 2000, and are also used for 5-day diagnostic simulations (IOP2). Sample figures showing spatial and temporal patterns of emissions are shown below. Description of emissions processing Fortran 90 codes written during this project are provided in the Appendix.

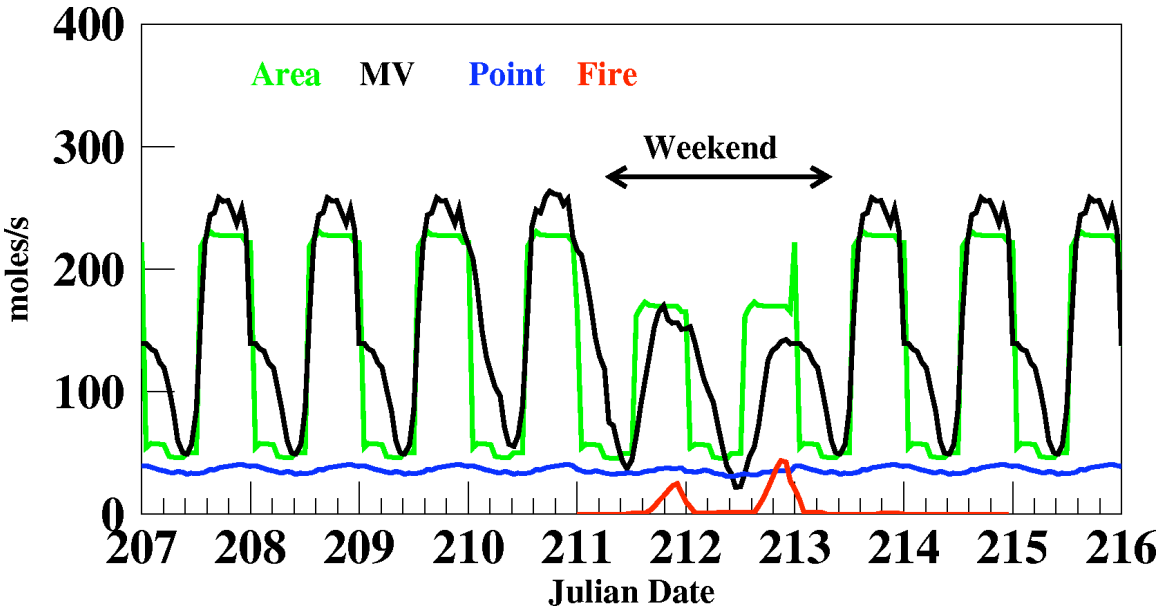

Figure 6a: NO_x emission profiles summed over the domain by source category. The forest fire inventory is for days 211-216 only.

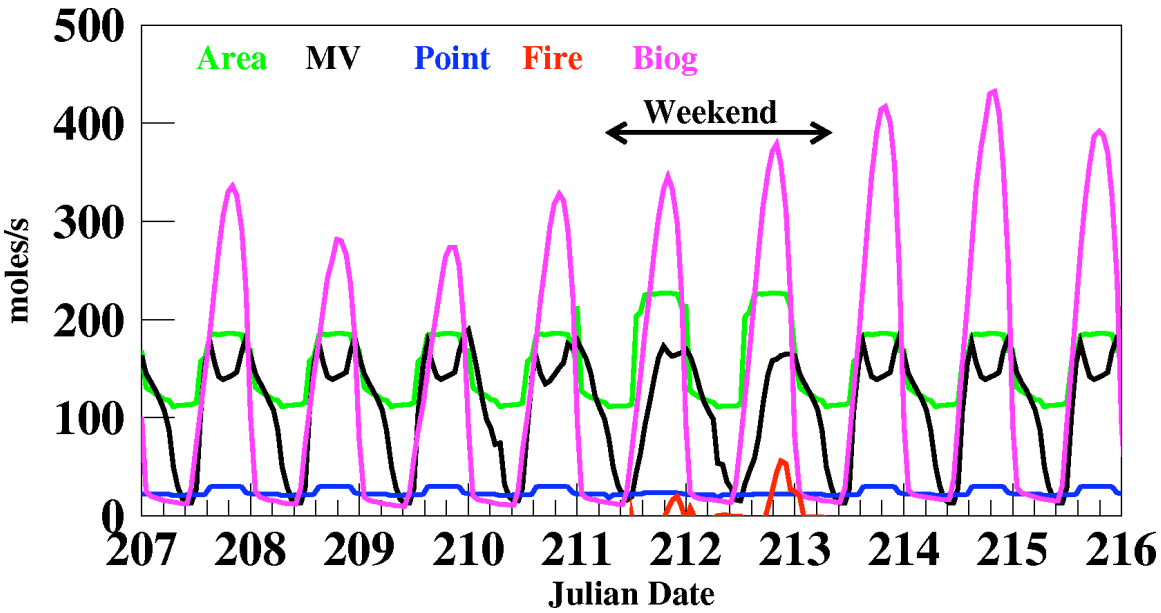

Figure 6b: VOC emission profiles summed over the domain by source category. The forest fire inventory is for days 211-216 only.

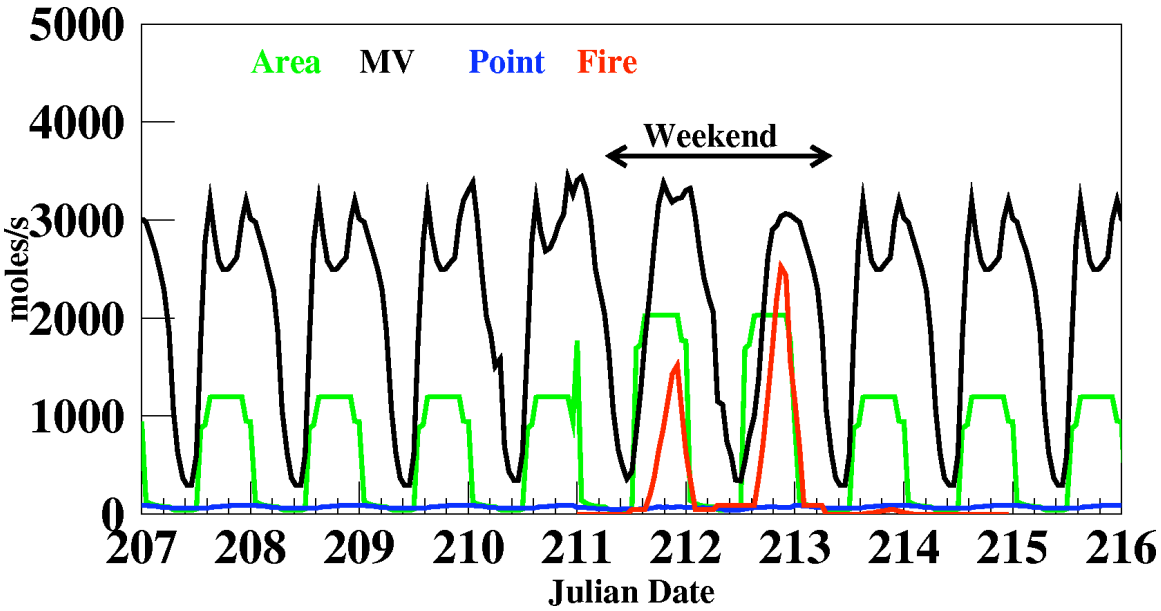

Figure 7: CO emission profiles summed over the domain by source category. The forest fire inventory is for days 211-216 only.

The spatial distribution of NO_x emissions within the study domain is shown in Figure 8.

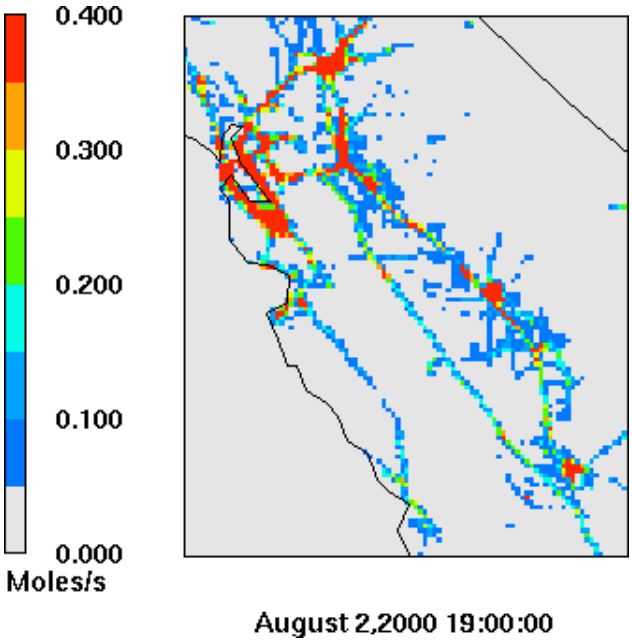

Figure 8: Spatial distribution of NO_x emissions at noon PDT. The urban centers of the SF Bay Area, Sacramento, and Fresno can be seen. Also prominent, extending in a NW to SE direction, are highways 101, I-5 and 99 going from left to right, respectively.

2.3 Boundary Conditions

Boundary conditions (BC) must be specified on a perimeter of grid cells surrounding the main domain, with the same number of layers as the main domain, and with concentration defined for every species. The Boundary conditions are time-independent; i.e., the same boundary concentration values are used throughout each simulation.

Boundary Concentrations: Since the western boundary is over the Pacific Ocean, many species are assigned less polluted values on that boundary. Table 3 lists the boundary values used for all species. O_3 has a vertically varying profile based on [Newchurch, 2003] ozone sonde measurements made at Trinidad Head, CA over several years, and taking the August average. This profile is applied to the western boundary. The other three boundaries adopt the same profile at higher altitudes but have higher O_3 at the surface. The value for NO_x is 1.05 ppb, higher than typically clean conditions over the Pacific, and is based on aircraft measurements offshore [Buhr, 2001 and Fujita, 2005] made during the CCOS IOP2 episode. The value is consistent with NO_x measured in Asian plume transits during 2002 experiments [Tang, 2004]. The bases for the CO and alkane values for the western BC are similar. Further study of boundary conditions will be necessary, and assignments for the four boundaries may be modified in the next phase. An alternate simulation has been also conducted with cleaner BC values of CO, NO_x and alkanes on the western boundary [Goldstein, 1995 and Goldstein, 2004].

Boundary Fluxes: The degree to which a boundary value is influential depends on the baseline value of the BC concentration, and whether it is predominantly an inflow or an outflow boundary. Ideally we should be very confident of inflow BC's and would not be very concerned about outflow BC's. In reality, the meteorology dictates when a boundary is an inflow or an outflow boundary. The next four figures show the density-weighted winds (relative density multiplied by perpendicular wind component) through each of the four boundaries, separately as a function of time and space, and separately for low and high altitudes. Fluxes were calculated without ozone weighting. Although, conclusions are not changed if ozone weighting of the fluxes is included because velocity determines the sign of the flux. The signs (+ or –) are of particular relevance, signifying inflow and outflow depending on the boundary. The winds and density are extracted from the meteorological input file.

Figure 10 contains four panels where the data are presented as box scatter plots, similar to normal scatterplots except that different sized boxes are used to denote areas with larger numbers of data points, to prevent over-crowding. A bigger box implies more entries. The two upper panels in each figure are for Layers 1-15 (ground to 1 km), and the two lower panels for Layers 16-20 (1 km to 3 km). The data are from Julian date 206 (July 24, 2000) and extend for 15 days.

Table 3: Boundary species concentrations. Values at selected heights are given because O_3 has a vertically varying profile.

Species	Western BC (ppb)	N/E/S BCs (ppb)	Clean Western BC (ppb)
CO	200	200	80
NO	0.05	0.05	0.05
NO_2	1	1	0.05
O_3 at surface	22	40	22
O_3 at 1km	44	48	44
O_3 at 2km	60	60	60
O_3 at 3km	60	60	60
HCHO	2	2	2
RCHO	0.5	0.5	0.5
PAN	0.005	0.005	0.005
ACETONE	1	1	1
ALKANE-1 (mainly C_2H_6)	6	10	1
ALKANE-2 (~C_3H_8, C_2H_2)	1	2.5	0.35
OLEFIN-1	0	0.5	0
OLEFIN-2	0	0.2	0
AROMATIC-1	0	0.35	0
AROMATIC-2	0	0.25	0
ISOPRENE	0	0.1	0

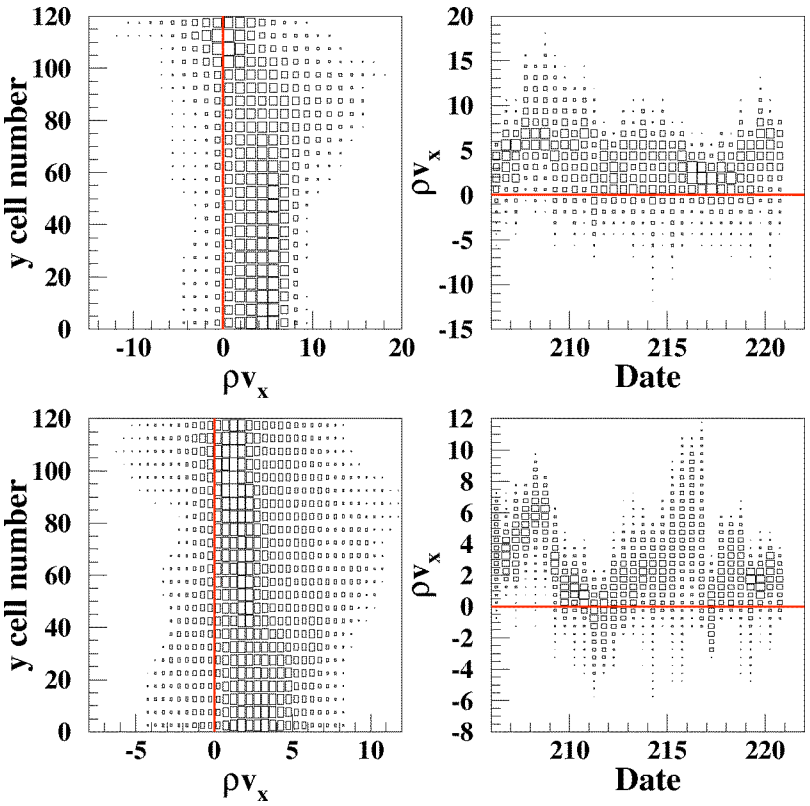

Figure 9: Western boundary flux. Top left: The spatial dependence of the x wind component (layers 1-15), plotted against the 117 cells that lie along the western boundary (axes are switched to resemble the alignment of the grid and the western boundary is vertical to the reader). Data from all timesteps are lumped in this plot. A positive value (to right of red line) indicates inflow, and negative, outflow. Box size is determined by the number of entries for each cell at a particular flux on the western edge for all timesteps. Bottom left: Similar plot for layers 16-20. Top right: The x wind flux component on the West boundary, (for all cells) versus time. Bottom right: Similar plot for layers 16-20.

As seen in Figure 9, the western boundary is mostly an inflow boundary, and it is also an inflow boundary, in both the lower and upper layers; however there is slightly more outflows on this boundary for the upper levels on Days 211 and 217.

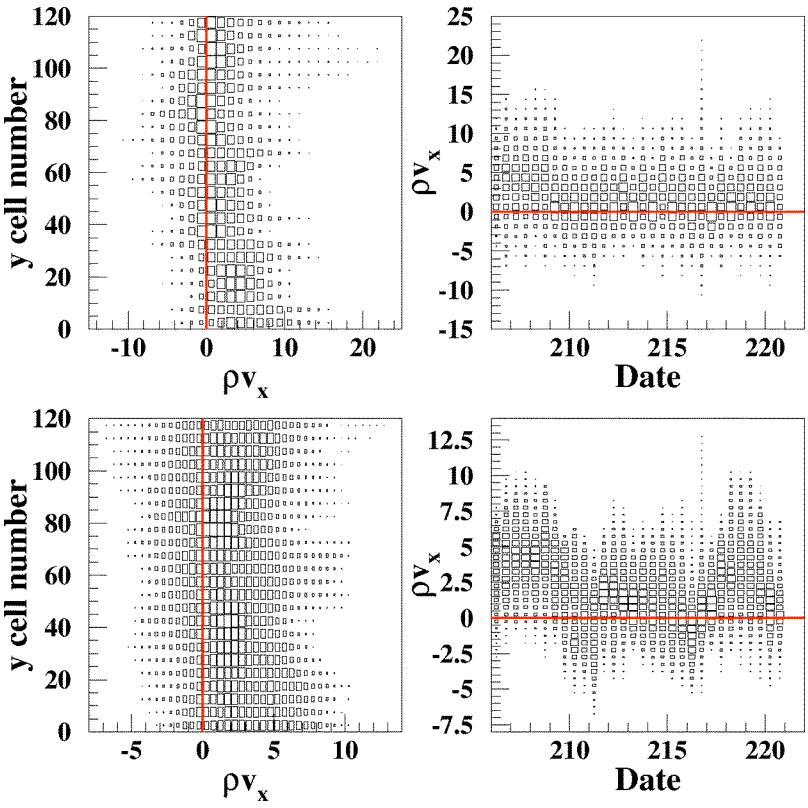

Figure 10: Eastern boundary flux. Top left: The spatial dependence of the x wind component (layers 1-15), plotted against the 117 cells that lie along the eastern boundary. Data from all timesteps are included in this plot. Positive values (to right of red line) indicates outflow, and negative, inflow. Bottom left: Similar plot for layers 16-20. Top right: The x wind flux component (for all cells) versus time. Bottom right: Similar plot for layers 16-20.

As seen in Figure 10, the eastern boundary especially towards the southern end, tends to be an outflow boundary. Significant inflow does occur through the northern portion of the eastern boundary; more inflow is associated with the upper layers where the north/south distinction is lost. The inflow-outflow ratio is time-dependent and increases on Days 211 and 217.

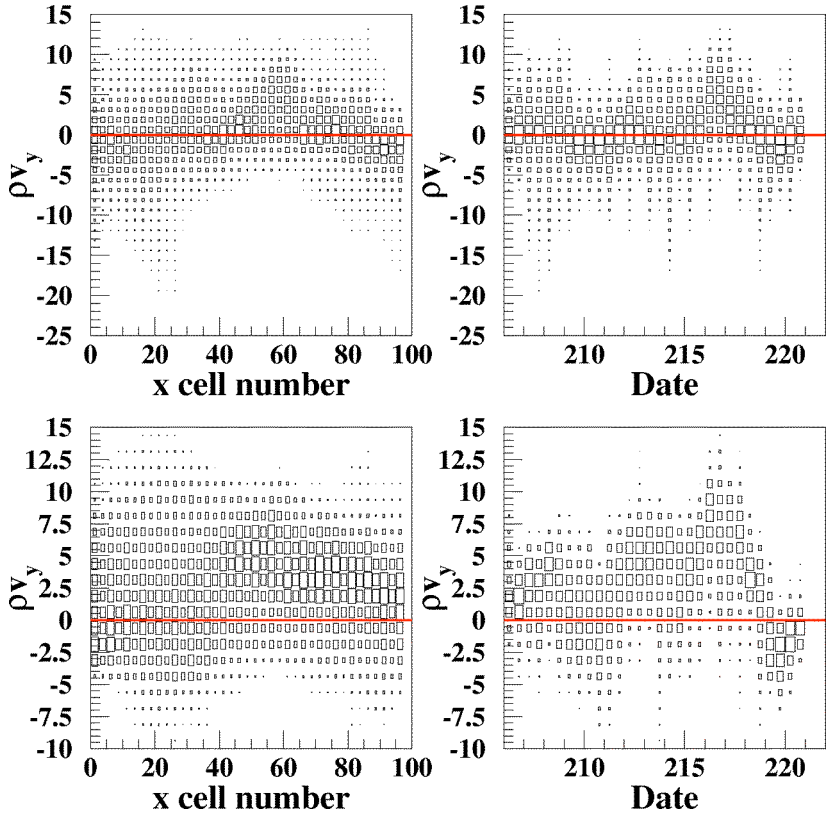

Figure 11: Northern boundary flux: Top left: The spatial dependence of the y wind component (layers 1-15) plotted for the 97 cells that lie along the northern boundary. Data from all timesteps are included in the plot. Positive values (above the red line) indicate outflow; negative values are inflow. Bottom left: Similar plot for layers 16-20. Top right: Time dependence of the same data. The y wind flux component (for all cells versus time. Bottom right: Similar plot for layers 16-20.

The northern boundary is dominated by outflow, but inflow is certainly apparent in both the lower and upper layers. The relative amounts of inflow and outflow vary with time; e.g., day 220 is mostly inflow at the higher altitudes, while previous days (215-219) are dominated by outflow.

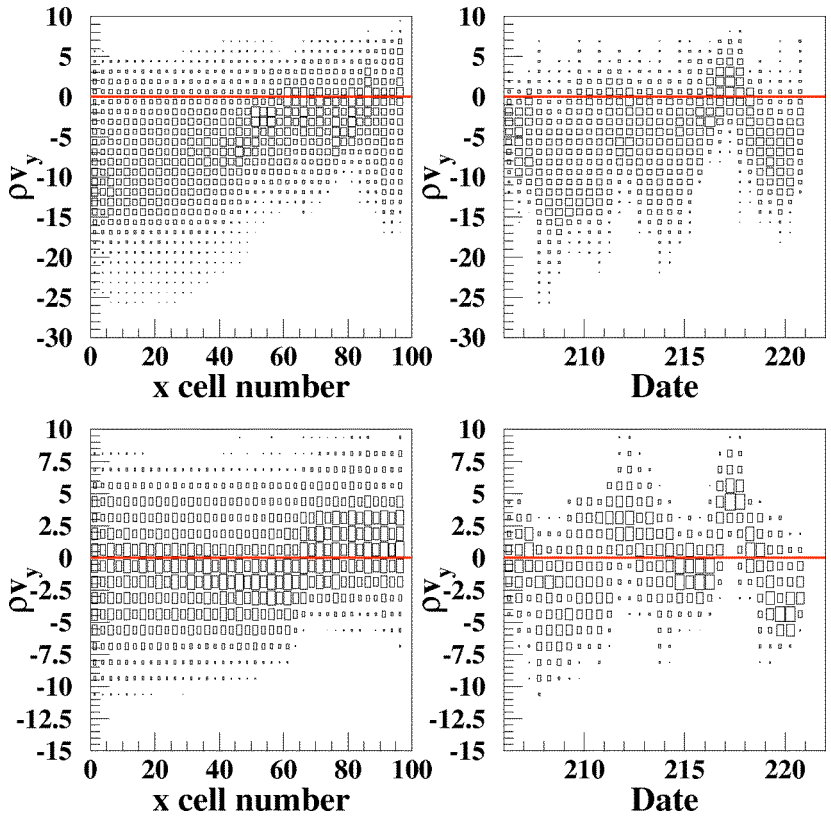

Figure 12: South boundary flux: Top left: Spatial dependence of the y wind component (layers 1-15) plotted for the 97 cells that lie along the southern boundary. Data from all time steps are included in the plot. Positive values (above the red line) indicate inflow; negative values are outflow. Bottom left: Similar plot for layers 16-20. Top right: The y wind flux component (for all cells) versus time. Bottom right: Similar plot for layers 16-20.

The southern boundary is an outflow boundary most of the time for the lower layers, except at its eastern edge where there is increased inflow. Upper layers behave in a spatially similar fashion. In the lower layers, there seems to be more inflow for days 216-217. The flow in and out of the boundary oscillates with time, especially in the upper layers. In the upper layers, the boundary flows are dominated by the inflow for a few days then are dominated by outflow.

Upper layer behavior seems to be more synoptic, with oscillations from inflow to outflow lasting several days. With the possible exception of the northern boundary, lower layers do not exhibit the oscillatory behavior. It is also helpful that the majority of boundary fluxes are outflow fluxes; however, inflow fluxes are important especially at northern and southern boundaries and appear to become more important aloft. The influence of boundary conditions aloft will be examined subsequently. Also note, that boundary flux sign varies with time, especially for the southern boundary. In summary, we cannot really ignore inflow at any of the boundaries for all days at all times. It is important to

recall that boundary condition influence on model results is expected to decrease when using the larger 190×190 CCOS domain.

2.4 Initial Conditions

The initial condition file contains an initial value in every grid cell for every species concentration. Replicating the actual initial conditions is difficult because they are not known for all species in the domain, and even a chemically and physically plausible set of concentrations is challenging to assemble. Plausible initial conditions can be assembled using extra "spin-up" days of air quality model simulations. This is achieved by running the model for a spin-up period of about 72 hours, and using the concentrations at the final timestep as initial conditions thereafter. After 72 hours of spin-up, predicted concentrations are largely independent of the initial conditions that were used to initiate the spin-up run, as we subsequently show using sensitivity calculations.

2.5 Actinic Flux

In order to simulate the chemical kinetics accurately, photolysis rates need to be calculated correctly. These rates determine the formation of radicals that drive O_3 production, and for this, correct calculation of temporal and spatial variations in the actinic flux is critical. Actinic flux is affected by the earth's surface albedo as well as by various atmospheric scatterers and absorbers, such as O_3, aerosols and clouds. Surface albedo data obtained from moderate resolution imaging spectrometer (MODIS) satellite retrievals show as much as a factor of four difference in surface albedo across our modeling domain. In the diagnostic simulations sub-section below, we show results of CMAQ simulations in which surface albedo was perturbed by zeroing, doubling, and tripling it in different simulations.

3. Air Quality Model and Computing Platform

3.1 Community Multi-scale Air Quality Model (CMAQ)

CMAQ [Byun, 1999] incorporates up-to-date representations of atmospheric chemistry and physics, is peer-reviewed, and is publicly available. CMAQ is a multi-scale, multi-pollutant model that has been evaluated for numerous ozone and particulate matter studies. It contains the Carbon Bond (CB-IV and CB-V), Regional Acid Deposition (RADM) and SAPRC97/99 [Carter, 2000] chemical mechanisms. For gas-phase problems, chemical kinetics are calculated with the Sparse Matrix Vectorized Gear (SMVGEAR) and the Euler Backward Iterative (EBI) ordinary differential equation solvers. Advective transport is treated with the piecewise parabolic method. CMAQ includes an optional plume-in-grid module for more realistic representation of near-stack chemistry and transport. A useful feature is the Process Analysis module, used to quantify the contributions of individual physical processes and chemical reactions to the predicted concentrations of chemical species.

Initially CMAQ V4.3 was used in this research, with updates to V4.4 and most recently V4.5 in November 2005. Revised versions of CMAQ contain new algorithms and algorithmic improvements that have been rigorously tested. In addition there are corrections for programming errors that had escaped the initial evaluation efforts. When we install a new version, we conduct model evaluations by repeating benchmark simulations, comparing new and old versions for accuracy, testing and timing the chemistry solvers, and measuring computational times used for different degrees of parallel processing.

The main improvement in going from V4.3 to V4.4 was an improved horizontal advection algorithm which permitted the internal time step of the horizontal advection module to vary according to the Courant number of the layer, thus allowing larger time steps to be used in layers with lower wind velocity, i.e., lower altitude layers. Previously all layers were constrained to using the highest Courant number in all layers taken together, which was unnecessarily restrictive. The main benefit of this change is computational speedup.

CMAQ V4.5 features an improvement in the piecewise parabolic advection solver, which rectifies a mass conservation problem which had plagued earlier versions. These had occasionally resulted in species mass errors of up to 20%, and had been patched by an *a posteriori* correction. The new treatment of advection satisfies the continuity equation using the density computed in MM5. The SMVGEAR solver gained almost a factor of two speedup from V4.3 to V4.5. CMAQ 4.5 also features a fast, accurate Euler Backward Iterative (EBI) solver for chemical kinetics. This provides a speedup of a factor of eight over SMVGEAR, while preserving the accuracy of the chemical concentrations. An earlier, less accurate version of EBI, the MEBI solver (Modified Euler Backward Iterative) was included in CMAQ V4.3 and V4.4. Aside from some of the sensitivity simulations described below, all results presented here use CMAQ V4.5, and are generally obtained using the EBI solver. The SMVGEAR solver must be used if process analysis of chemistry is required.

In addition, we have conducted sensitivity analysis calculations using a 3-D version of the Decoupled Direct Method (DDM) [Dunker, 1984], implemented in CMAQ by Russell and coworkers [Cohan, 2005]. In DDM the first-order model sensitivities to an input variable are propagated in time through transport and chemical equations in much the same way that the species concentrations themselves are propagated. Modified versions of the transport and chemical equations are derived from the original equations to propagate the sensitivity. The same Jacobian matrix used to propagate the species concentrations is also used to propagate the sensitivities, saving considerably on computing time since determining Jacobian elements involves expensive evaluations of reaction rates. Multiple output variable-input variable combinations can be calculated in a single CMAQ/DDM simulation. The current implementation of DDM uses the MEBI solver of CMAQ V4.3. Typically we have examined O_3 sensitivities in our sensitivity studies. Input variables to be studied can be selected from species initial concentrations, boundary conditions, or emissions. When calculating sensitivities to emissions, the

sensitivities can be restricted to emissions from user-specified sub-domains of the grid and/or to emissions from particular time intervals.

3.2 Computing Platform

CMAQ model simulations are performed on a Beowulf-style Linux cluster computer using a distributed parallelization model. The Mariah cluster was purchased with DOE support in 2003, and is located at Lawrence Berkeley National Laboratory. Maintenance and upkeep have been supported by the laboratory's Scientific Cluster Support Program. Mariah has 28 nodes; each node has two Athlon processors running at 2.5 GHz, and 2 GB of RAM. A fast 2 Gbit/s Myrinet interconnect system is used to transfer data between nodes during parallel execution of CMAQ.

Distributed parallelization is implemented in CMAQ by partitioning the domain into sub-domains at the beginning of the simulation and assigning one processor element (PE) to the calculations in each sub-domain. The Message Passing Interface (MPI) is used to send/receive data between PEs, and MPI subroutine calls are embedded in CMAQ to support the needs of a PE for data from adjoining cells in a neighboring sub-domain. Typically we divide the 96×117 grid by three in each direction and use 9 PE's. In this configuration current run-times (96×117 domain, 27 layers, 15 day simulation, SAPRC mechanism with 72 species) are 18 hours with the EBI solver and 144 hours with the SMVGEAR solver. Typical input and output disk file sizes are 8 GB for the meteorological files, 7 GB for the emission file, and 1.2 GB for an output file containing average concentrations of 15 species for 5 vertical layers.

Although we could in principle use a larger number of PEs, a penalty is incurred as one increases the number of PEs assigned to a problem, as shown in Table 4. Reasons are:

1. Load imbalance: Computational load is not balanced between PEs, as grid sub-domains with more emissions and more chemical activity require more CPU time. PEs with a lighter load complete their calculations first and must wait for the others. As the number of sub-domains is increased so does the probability of larger load discrepancies between PEs.
2. Smaller sub-domains result in higher cost for inter-PE communication. This can be seen by looking at the perimeter to area ratio of the sub-domain: cost of scientific calculations depend on area and is proportional to N^2, whereas communication depends on perimeter and varies as N.
3. Portions of the code are either not parallelizable, or do not benefit from parallelization, and so are redundantly calculated on all PEs.

Table 4: Performance as a function of number of PEs. Scalability indicates the relative PE effectiveness. Effective number of PEs is Scalability multiplied by number of PEs.

No. of PEs	CPU Time (seconds)	Scalability	Effective no. of PEs
1	4500	100%	1.0
2	2431	92%	1.8
6	1019	74%	4.4
12	739	50%	6.0
24	539	35%	8.4

4. Analysis of Model Results

The output from CMAQ 15-day simulations includes hourly averaged concentrations of O_3, NO, NO_2, and CO at every grid cell and hour, for layers 1-5 (0 to 100 m). Visualization of model output was done using PAVE, and the data can also be interrogated in a more detailed fashion and correlated with emission, boundary and meteorological inputs using our data analysis tools, described later. Comparisons of simulated and observed O_3 are presented below as time series and also in statistically aggregated form. Statistically aggregated results are also shown for CO, NO_x and NO_y. In addition to the 15-day simulation, several diagnostic simulations were conducted over 5 days (IOP2 from July 29 to August 2) to investigate the effects of various input and operational modifications. Model sensitivities to initial conditions, boundary conditions, emissions from all or part of the domain, and emissions at particular times of day were evaluated using an online sensitivity analysis tool (CMAQ with DDM-3D). Finally, process analysis was used to quantify changes in chemical processes that contribute to weekday/weekend O_3 differences.

4.1 Simulation of 15-Day Period

The 15-day simulations extend from 12 am GMT on Monday July 24 (Julian day 206) to 12 am on Tuesday August 8, 2000 (day 221). These simulations use unnudged meteorological fields provided by NOAA, and date-specific emission files assembled at LBNL. Two different simulations have been conducted: a base case and a second simulation with cleaner western boundary conditions, as shown in Table 3. Figure 13 shows maps of ground level O_3 predictions at 3 pm PDT on the 3rd, 8th and 13th days of the simulations to give an idea of general patterns. There are day-to-day variations in O_3 concentrations; however "hot spots" are commonly observed in the Bay Area (Livermore and San Jose areas), in Sacramento, and in the San Joaquin Valley (near Bakersfield and Fresno).

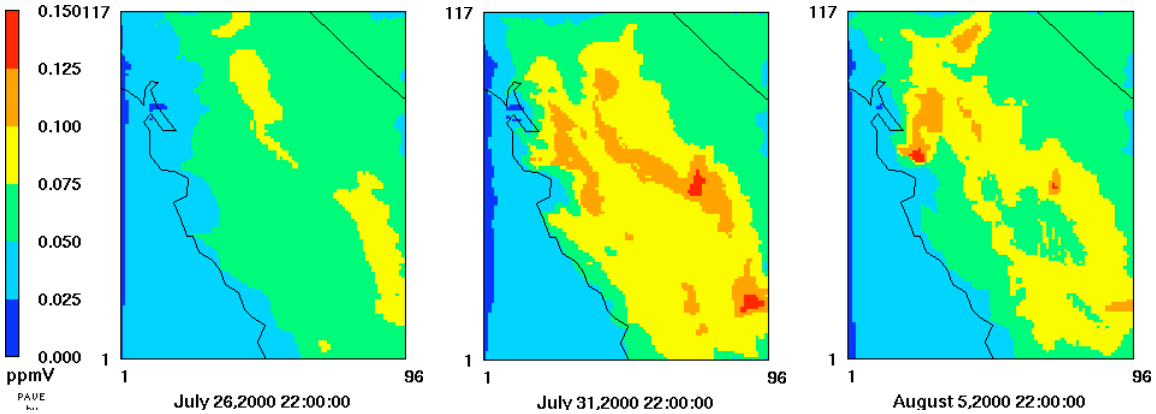

Figure 13: Spatial distribution of O_3 at 3 pm PDT on the 3rd, 8th, and 13th days of the simulation.

Domain-wide comparisons: Comparisons of predicted and observed hourly averaged O_3, NO_x, NO_y, and CO are presented as time series and in statistically aggregated form. The following statistical metrics of model performance are considered:

$$\text{Mean Bias} = \frac{1}{N}\sum_{i=1}^{N}(C_{\text{model},i} - C_{\text{obs},i})$$

$$\text{Root Mean Squared Error (RMSE)} = \sqrt{\frac{1}{N}\sum_{i=1}^{N}(C_{\text{model},i} - C_{\text{obs},i})^2}$$

$$\text{Mean Normalized Bias (N. Bias)} = \frac{1}{N}\sum_{i=1}^{N}\left(\frac{C_{\text{model},i} - C_{\text{obs},i}}{C_{\text{obs},i}}\right)$$

for i where $C_{\text{obs},i}$ > cutoff

$$\text{Mean Normalized Gross Error (N. GrossErr)} = \frac{1}{N}\sum_{i=1}^{N}\left|\frac{C_{\text{model},i} - C_{\text{obs},i}}{C_{\text{obs},i}}\right|$$

for i where $C_{\text{obs},i}$ > cutoff

Table 5: Summary statistics with base case boundary conditions across the whole domain

	O_3		NO_x	NO_y	CO	VOC[2]
Mean Bias[1] (ppb)	4		0	0	-121	10
RMSE[1] (ppb)	18		17	15	349	193
Mean Bias (ppb)	1		0	-1	-183	-3
RMSE (ppb)	18		19	15	384	232
N. Bias	10%	-13%	11%	9%	-27%	39%
N. GrossErr	33%	20%	67%	49%	42%	71%
Sample size	34990		12881	6646	15782	34
Cutoff value (ppb)	20	60	7	5	300	50

1 no cutoff applied

2 in ppbC, simulated VOC species are compared to total identified NHMC

The purpose of Table 5 is to present model performance across the full range of species concentrations, including both daytime and nighttime. Therefore we used the 25th percentile of the observations as cutoff values. Past studies (summarized by Seigneur et al.) have typically used 60 ppb as the cutoff in evaluating model performance for ozone. In order to compare our performance statistics to previous studies, we also show ozone metrics with 60 ppb as the cutoff value (see Table 5). The normalized gross error is reduced as the cut-off is increased.

One can see from Table 5 that CMAQ has low mean bias associated with predictions of O_3, NO_x, and NO_y across the whole domain and throughout the 15-day period. On average, CMAQ under predicts CO. Mean normalized gross errors indicate that CMAQ predicts ozone more accurately than the other species.

Selected ozone time series plots for each of the air basins: San Joaquin Valley (SJV), Sacramento Valley (SV), San Francisco Bay Area (SFB), Mountain County (MC), South Central Coast (SCC), and North Central Coast (NCC) are presented in Figures 14-19. The selection criterion is to choose sites close to the median value of RMSE in each air basin. Observed values are shown along with two sets of model predictions (base case, labeled "Dirty BC", and a modified case with clean BC). Modeled ozone time series track the observations in general, except at coastal sites, where ozone is overpredicted, and for some ozone peaks observed during the middle 5 days, which are underpredicted. Simulations with base vs. clean BC show differences of 10 to 15 ppb at the coastal sites (lower ozone with clean BC), and very little difference elsewhere.

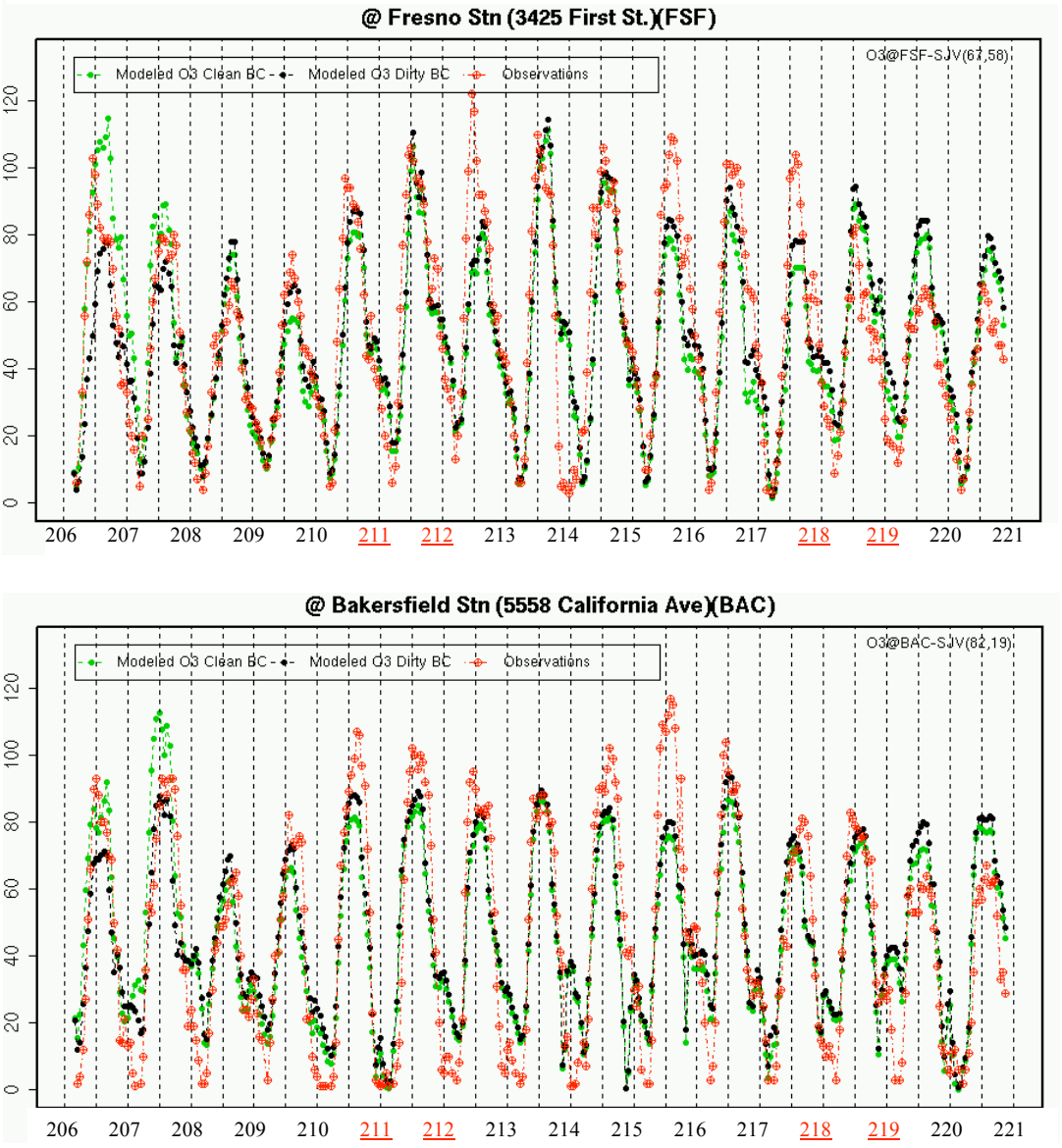

Figure 14: Predicted and observed O_3 (ppb) at two San Joaquin Valley stations (underlined/red Julian days along time axis denote weekends)

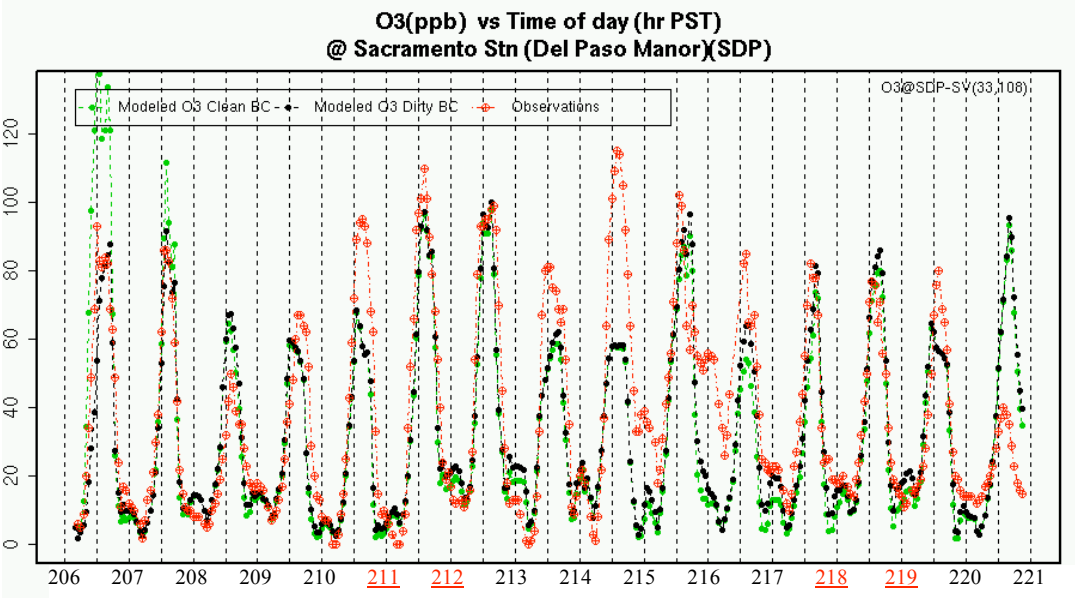

Figure 15: Predicted and observed O_3 (ppb) at a Sacramento Valley station (underlined/red Julian days along time axis denote weekends)

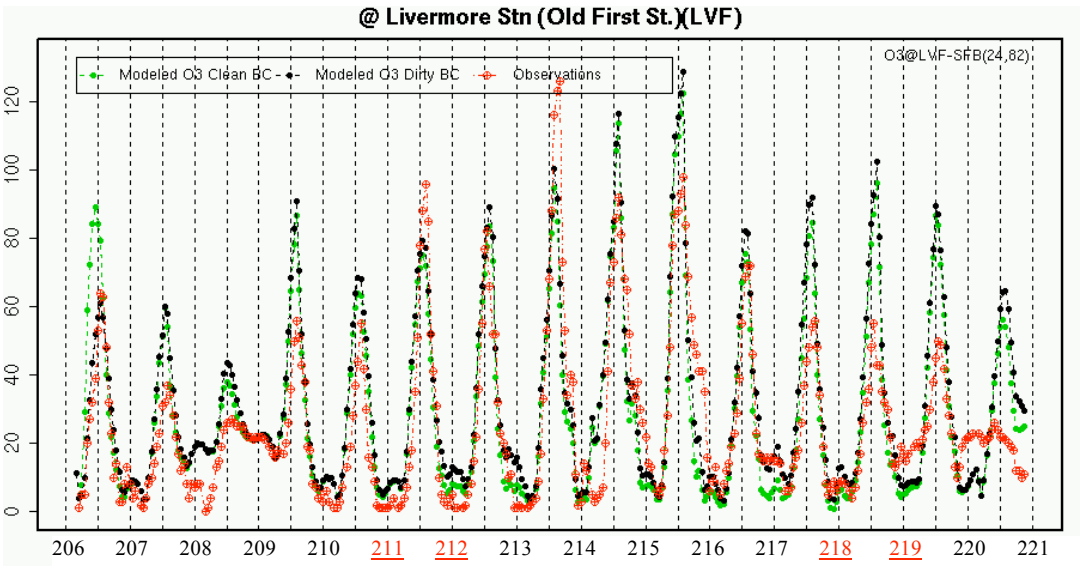

Figure 16: **Predicted and observed O_3 (ppb) at a San Francisco Bay Area station (underlined/red Julian days along time axis denote weekends)**

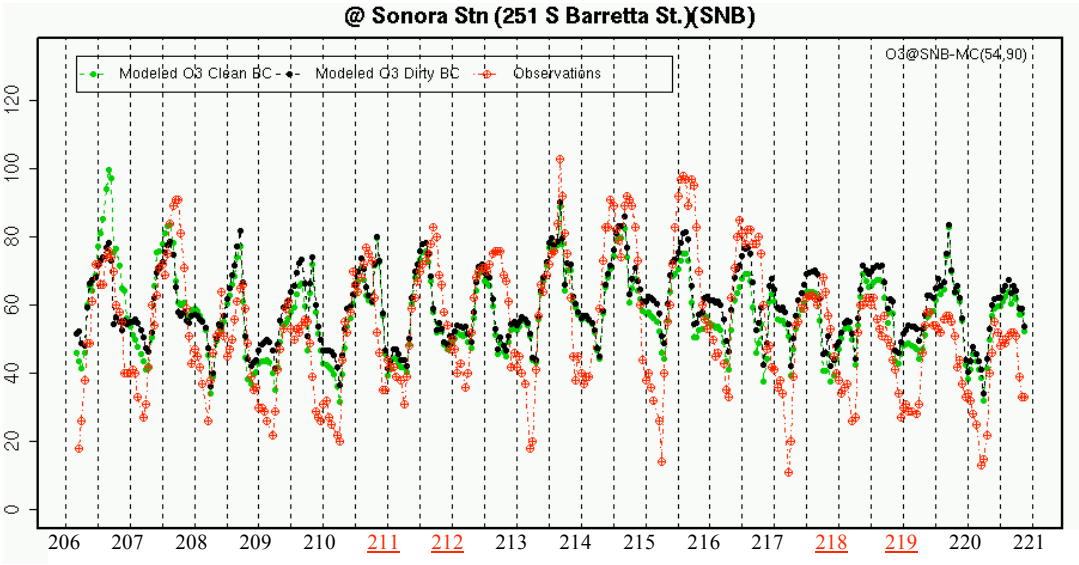

Figure 17: Predicted and observed O_3 (ppb) at a Mountain County station (underlined/red Julian days along time axis denote weekends)

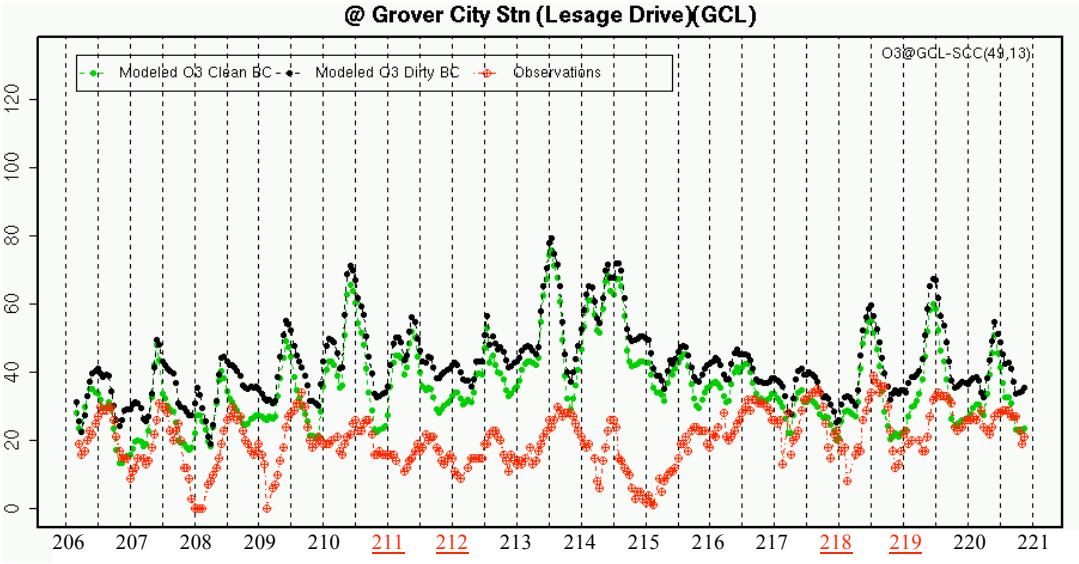

Figure 18: Predicted and observed O_3 (ppb) at a South Central Coast station (underlined/red Julian days along time axis denote weekends)

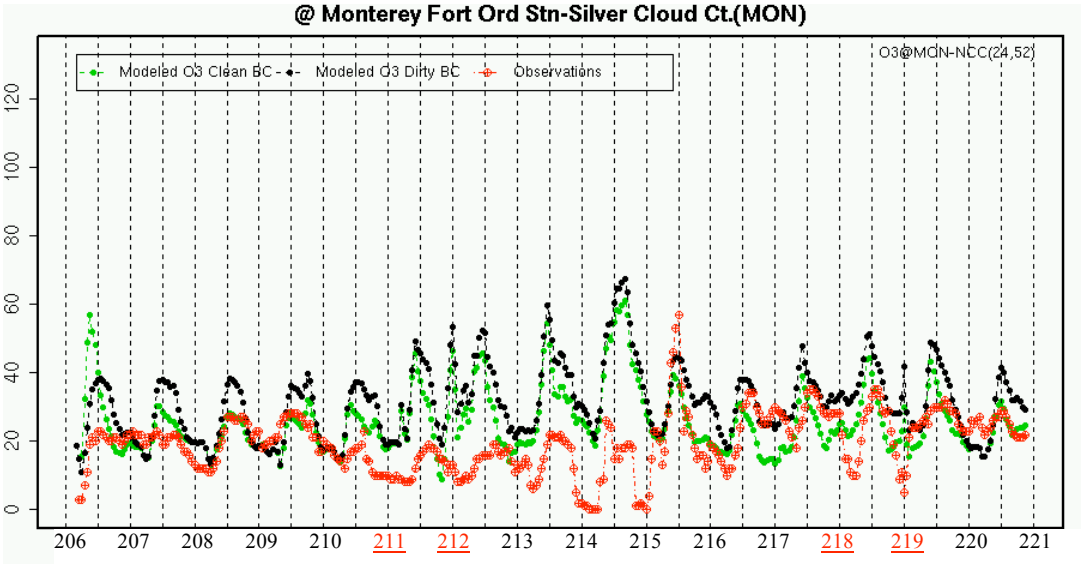

Figure 19: Predicted and observed O_3 (ppb) at a North Central Coast station (underlined/red Julian days along time axis denote weekends)

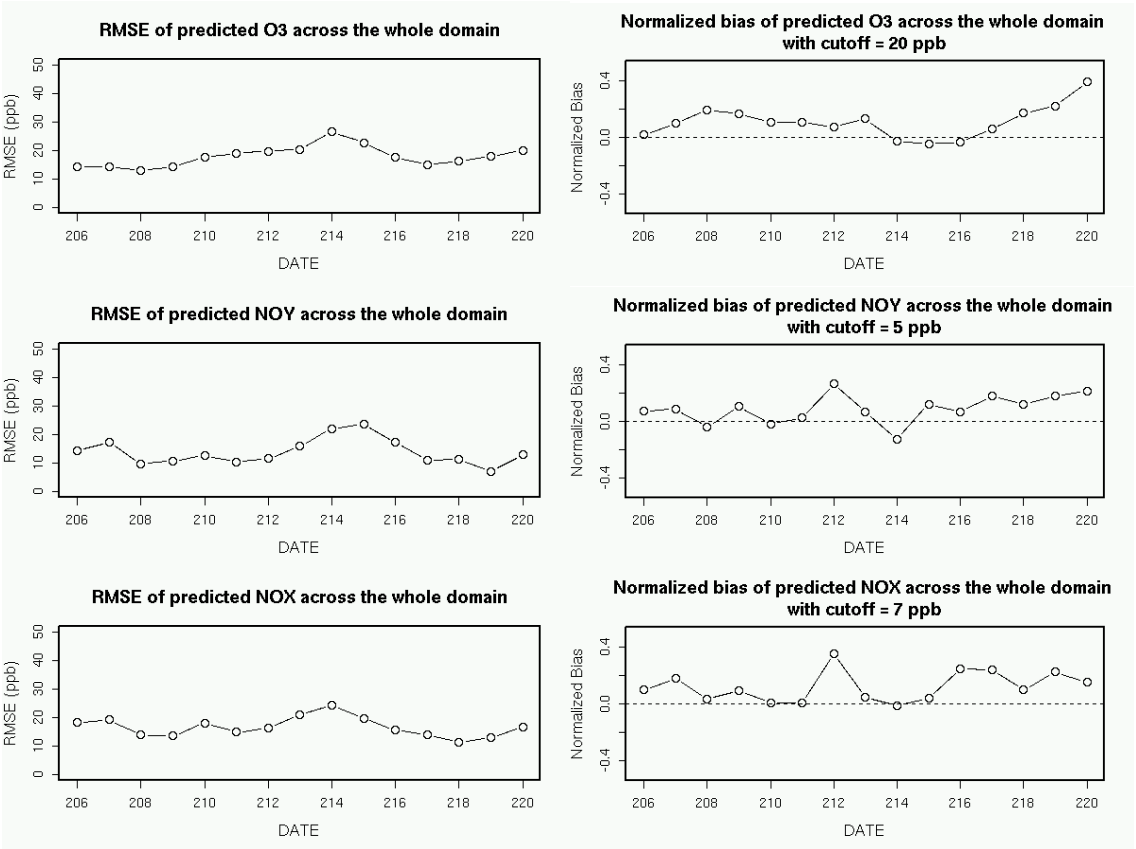

Figure 20: Temporal variability in root mean squared error and normalized bias for O_3, NO_y, and NO_x. Cutoff values are chosen so as to include the top 3 quartiles of the observed data.

Figure 20 shows how the accuracy of model predictions varies from day to day, plotting two evaluation statistics, mean normalized bias and RMSE, for O_3, NO_x, and NO_y. Note IOP2 includes days 211-216, for which the RMSE is high compared to the 5-day periods before and after it, when observed ozone levels were lower.

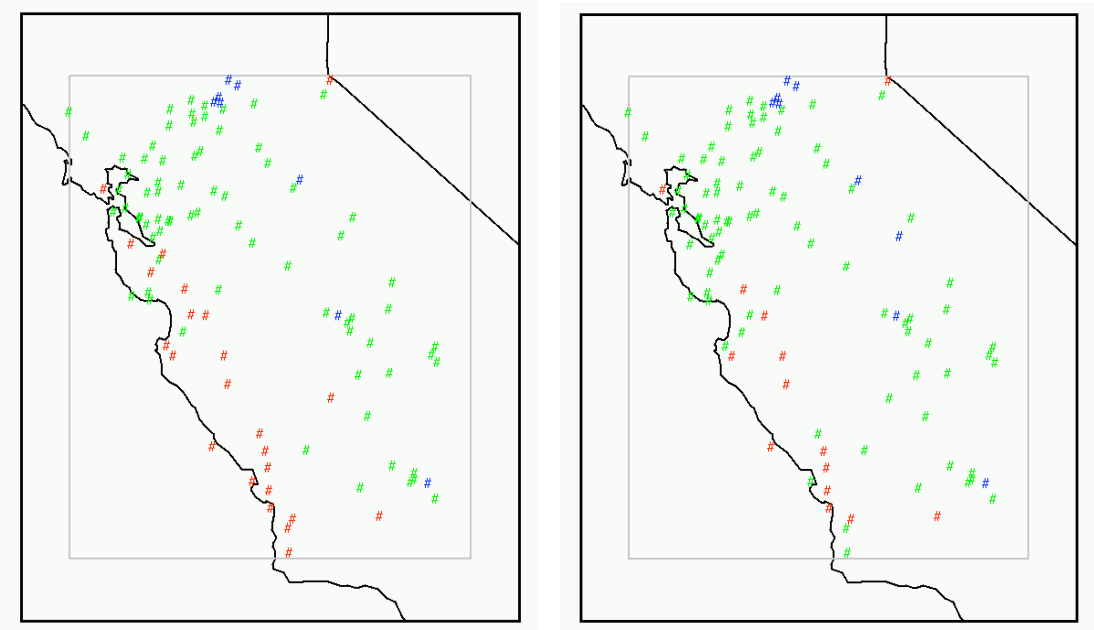

Figure 21: Spatial distribution of mean bias (ppb) for ozone at surface measurement sites. Left panel: Base Boundary Conditions. Right panel: Clean Boundary Conditions (western BC only). Red: Bias > 10 ppb. Green: Bias -10 to 10 ppb. Blue: Bias < -10 ppb.

Figure 21 shows the spatial distribution of mean bias for ozone using all hourly data from all 15 days of the simulation period (no cutoff was used as these are un-normalized model-measurement comparisons). The model generally overpredicts ozone along the coast, with better agreement farther inland. Comparison of the two figures indicates that the simulation using clean boundary conditions has better performance along the coast, with no significant differences inland.

Table 6: Ozone summary statistics for different air basins

Cutoff value =40ppb	All Air Basins		SJV		SV		SFB		SCC		NCC	
	Base BC	Clean BC	Base BC	Clean BC	Base BC	Clean BC	Base BC	Clean BC	Base BC	Clean BC	Base BC	Clean BC
Mean Bias[1] (ppb)	4	1	1	0	-3	-4	5	3	15	9	14	8
RMSE[1] (ppb)	18	18	19	19	18	20	16	17	21	18	19	16
Mean Bias (ppb)	-5	-7	-5	-6	-10	-11	-2	-5	1	-4	10	4
RMSE (ppb)	19	21	17	19	23	26	25	29	15	15	18	17
N. Bias (%)	-5 | -13*	-8 | -14*	-5 | -10*	-7 | -11*	-14 | -18*	-15 | -17*	-1 | -12*	-8 | -17*	5 | -10*	-3 | -15*	20 | 7*	9 | 0*
N. Gross Err (%)	23 | 20*	25 | 23*	20 | 18*	22 | 20*	29 | 26*	32 | 30*	36 | 29*	40 | 22*	20 | 15*	20 | 19*	28 | 18*	24 | 18*
Sample size	34990	34990	9568	9568	5359	5359	9190	9190	3374	3374	3793	3793

1: no cutoff value applied
*: cutoff value = 60 ppb

Table 7: One-hour peak ozone comparison statistics
(matched in location, to within three hours of the observed peak hour)

Cutoff value = 40 ppb	All Air Basins		SJV		SV		SFB	
	Base BC	Clean BC	Base BC	Clean BC	Base BC	Clean BC	Base BC	Clean BC
Mean Bias[1] (ppb)	8	6	0	-1	1	0	20	18
RMSE[1] (ppb)	24	26	22	25	27	29	28	30
Mean Bias (ppb)	0	-1	-3	-4	-4	-4	16	16
RMSE (ppb)	22	26	19	23	25	27	28	33
N. Bias (%)	4 | -2*	3 | -2*	0 | -3*	-1 | -3*	-1 | -5*	-2 | -6*	26 | 15*	26 | 17*
N. Gross Err (%)	22 | 18*	24 | 21*	18 | 16*	20 | 18*	24 | 21*	25 | 24*	35 | 24*	36 | 27*
Sample size	1128	1128	322	322	193	193	329	329

1: no cutoff value applied
*: cutoff value = 60 ppb

Table 8: Peak ozone (8-hour average) comparison statistics
(matched in location, to within three hours of the observed peak hour)

Cutoff value = 40 ppb	All Air Basins				SJV				SV				SFB			
	Base BC		Clean BC		Base BC		Clean BC		Base BC		Clean BC		Base BC		Clean BC	
Mean Bias[1] (ppb)	4		1		-3		-3		-5		-5		13		10	
RMSE[1] (ppb)	17		18		16		18		19		21		18		19	
Mean Bias (ppb)	-3		-3		-4		-4		-7		-6		7		5	
RMSE (ppb)	16		18		14		17		19		21		15		16	
N. Bias (%)	0	-8*	-2	-8*	-2	-7*	-3	-7*	-5	-13*	-5	-11*	16	0*	11	0*
N. Gross Err (%)	18	15*	19	18*	15	13*	17	16*	20	19*	23	24*	23	11*	22	16*
Sample size	1203		1203		346		346		203		203		315		315	

1: no cutoff value applied
*: cutoff value = 60 ppb

Basin-by basin comparisons: Ozone summary statistics computed for individual air basins are provided in Table 6. A cutoff value of 40 ppb, which is close to the median of observed ozone, was used in all but the top two table entries. Examination of Table 6 reveals that the model performs best in the San Joaquin Valley. The performance is not as good in the San Francisco Bay area.

Tables 7 and 8 display summary statistics for 1-hour and 8-hour average peak ozone for the whole domain and for the San Joaquin Valley, Sacramento Valley, and SF Bay area, where high ozone concentrations are typically observed. The cutoff values are chosen so that the top two thirds of the peak values are used in evaluating model performance in predicting daily maximum ozone concentrations. The model shows good performance in the San Joaquin Valley and in the small portion of the SV that is included in the SARMAP domain. The model on average over-predicts peak ozone in the SF Bay area. Changing boundary conditions from the base case to clean values on the western boundary has little impact on performance. Performance is better for the 8-hour average values than for the 1-hour average values of ozone concentration. This is especially true for the SFB basin.

4.2 Diagnostic simulations

During the course of this study, we investigated differences between model predictions and observations, and hypothesized as to the cause. A set of simulations summarized in Table 9, mostly over the 5-day IOP2 period (i.e., July 29-August 2), was conducted to investigate:

1. Deposition velocity of O_3 to ocean
2. Vertical mixing: minimum value for eddy diffusivity coefficient
3. Attenuation of light by low altitude coastal stratus
4. Surface albedo influence on photochemistry
5. Nudged vs. unnudged wind fields
6. Time averaged wind fields vs. instantaneous wind fields
7. O_3+NO_2 comparison to observational O_3+NO_2

The first three items were motivated by the consistent over-estimation of O_3 by the model compared to observations at coastal stations.

4.2.1. Deposition velocity of O_3 to ocean

We investigated if MCIP's O_3 dry deposition velocity over the ocean (set to zero) was set too low. Studies [Wesley, 2000] showed that ozone deposition velocity over the ocean is higher (~0.03-0.05 cm/s). To explore the effect of the change on predicted coastal ozone values, we conducted three simulations in which the O_3 dry deposition velocity over the ocean was increased relative to the default CMAQ value of zero by 0.05 cm/s, 0.1 cm/s and 0.5 cm/s. In all the three simulations with perturbations, ozone concentrations are decreased through out the domain compared to the base simulation. Ozone concentrations at coastal sites are only moderately sensitive to dry deposition velocity over the ocean. At central coastal sites, reasonable increases in ozone dry deposition velocity (i.e., 0.05 to 0.10 cm/s) resulted in decreases of approximately 5 ppb in ozone concentrations. Ozone sensitivities are smaller during the day than at night (and early morning). Since dry deposition contributes more to ozone changes when photochemistry is diminished, we examined its effect at a

Table 9: Summary of Diagnostic Model Simulations

No.	Run ID	Process or Parameter Adjusted	Most Affected Species / Geographic Areas
1	O_3_BC	Ozone sensitivity calculated by DDM to boundary ozone, and its precursors (NO, NO_2, and VOC). Brute force perturbation at different layers.	Coastal/near boundary sites are most affected. The effects of these perturbations are strongest locally in both horizontal and vertical.
2	Constant BC vs Vertically Varying BC	Change constant ozone boundary (40ppb at all layers) to a vertically varying profile (~20 ppb at surface, increasing aloft) derived from Trinidad head measurements.	A decrease in modeled coastal ozone, and an increase in inland ozone, by ~5 ppb.
3	O_3_EMISNOx	Ozone sensitivity calculated by DDM to emitted NOx.	Large positive sensitivity in rural areas, and negative sensitivity in NOx rich areas (urban).
4	O_3_EMISVOC	Ozone sensitivity calculated by DDM to emitted anthropogenic VOC.	Positive throughout the domain, and highest in NOx rich urban areas.
5	K_{zmin}	Change default value of minimum vertical eddy diffusivity in CMAQ from 0.5 to 0.1 m^2s^{-1} based on Jacobson (1999).	Lowered nighttime and some morning O_3 by ~10 ppb.
6	V_{d_O3}	Brute force sensitivity conducted by adding 0.05 cm/s, 0.1 cm/s, and 0.5 cm/s to default ozone dry deposition rate. Change zero ozone dry deposition rate to 0.04 cm/s based on Wesley (2000) and measurements by Faloona (2006).	Nighttime ozone and ozone at coastal sites are most sensitive to ozone dry deposition rate.
7	Wind fields	Conducted CMAQ simulation for 5-day ozone episode, using nudged vs. un-nudged wind fields, and time averaged wind fields.	No significant or systematic differences.
8	Nighttime Titration	Compare simulated NO_2+O_3 to observed values.	Eliminates titration effects when there are nearby NOx sources. Improved agreement at nighttime.
9	Coastal Stratus	Reduce coastal cloud transmissivity by 60% based on ground radiometer observations.	Coastal sites
10	Surface Albedo	Zero-out, double, and triple surface albedo	Urban areas where photochemistry is most active.

coastal site. Figure 22 compares O_3 from the various simulations at Salinas. For our 15-day simulations the O_3 dry deposition velocity over the ocean (i.e. Land-use category = "water") has been set uniformly in space and time to 0.04cm/s. [I. Faloona, personal comm., 2006].

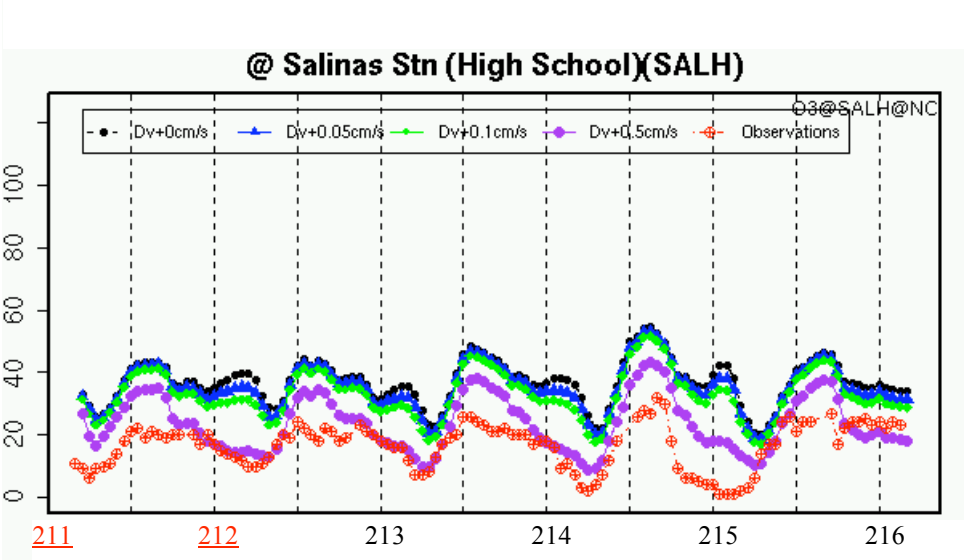

Figure 22: Observed and predicted O_3 (ppb) for different values of O_3 deposition velocity over water, at a site near the coast. Days 211-212 are Saturday-Sunday.

4.2.2. Vertical mixing:

In CMAQ, coastal O_3 readings are consistently higher than observed values, and appear in time series as an offset above them, whether day or night. Dr. Jinyou Liang of CARB pointed out that this might be caused by excessive vertical mixing in CMAQ due to the use of a minimum eddy diffusivity of vertical diffusion more suited to over-land than over-water values. We notice in the simulations that the vertical O_3 profile at the boundary degrades quickly as one moves eastward from the western boundary, with mixing from above which should not happen so quickly in a stable marine layer. Back of the envelope calculations show that it is physically justifiable [Jacobson, 1999] to reduce the minimum eddy diffusivity (KZMIN) value over the ocean from 0.5 to 0.1 m/sec^2. Assuming wind speeds of about 10 m/s and surface roughness lengths for the ocean to be between the suggested values of 1.5×10^{-5} and 1.5×10^{-3} m., we calculated KZ to be between 0.0015 and 0.15 m/sec^2. We conducted CMAQ simulations with chemistry disabled, with KZMIN=0.5 and 0.1, and compared the vertical O_3 profiles at several locations near the western boundary. With KZMIN = 0.1 the mixing from above was reduced by about 4 ppb by the time the coastline was reached. We also conducted simulations with chemistry and compared O_3 concentrations. The following time series in Figure 23 are O_3 at ground level at two coastal observation stations. The KZMIN = 0.1 simulation results in consistently lower values of O_3 at all times of day, due to a reduced rate of O_3 being diffused from above. Surface O_3 reductions of 5-10 ppb result when KZMIN is reduced.

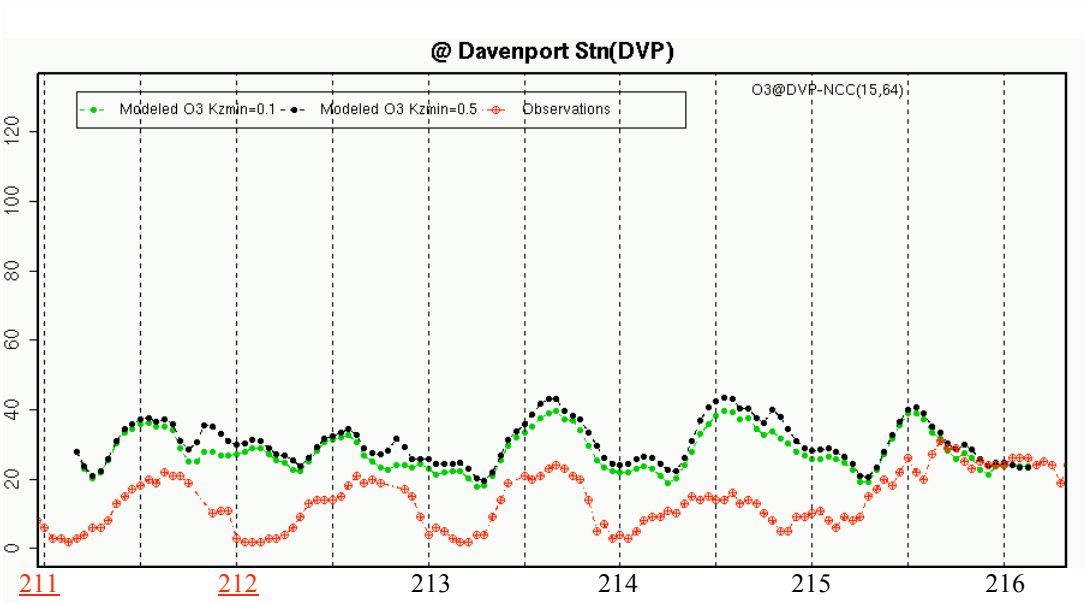

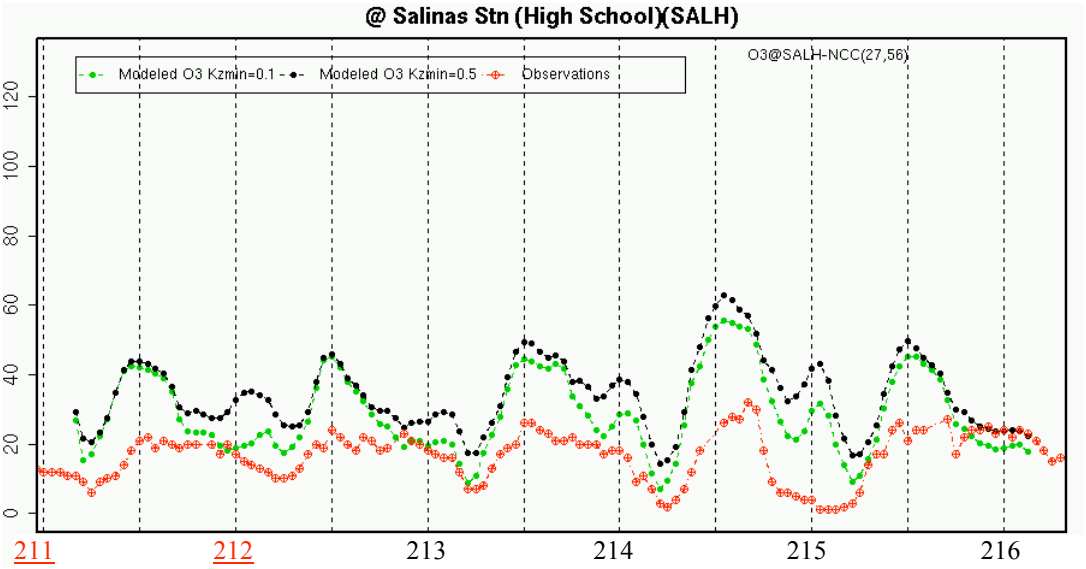

Figure 23: Time series of surface O_3 at Davenport and Salinas High coastal stations, comparing observations to model simulations with minimum eddy diffusivity (KZMIN) set to 0.5 and 0.1 m/sec^2. Days 211-212 are Saturday-Sunday.

4.2.3. Attenuation of light by low altitude coastal stratus:

In our search for factors responsible for the over prediction of coastal O_3 concentration, we investigated the treatment of light attenuation by clouds in CMAQ by focusing on the coastal fog/stratus off the California coast. The MCIP 3.0 processor obtains cloud liquid water content and cloud heights from MM5 and translates it to liquid water path, cloud fraction, cloud optical depth and finally into a corrective attenuation factor that is subsequently multiplicatively applied to the photolytic reaction rates in CMAQ. The attenuation values

were compared to ground radiometer observations from CIMIS (California Irrigation Management Information System) sites located in coastal areas, and the results indicate that attenuation in CMAQ is occasionally severely underestimated. This could have consequences for photochemistry, and possibly indicate a problem with higher (non-stratus) clouds. We will examine this further with the NOAA group, with the aim of implementing algorithmic improvements. The attenuation depends mainly on cloud water content and cloud height. Coastal stratus clouds have low values for both of these quantities and CMAQ treats stratus clouds as being nearly transparent. Radiometer readings such as those in Figure 24 show that actually as much as 60% of the incoming radiation is being reflected or absorbed before reaching the ground. Clear days show no attenuation and the diurnal behavior is caused by solar zenith angle. On very foggy days (e.g., the red curve) the attenuation can be as much as 60%. Figure 25 shows the actual cloud conditions which prevailed at noon on the day corresponding to the red curve in Figure 24.

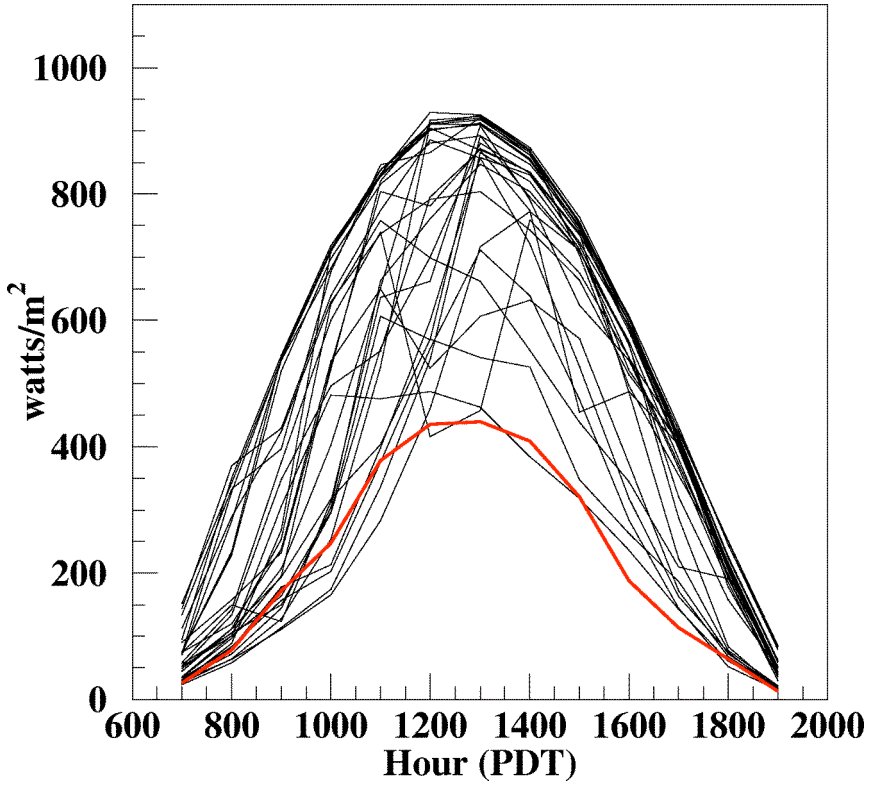

Figure 24: Radiometer readings (W/m^2) at Castroville CIMIS station near Monterey Bay, as a function of time of day for approximately 25 days.

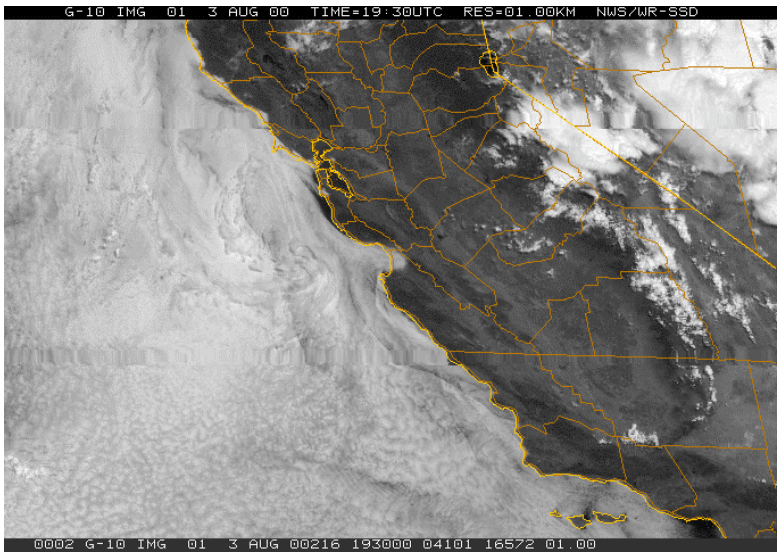

Figure 25: GOES satellite image corresponding to noon on the red curve from the preceding plot (Figure 24).

We conducted a model simulation with stratus cloud transmissivity diminished by 60%, to replicate the level of the attenuation seen on the red curve at Castroville. Figure 26 shows the change in O_3 concentration when compared to a base case. Below the cloud (layer 1, left panel) we see a decrease in O_3 of 1-2 ppb, while above the cloud (layer 15, right panel) we see an increase of 3-4 ppb due to increased reflection from the top of the cloud, which increases the rates of photolytic reactions. This analysis was performed before we decreased the value of KZMIN, so the effect at the surface may be diminished by too much vertical mixing.

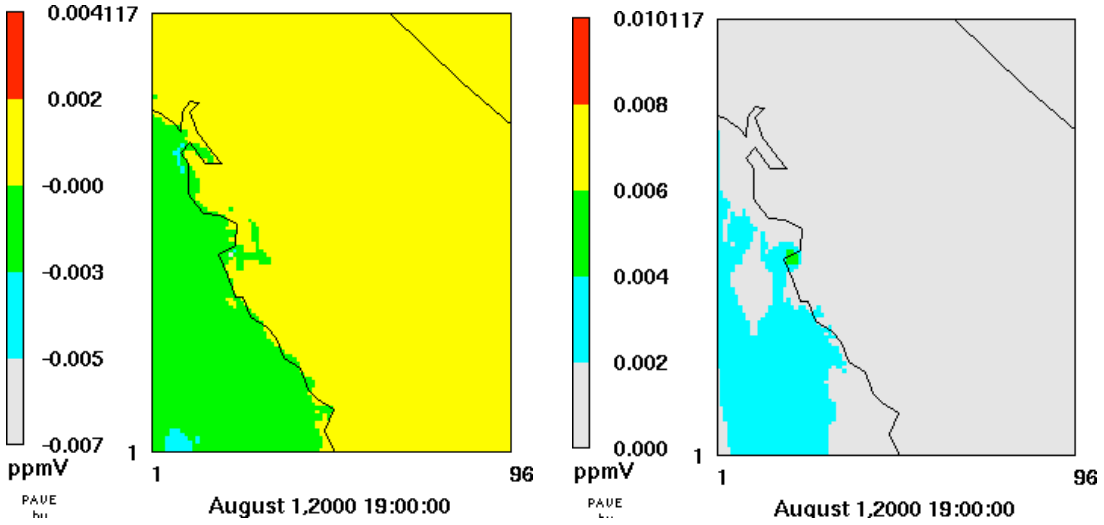

Figure 26: Difference in O_3 concentration seen at surface (left panel) and at 1 km (right panel), given a 60% reduction in solar radiation .

4.2.4. Albedo

The reflection of incident solar radiation from the earth's surface, or albedo, is calculated in CMAQ as a function of wavelength, with no variations with respect to land use type and surface properties. Our examination of surface albedo data obtained from the MODIS satellites shows as much as factor of four difference in surface albedo across the modeling domain. Figure 27 shows the albedo as a function of wavelength for selected locations. The two rural sites, Yosemite and Piedras Blancas on the south central coast, differ significantly from the values used in CMAQ for the short wavelength albedo.

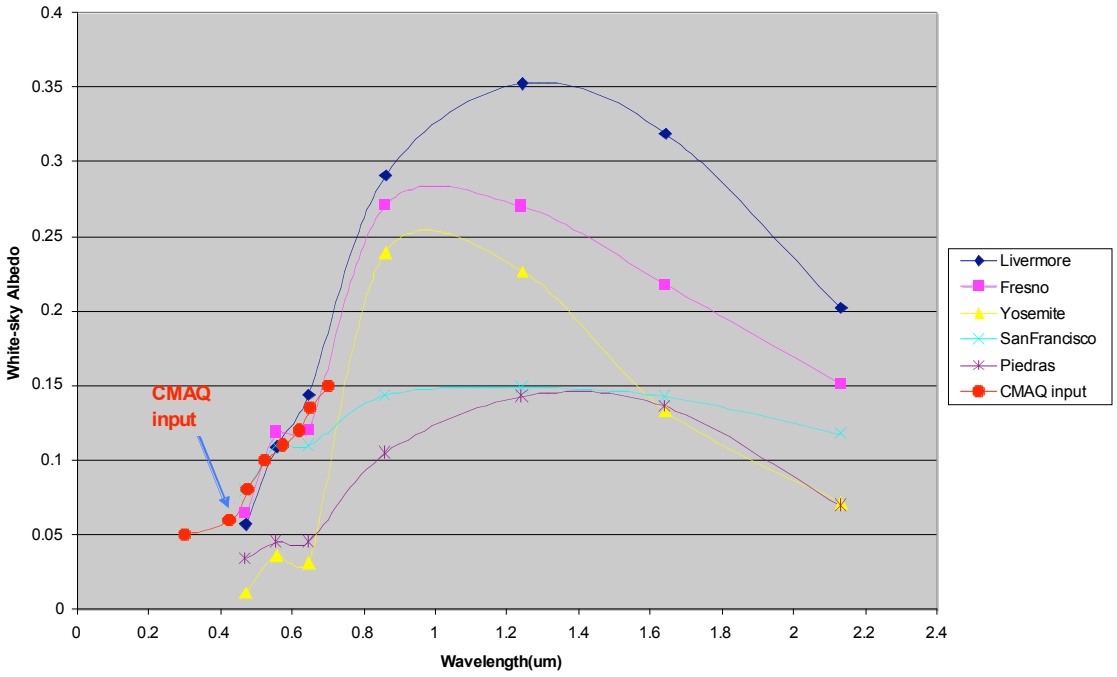

Figure 27 The variation of surface albedo at several locations in the domain.

We conducted a set of albedo perturbations simulations by zeroing, doubling, and tripling CMAQ's value of surface albedo, and examined the change in O_3 concentrations. The left panel of Figure 28 shows O_3 time series for the different multiples of albedo input. As seen in Figure 28, the ozone sensitivity to albedo is positive and of moderate value. Tripling the albedo results in a 5-10 ppb increase in O_3 in some locations.

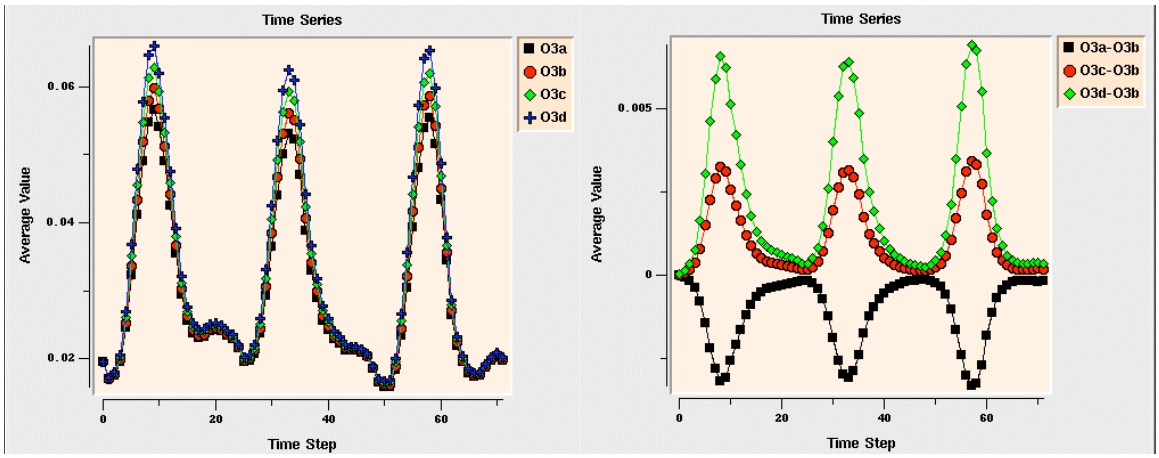

Figure 28: Left panel: O_3 time series in SF Bay region using different values of albedo. Legend: O3a: Zero albedo O3b: Base case albedo O3c: Double albedo O3d: Triple albedo.
Right panel: Differences of the three albedo perturbation simulations with respect to the base case. Legend: O3a-O3b: Zero-base albedo O3c-O3b: Double-base albedo O3d-O3b: Triple-base albedo

The differences in O_3 concentration observed are enough to warrant effort to improve the representation of surface albedo in CMAQ. The current albedo used in CMAQ is outdated. We are currently using satellite albedo products from MODIS and TOMS to construct new surface albedo maps according to radiation wavelength, surface land type, and time of the day for the summer 2000 season.

4.2.5. Wind fields: Nudged vs. unnudged

Four-dimensional assimilation of observed wind data (nudging) forces the meteorological model to follow measured values more closely than in unnudged simulations. The process of nudging is labor intensive, involving detailed examination of the observed wind data, and multiple MM5 simulations. While nudging improves agreement of modeled winds with observed winds, its effect on ozone concentration might be smaller. We evaluate the effect of using nudged wind fields on CMAQ simulations, using observed O_3 concentration as a metric by conducting CMAQ simulations with nudged and unnudged wind fields and comparing the calculated and observed O_3 observations. Results are shown in Fig. 29 and 30.

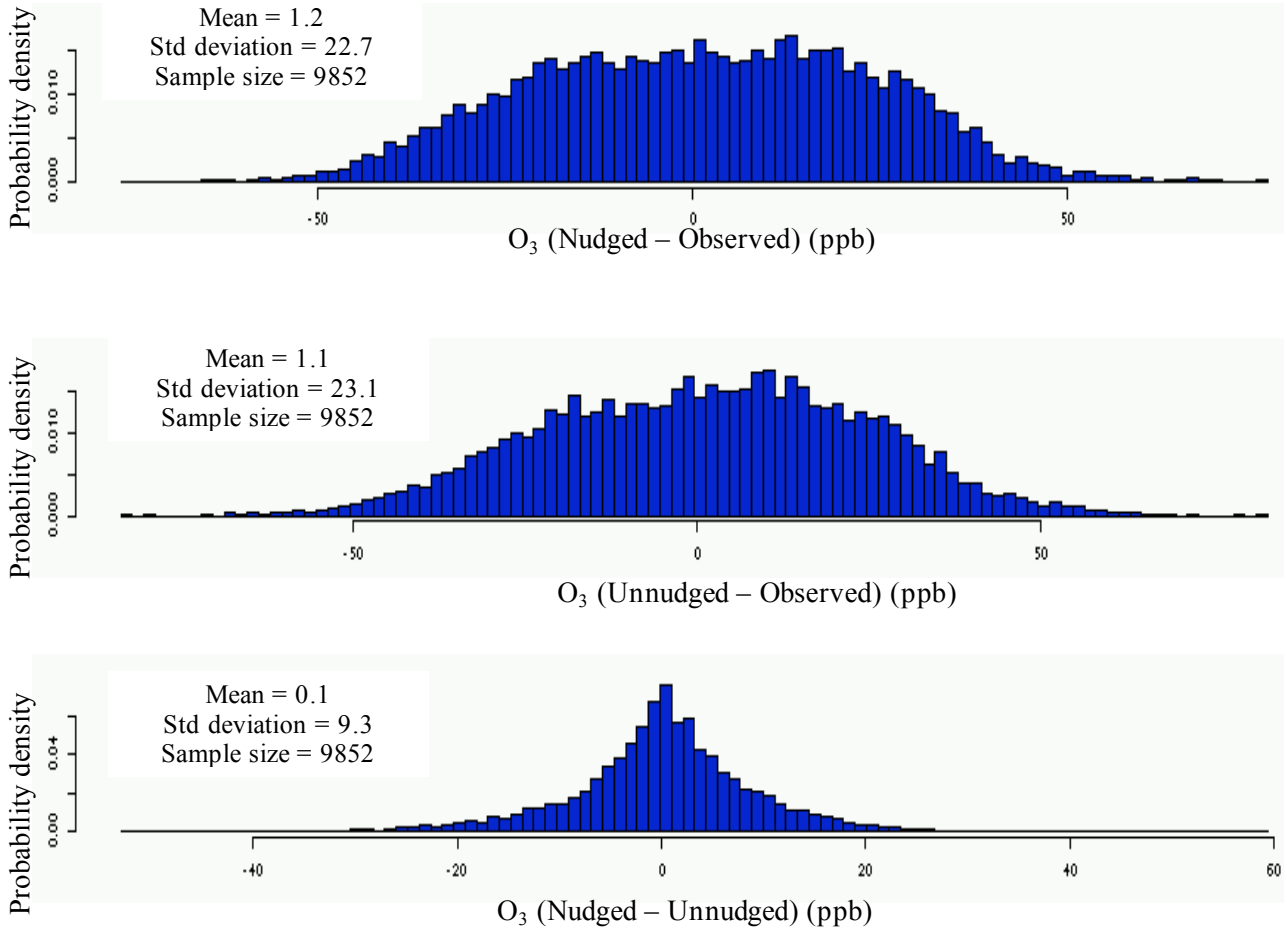

Figure 29: Distributions of the O_3 difference between nudged simulations and observations, unnudged simulations and observations, and nudged and unnudged.

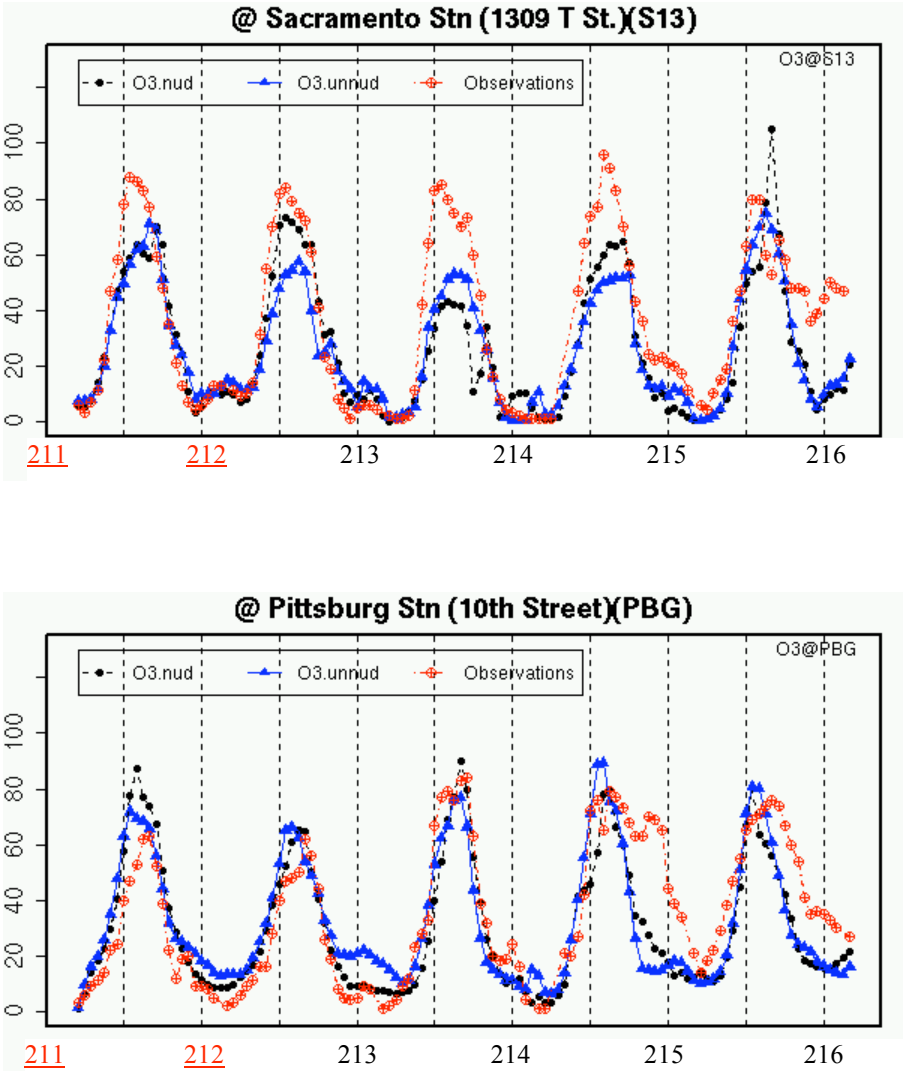

Figure 30: Observed and predicted O_3 (ppb) using nudged and unnudged simulations, at two stations. Days 211-212 are Saturday-Sunday.

Figures 29 and 30 indicate that there are differences between O_3 concentrations calculated with nudged and unnudged wind fields, and the difference is significantly smaller than the difference of either of these and the observations. This indicates that at the current level of model performance, unnudged wind fields are satisfactory. This conclusion may change in the future as the model is improved. The time series shown in Fig. 30 also shows that nudging effects are somewhat location dependent. Pragmatically, when faced with choosing (in fall 2005) unnudged meteorological simulations over a longer simulated period over nudged meteorological simulations over a shorter period, we selected the former.

4.2.6. Wind fields: Time averaged vs. instantaneous

Traditionally with MM5/CMAQ applications, wind fields at a particular instant are calculated by interpolating the instantaneous wind values that MM5 calculates out at the top of each hour. This practice could result in omissions of the effects of wind fluctuations occurring on time scales of less than one hour. As a possible replacement to interpolated wind fields, we investigated the benefit of using wind fields that are averaged by MM5 over the course of an hour using values calculated every few minutes, so that short-lived fluctuations in speed and direction are represented to some extent. This does not change the physics of the MM5 calculation, and only modifies what is actually written to the MM5 output file. The results are shown in Figure 31. Examination of the figure reveals there is very little difference in O_3 concentration determined with the interpolated and averaged wind fields. Wind fluctuations on time scales less than one hour do not make a significant change in O_3 predictions.

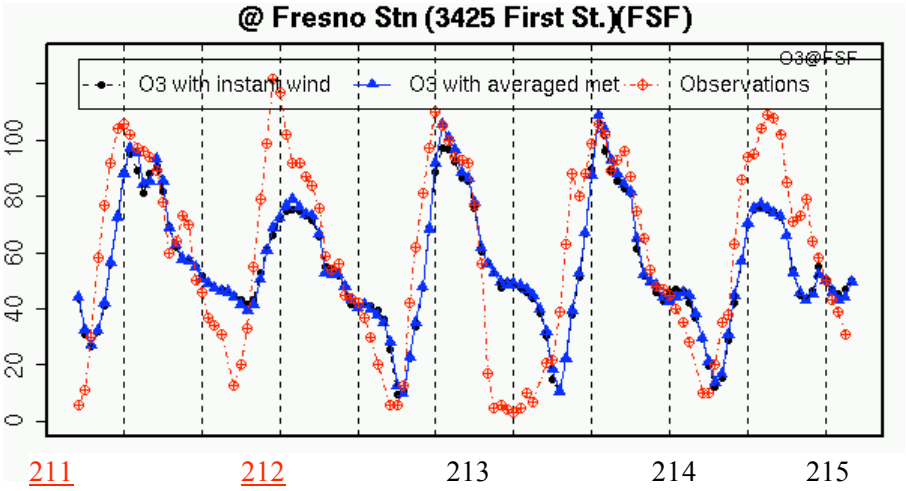

Figure 31: Observed and predicted O_3 (ppb) using instantaneous vs. hourly averaged winds. The two sets of model predictions are almost indistinguishable.

4.2.7. Possibility of local O_3 titration at stations: O_3+NO_2 comparisons:

We observed that the model overestimates ozone concentrations at night at many locations. Many nighttime surface observations are probably influenced fresh NO_x emissions. The over prediction of ozone could result from titration by NO_x. If titration is the reason for nocturnal O_3 overestimates, we expect the sum O_3+NO_2 to be predicted more accurately by the model than O_3 alone, which is shown to be the case in the following plots. Distributions of biases for both daytime and nighttime are presented for predicted O_3+NO_2, as well as O_3 alone. One can see that nighttime over-prediction is reduced from 10.5 ppb to 3.5 ppb after titration effects are accounted for.

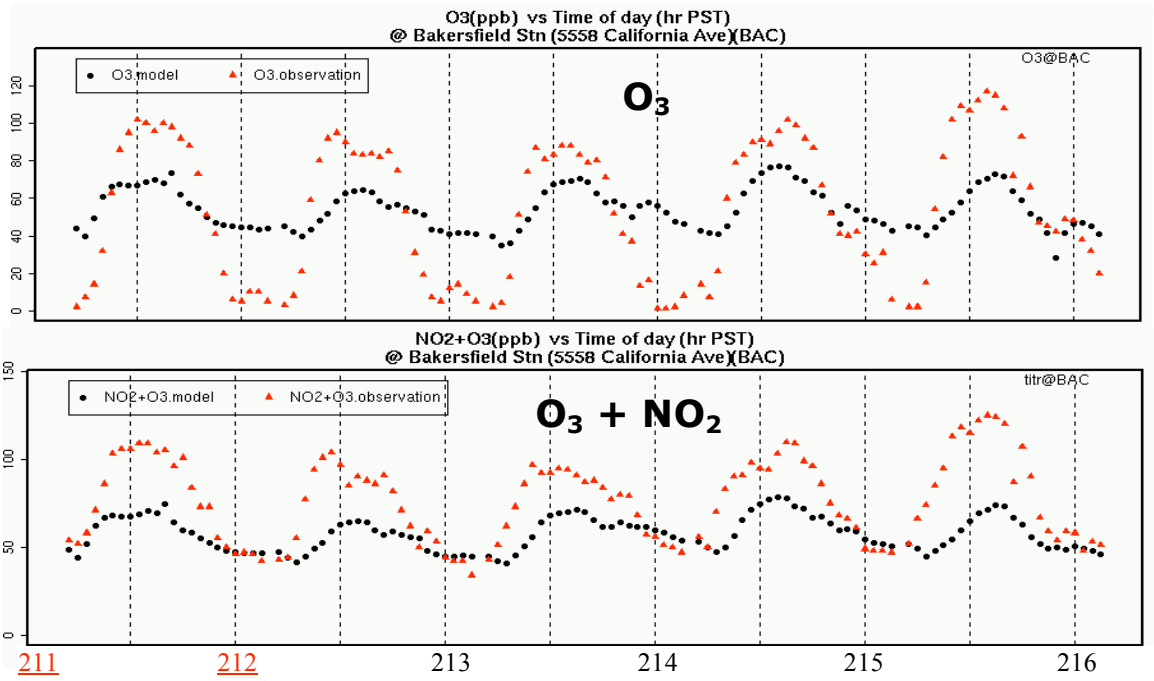

Figure 32: Observed and predicted O_3 (ppb) at Bakersfield station to show the effect of including NO_2 when comparing with observations. Days 211-212 are Sat-Sun.

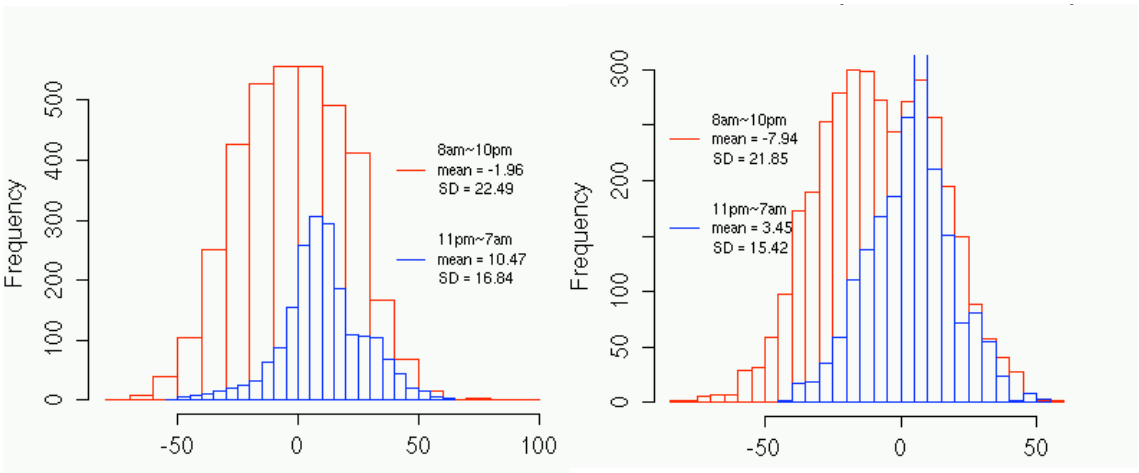

O_3 biases (ppb)

O_3 + NO_2 biases (ppb)

Figure 33: Distribution of biases in predicted O_3 and O_3 + NO_2 concentrations. The daytime biases are colored in red and nighttime biases in blue.

4.3 Sensitivity Analysis

Sensitivity analyses were undertaken for four purposes:

1. To determine whether a 72 hour spinup period is sufficiently long
2. To translate our estimates of uncertainty in boundary concentrations and emissions into uncertainty for O_3 within the domain and determine whether further efforts to reduce that uncertainty will be worth the effort.
3. To translate observed daily variability in boundary conditions and emissions into a daily variability for O_3.
4. Sensitivity analysis provides guidance on the weight that should be given to a prediction at a location/time. A prediction with a high sensitivity to an input variable that has a large uncertainty or an unknown day-to-day variability will inherit some of the uncertainty/variability and should be treated as such when statistical measures are calculated.

The majority of our sensitivity calculations use the Decoupled Direct Method of CMAQ_DDM4.3, but a few calculations use the brute force approach whereby an input quantity is perturbed, the model is re-run, and the change in the observable of interest is quantified. The results are presented in semi-normalized form, i.e., the sensitivity value, which resembles a first derivative, is linearly extrapolated to show the change in the dependent variable that would have occurred had the change in the sensitivity (input) parameter been +100 % of its nominal value. The output (dependent) variable for all of our sensitivity calculations is O_3, and the semi-normalized sensitivity value has units of concentrations, ppb. The sensitivities calculated by DDM are first order; hence, care must be taken when interpreting the result and applying it to a larger perturbation. Generally extrapolations less than 25% perturbations [Vuilleumier, 1997] are acceptable.

4.3.1. Sensitivity to Initial Conditions: Sensitivity of O_3 to Initial Conditions (IC) of O_3, NO_x and VOC were calculated with CMAQ_DDM4.3. The results show that memory of initial conditions is lost after approximately 50 hours (Figure 34) and this validates our practice of producing a spinup IC file from a 72-hour simulation. There is some spatial variability, above the ocean the decay is much faster, while inland over the SJ valley decay is slightly slower. The spinned up IC file is still not a true initial condition, but a more physically realistic one than our initial arbitrary IC.

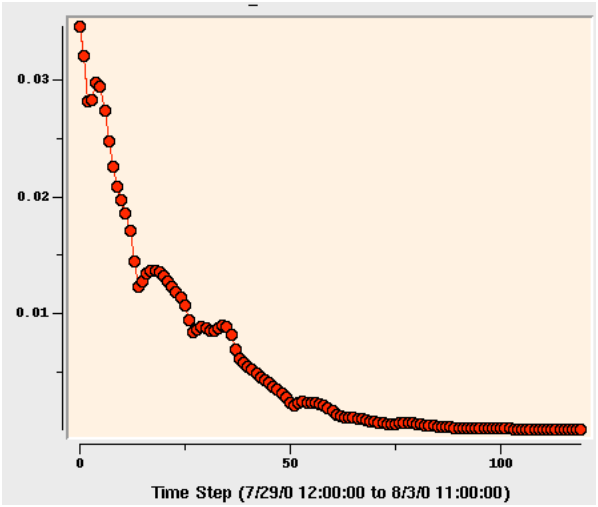

Figure 34: The semi-normalized sensitivity (ppb) of O_3 concentration to initial condition O_3 concentration as a function of time (hours).

4.3.2. Sensitivity to Boundary Conditions: Sensitivity of O_3 to boundary conditions is important to evaluate because of uncertainty as to the appropriate BC values. Boundary conditions are often in remote areas, vary vertically, have day-to-day and even hour-hour variability. Sensitivity of O_3 with respect to BC of O_3, NO_x, and VOC were calculated with DDM. Additional brute force sensitivities were conducted in which, the vertically varying O_3 BCs were separately perturbed for the lower, middle and upper model layers.

Figure 35 shows the sensitivity of O_3 concentration to the boundary concentration of O_3. The sensitivities, of course, are larger near boundaries. The sensitivity of O_3 in the San Joaquin Valley seems to be a 25% effect, i.e. a perturbation of 20 ppb in the boundary conditions produces a change of about 5 ppb in simulated O_3. The top right quadrant of the domain has the highest sensitivity, close to 100%. Our calculation of boundary fluxes (Figure 10) indicates that there is inflow on the upper half of the eastern boundary, which could account for the large sensitivity.

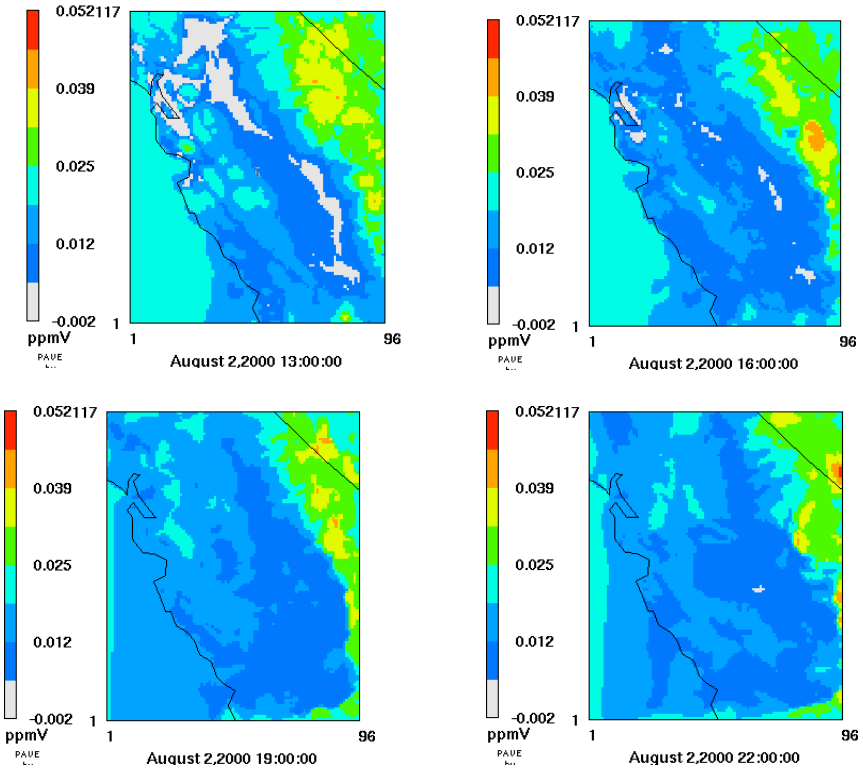

Figure 35: Sensitivity of O_3 to boundary O_3 at four times (in PDT) of the day: 6am, 9am, 12pm, and 3 pm. Times are GMT, which is 7 hours ahead.

The sensitivity of O_3 to the boundary concentration of NO_x and to anthropogenic VOC is shown in Figure 36. On the coast we see about 10 ppb change of ozone due to a 1 ppb increase of NO_x BC. The sensitivity to VOC seems to be high downwind of NO_x rich areas, one can see this is the case for the SF Bay area and Sacramento. The sensitivity to VOC is significant in parts of the SJ Valley, but is low on the coast.

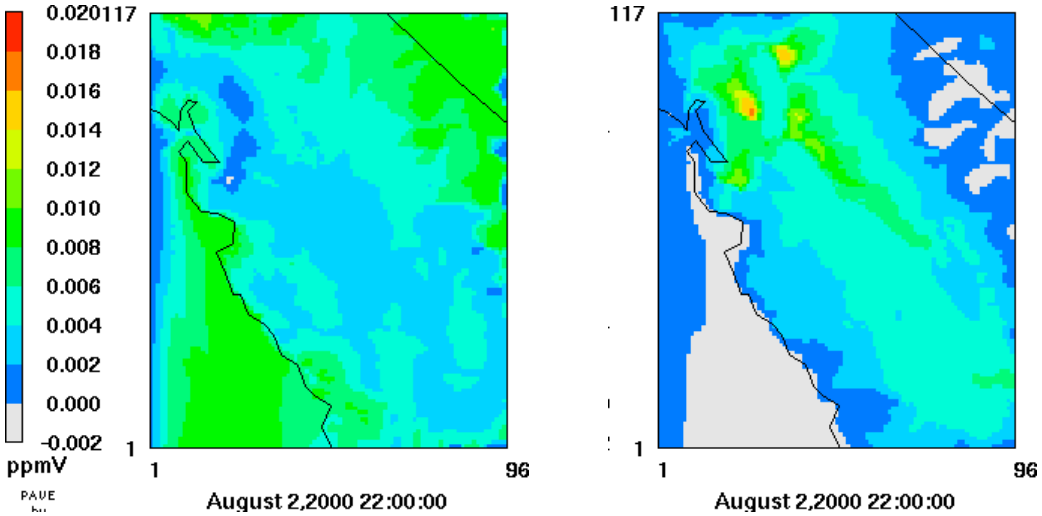

Figure 36: Sensitivity of O_3 to boundary NO_x (left) and anthropogenic VOC (right). Times are GMT.

Brute force sensitivity calculations were used to study the influence of the altitude dependence ozone BC on the computed O_3 concentrations. Multiplicative perturbations of ±20% were separately applied to the ozone BC at three different ranges of altitudes as described in Table 10.

Table 10: Vertical domain ranges over which BC perturbations were applied

Layers	Altitude range (meters)	Name
1 to 15	0 – 1067	low
16 to 21	1067 – 4242	middle
22 to 27	4242 – 16667	high

5-day simulations were conducted with the modified ozone BCs, starting on day 211 (July 29) at 1200 GMT. The computed ozone concentrations were compared to a base case.

Figure 37 shows the spatial variation of the difference in O_3 at the surface observed for the low and middle BC perturbation cases. As expected, surface O_3 is most affected by perturbations near the surface, and less so for the "middle" perturbations. Perturbations in the middle range only affect the surface at places where the terrain is elevated, such as the Sierra Nevada and coastal ranges. This is verified from comparing to terrain height information provided in the meteorological input files.

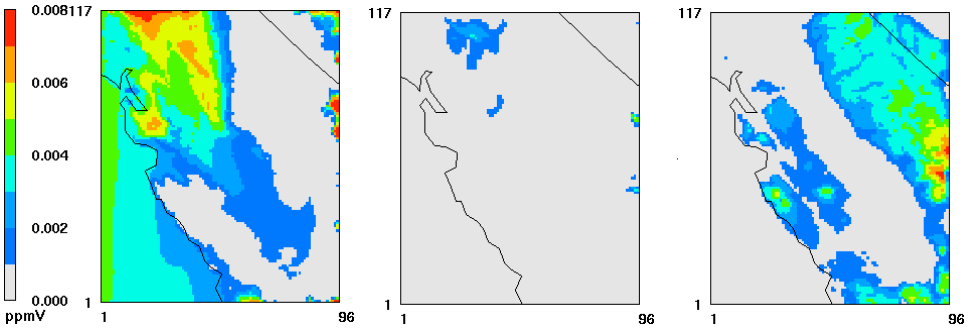

Figure 37: Sensitivity of O_3 to O_3 BC perturbations at different levels.

Left panel: O_3 change seen at layer 1 when perturbation of +20% is applied to low layers.

Middle panel: O_3 change seen at layer 18 when perturbation +20% is applied to low layers.

Right panel: O_3 change seen at layer 1 when perturbation +20% is applied to middle layers.

Changing the sign of the perturbation while fixing the magnitude produced changes in computed ozone of nearly equal magnitude but opposite sign. Changes noted in Figure 37 for a negative perturbation would be of opposite sign for a position perturbation.

Table 11: The absolute and relative (percentage) O_3 difference seen in selected layers for a perturbation of +20% in low layers (layers 1 to 15)

subdomain	differences	layer 1	layer 7	layer 15	layer 18	layer 22	layer 25
SFBAY	abs in ppbV	3.34	3.85	1.56	0.07	low	low
	%	20.07	11.88	2.96	0.11	low	low
SACRA	abs in ppbV	2.99	3.57	3.24	0.45	low	low
	%	11.6	7.85	5.46	0.66	low	low
FRESNO	abs in ppbV	0.84	1.04	0.26	low	low	low
	%	2.23	1.59	0.33	low	low	low
MONTEBAY	abs in ppbV	4.28	4.3	2.59	low	low	low
	%	16.83	14.45	5.49	low	low	low
EMOUN	abs in ppbV	0.11	0.11	low	low	low	low
	%	0.19	0.17	low	low	low	low
WMOUN	abs in ppbV	0.6	0.56	0.09	low	low	low
	%	0.96	0.79	0.14	low	low	low

Color legend:

	extremely high > 15%
	10% < very high < 15%
	5% < high < 10%
	1% < low < 5%
	0.1% < very low < 1%
	extremely low < 0.1%

-absolute differences : O_3ref-O_3disturbed
-relative differences (%) : (O_3ref-O_3disturbed)*100/O_3ref

Subdomain definition:

Subdomain	***full name***	***x min***	***x max***	***y min***	***y max***
SFBAY	San Francisco Bay Area	6	24	68	92
SACRA	Sacramento Area	28	37	104	111
FRESNO	Fresno	59	71	54	66
MONTEBAY	Monterey Bay	4	14	53	63
EMOUN	East Mountains	62	82	82	100
WMOUN	West Mountains	28	36	37	45

Table 11 summarizes the changes in O_3 concentrations in various layers when boundary conditions were perturbed by (-20%) in the low layers as defined in Table 10. As seen from the Table, low altitude perturbations do not affect calculated O_3 concentrations in the high layers. Generally, small effects are observed in middle layers from low altitude perturbations. Influence on low layers varies according to the basin area being studied; specifically, it ranges from very low in mountainous areas to high and extremely high in SF bay, Sacramento and Monterey Bay, i.e., areas with lower layers near sea level. Other calculations revealed that perturbations in the middle layers influence middle layers most strongly. The middle layer perturbations influence low layers quite modestly (1 to 5%) and their influence grows as layer height increases (layer 15, often 5 to 10%). The middle layer perturbations exert very little influence on the top layer.

We also investigated the effects of perturbing the boundary conditions in the high layers. Perturbations in the high layers strongly affect the high layers, and changes in computed ozone between 10 and 20% are observed. Often perturbations in the high layers exert little influence over computed ozone in the middle and low layers, but there are exceptions especially in the mountainous areas. In the Eastern mountain region, computed ozone changes greater than 5% were observed in all layers. Changes were significant but less than 5% in the Western mountain region for all layers.

4.3.3. Sensitivity to Emissions: Sensitivities of O_3 to emissions of NO_x and anthropogenic VOC (AVOC) and biogenic VOC (isoprene and mono-terpenes) were calculated with DDM, and are shown in Figure 38. Sensitivity to NO_x emissions is both positive and negative and depends on conditions. The very negative values are likely to result from a combination of titration and OH termination with NO_2. In NO_x-rich areas, there is high positive sensitivity to VOC emissions that is countered by a high negative sensitivity to NO_x emissions. Sensitivity to both anthropogenic and biogenic VOC emissions is especially high in NO_x rich areas. Regions of negative sensitivity to NOx sensitivity (see leftmost panel of Figure 38 below) indicated a NO_x-satured regime.

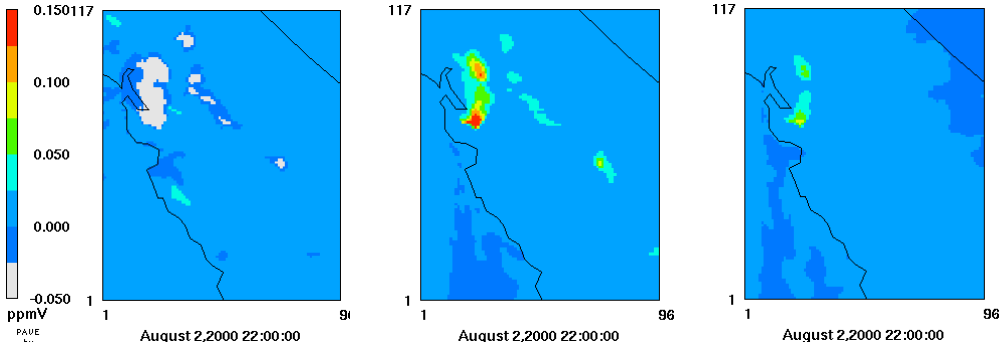

Figure 38: Sensitivity of O_3 (ppb change in layer 1), normalized to 100% change in emissions of NO_x, anthropogenic VOC and biogenic VOC. Times are given in GMT.

4.4 Investigation of Weekend Effect

Some urbanized areas see higher concentrations of ozone on weekends vs. on weekdays. This "Weekend Effect" appears to be paradoxical since it is known that the total anthropogenic emissions of NO_x are typically lower on weekends. We have conducted model simulations of weekday and weekend conditions, and calculated concentrations and process analysis variables. With the help of process analysis one can quantitatively track species and thereby gain insight into the factors causing the Weekend Effect focusing on the time-dependence of the emissions and actinic flux. We have analyzed the results with the data-interrogation tool, PAW.

Two hypothetical emissions scenarios were constructed using the following day-of-week specific emission rates:

1. Thursday Friday Saturday Sunday Sunday
2. Thursday Friday Monday Monday Monday

The two scenarios are identical for the first 48 hours, and for the last 72 hours, one contains weekend emissions, and the other, weekday emissions. Figure 39 shows the summed emissions, from all emission categories, for the first four days. There is appreciable difference in weekend NO_x emissions, and a much smaller difference in VOC emissions.

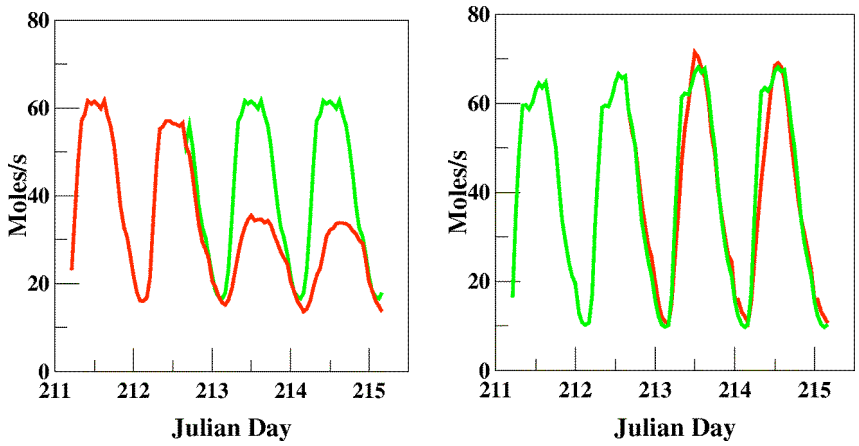

Figure 39: NO_x (left) and VOC (right) emissions summed over the whole domain for weekday scenario (green) and weekend scenario (red) for the first four days of the simulation. Note both scenarios have identical emissions on the first 2 days, so only one color is visible.

Initial, boundary, photochemical rate and meteorological conditions were identical in both simulations. Examination of the simulated O_3 concentrations revealed that, in some locations, the O_3 concentrations on the weekends are higher than those seen on weekdays. Figure 40 shows the spatial dependence of the weekend O_3 excess. The Weekend Effect is observed in the SF Bay and metropolitan Sacramento areas. All further data shown here will be taken from a region represented by grid cells to the east of SF bay near Pittsburgh.

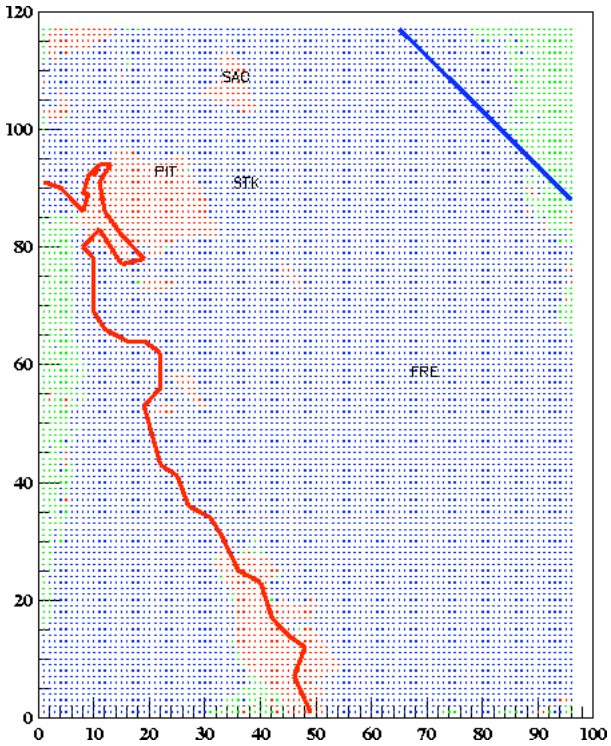

Figure 40: Effects of weekday-weekend emission changes on ozone at 3 pm on the fourth day. Grid cells are colored depending on whether the weekend O_3 is greater than (red), equal (green) or less than (blue) weekday O_3. The coast is marked red, the CA-NV border is blue, and the cities of Pittsburgh, Sacramento, Stockton and Fresno are shown.

Since NO emissions are lower on the weekend, reduced titration of O_3 by $O_3+NO \rightarrow NO_2$ could be a contributing factor. The extent of this effect can be determined by plotting ($-\Delta NO_2$), the negative of the difference between weekend and weekday NO_2, against ΔO_3, the difference between weekend and weekday O_3, for all grid cells and timesteps as shown in Figure 41. If titration were the only relevant factor, then points would lie close to the black line. Points below the line indicate that extra weekend O_3 is not compensated for by a deficit in NO_2, and so is being produced by some other means. Titration accounts for some of the change, but there is also an odd oxygen excess, accounting for 30-50% of ΔO_3, where odd oxygen is the sum of O_3+NO_2 concentrations. The plot is color coded, showing that overnight and 6-9 AM, weekday-weekend differences are dominated by titration effects (blue, cyan), while for 9 AM-6 PM, an odd oxygen excess occurs that must involve other explanations than titration (yellow, red).

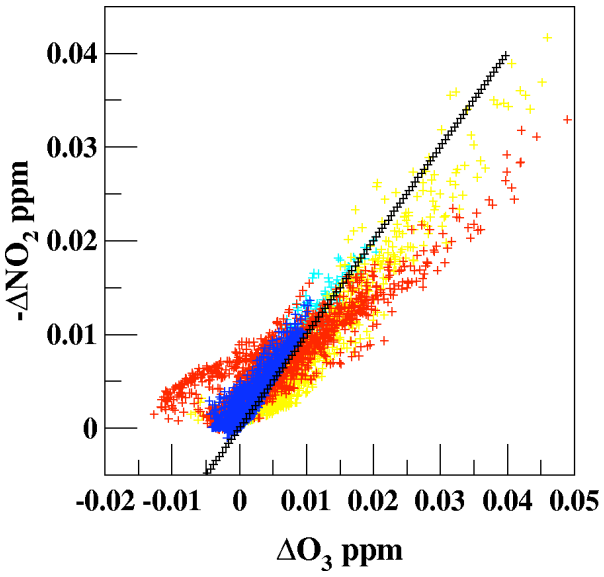

Figure 41: Scatterplot of ($-\Delta NO_2$), the negative of weekend-weekday NO_2, vs. ΔO_3 weekend minus weekday O_3 for every column-averaged grid cell. The color coding shows time of day: Cyan: 6 am-9 am, Yellow: 9 am-Noon Red: Noon-6 pm, Blue: 6 pm onward.

The reason for the odd oxygen excess can be investigated using process analysis. Figure 42 shows a partitioning of the integrated hourly change of odd oxygen into the contributions to NO_2 production from reactions of NO with HO_2 and RO_2. There is high correlation, and quantitatively (by looking at the limits on the axes), one can see that the two reactions account for nearly all of the odd oxygen production.

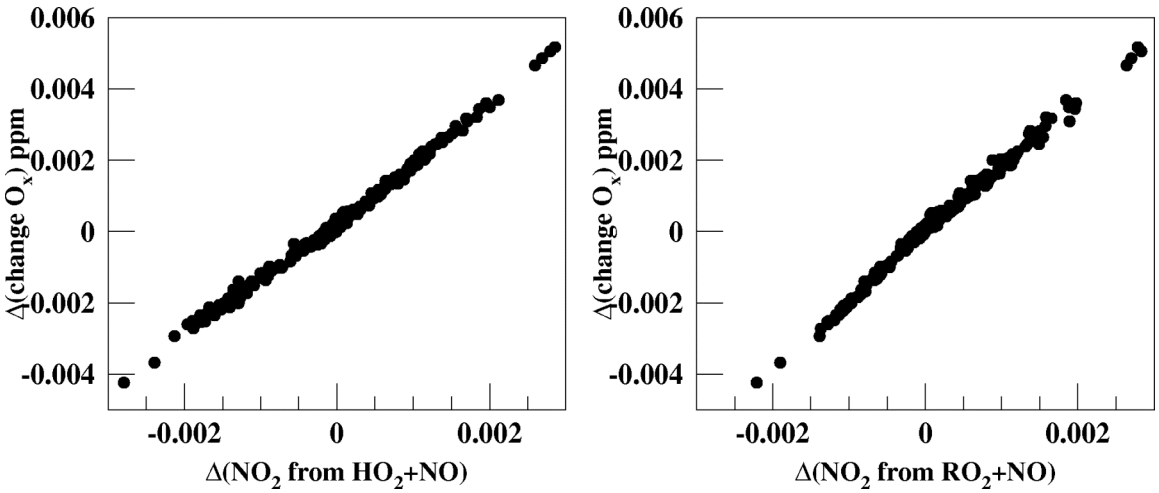

Figure 42: Integrated hourly change in odd oxygen vs. contributions from HO_2+NO and from RO_2+NO. One data point is given for every grid cell for every hour.

We investigated possible reasons for the increased HO_2+NO and RO_2+NO by examining the weekend-weekday differences for "new" OH production, where "new" OH excludes OH produced from the HOx cycling reaction $HO_2+NO \rightarrow NO_2+OH$. Process analysis revealed that

OH originating from ozone photolysis: $O_3+hv \rightarrow O_2+O(^1D)$, where the $O(^1D)$ reacts via: $O(^1D)+H_2O \rightarrow 2OH$ is responsible for most of the "new" OH production. Weekend production of OH by this means is larger than weekday production. Not only is there higher production of new OH on weekends, but also OH removal rate through the reaction $OH+NO_2 \rightarrow HNO_3$ is lower. This is the termination reaction by which OH leaves the HO_X cycle, removing one odd oxygen and one OH in the process. This results in more OH reacting with VOC on weekends to produce more HO_2. Weekend emissions of VOC are about the same as weekdays; hence, the underlying cause for the weekend excess is most likely extra OH availability.

The time dependence of the average rates of the reactions of OH with NO_2 and with VOC is shown in the left panel of Figure 43. The right panel in Figure 43 shows the weekend-weekday difference in OH loss from causes other than by $OH+NO_2 \rightarrow HNO_3$. It shows higher weekend OH reactivity with VOC at midday and early afternoon, followed by higher weekday reactivity in mid and later afternoon, as the Δ_{ED} ($OH_{effective}$) becomes negative. In mid to late afternoon, the weekend peroxy radicals (HO_2+RO_2) have difficulty finding NO to react with, and they undergo termination by self reaction, i.e., $HO_2 + HO_2 \xrightarrow{H, H_2O} H_2O_2 + O_2$. Termination of peroxy radicals is higher on weekends, and this causes the weekend effect to cease in mid-afternoon.

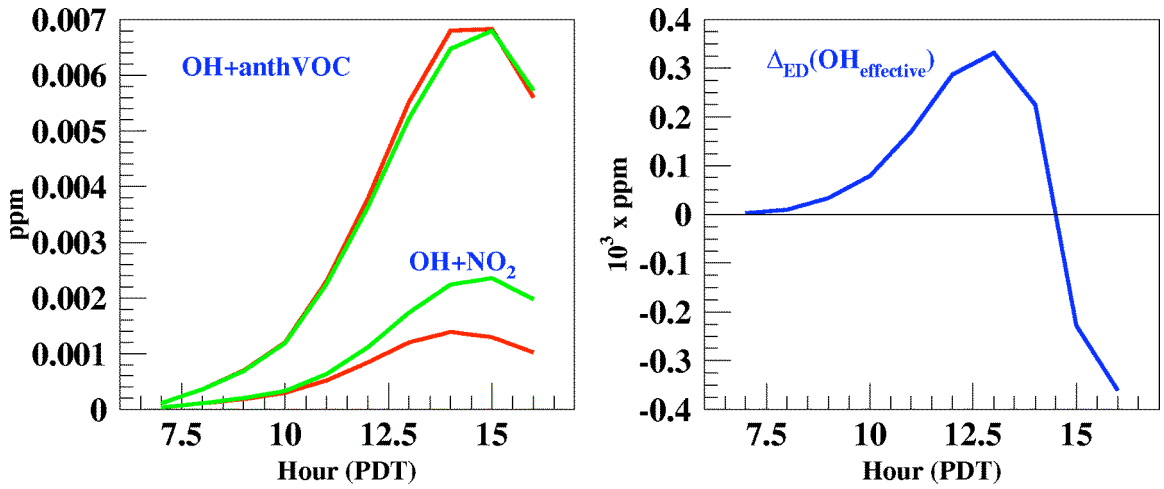

Figure 43: Left panel: Time dependence of the average rates of the reactions of OH with NO_2 and VOC on weekends and weekdays. Right panel: Weekend – weekday difference in effective OH loss, (where "effective OH loss" is defined as being OH loss not caused by termination with NO_2).

We summarize our analysis as follows:

1. The morning and midday weekend O_3 excesses can be attributed to the sudden transition from high to low NO emissions at the beginning of a weekend. This results in reduced titration, which leads successively to higher weekend O_3, higher weekend $O(^1D)$ and higher OH production from $O(^1D) + H_2O \rightarrow 2\ OH$.
2. Less termination via $OH+NO_2 \rightarrow HNO_3$ leads to a higher fraction of OH reacting with VOC on weekends.
3. Reduced emissions of NO lead to higher self-termination of peroxy radicals.
4. Increased competition for NO from higher weekend O_3 also leads to higher self-termination of peroxy radicals.

In conclusion, (1) and (2) are responsible for and enhance the Weekend Effect and (3) and (4) are responsible for its mid-afternoon termination.

5. Summary, Conclusions and Recommendations

We have assembled model inputs for, and have conducted a 15-day simulation of a portion of the CCOS 2000 period. Additionally we have conducted diagnostic simulations of other model inputs and operational parameters, and sensitivity calculations.

The model performance for the 15-day period shows its best agreement in the San Joaquin Valley. Absolute agreement (Mean Bias and RMSE) is better in the San Francisco Bay Area, but relative measures (Normalized Bias and Normalized Gross Error) are not as good. When model performance is considered on a day-to-day basis, it is seen to degrade slightly during the high ozone episode of IOP2, which covers the central 5 days of the 15-day period. The episode, the central five days of the 15-day period, tends to have higher ozone than the five days on either side of it.

From diagnostic simulations we conclude:

1. Deposition velocity of O_3 to ocean: A value of 0.04 cm/s is in agreement with experimentally measured values. It reduces modeled coastal O_3 concentrations by about 5 ppb.
2. Vertical mixing: minimum value for the eddy diffusivity coefficient: Reducing this value (from 0.5 to 0.1 m/sec^2) to more sensible over-water values reduces the mixing of O_3 from above, which provides better agreement with observed values. Mixing still appears to be over-estimated, and further research is necessary into whether the meteorological model MM5 is correctly predicting the variables which influence vertical mixing, and whether MCIP is interpreting and utilizing the variables in the most scientifically up-to-date manner.
3. Attenuation of light by low altitude coastal stratus: CMAQ occasionally severely underestimates this quantity. Our simulations show that this can result in a 1-2 ppb underestimate of O_3 below the cloud and 3-4 ppb overestimate above the cloud. The algorithms in MCIP might need to be brought up-to-date with the latest cloud algorithms available from the climate-change community.
4. Surface albedo influence on photochemistry: CMAQ's treatment of surface albedo ignores spatial variation of albedo completely. Our simulations indicate that increases of 5 ppb are possible in places if correct values are used. We aim to implement spatially and seasonally varying albedo fields as a CMAQ input.
5. O_3+NO_2 comparison to observational O_3+NO_2: Nighttime agreement of model to observation improves significantly if local O_3+NO → NO_2 effects are accounted for.

From calculations of sensitivity to boundary conditions we conclude:

1. The NO_x boundary concentration makes a large (10 ppb) difference on coastal O_3.
2. The VOC boundary concentration makes a large difference on O_3 near NO_x rich urban areas, such as SF Bay and Sacramento.
3. Upper layer (above 3 km) O_3 boundary condition values do not exert a significant influence on surface values anywhere in the modeling domain.

6. References

Benjamin, M.T. et al., Low-emitting urban forests: a taxonomic methodology for assigning isoprene and monoterpene emission rates. Atmos. Environ. **30**, 1437-1452 (1996).

Byun, D.W. and J.K.S. Ching, Science algorithms of the EPA Models-3 Community Multiscale Air Qualty (CMAQ) Modeling System. EPA/600/R-99/030, U.S. EPA. (1999).

Buhr, M.P. Donald L. Blumenthal Siana H. Alcorn Sonoma Technology, Inc., Measurements made aloft by two aircraft to support the Central California Ozone Study (CCOS). Final Report STI-900106-2131-DFR. Prepared for: San Joaquin Valleywide Air Pollution Study Agency (2001).

Carter, W.P.L., Documentation of the SAPRC99 chemical mechanism for VOC reactivity assessment. Report to the California Air Resources Board; University of California, Riverside, College of Engineering, Center for Environmental Research and Technology: Sacramento, CA, Contracts 92-329 and 95-308, (2000).

Cohan, D.S. et al., Non-linear Response of Ozone to emissions: Source Apportionment and Sensitivity Analysis. Environ. Sci. Technol. **39**, 6739-6748, (2005).

Dunker, A.M, The decoupled direct method for calculating sensitivity coefficients in chemical kinetics. J. Chem. Phys. **81**, 2385-2393 (1984).

FEJF, Fire Emission Inventory for the WRAP Region – Methodology and Emission Estimates. Final Report by Air Sciences Inc. for the Western Regional Air Partnership. (http://www.wrapair.org/forums/fejf/documents/emissions/FEJF1996EIReport_040325_final.pdf)

Fujita, E.M., D.E. Campbell, and T. Snorradottir, Central California Ozone Study (CCOS) Data Validation. Eric M. Fujita, David E. Campbell and Thorunn Snorradottir, Desert Research Institute. Final Report prepared for San Joaquin Valleywide Air Pollution Study Agency under contract 0021-CCOS (2005).

Geron, C.D., A.B. Guenther, and T.E. Pierce, An improved model for estimating emissions of volatile organic compounds from forests in the eastern United States, J. Geophys. Res. **99**(D6), 12773, (1994).

Goldstein, A.H., Impact of Asian emissions on observations at Trinidad Head, California, during ITCT 2K2. J. Geophys. Res. **109**, D23S17, (2004). doi:10.1029/2003JD004406

Goldstein, A.H., S.C. Wofsy, and C.M. Spivakovsky, Seasonal variations of non-methane hydrocarbons in rural New England: Constraints on OH concentrations in northern latitudes. J. Geophys. Res. **100**, D10, 21023-21033 (1995).

Grell, G.A., J. Dudhia and D.R. Stauffer, A description of the fifth-generation Penn State/NCAR mesoscale model (MM5). NCAR Technical Note, NCAR/TN-398+STR, 122 pp., NCAR, Boulder, CO (1994).

Guenther, A. et al., A global model of natural volatile organic compound emissions. J. Geophys. Res. **100**(D5), 8873-8892 (1995).

Guenther, A. et al., Estimates of global terrestrial isoprene emissions using MEGAN (Model of Emissions of Gases and Aerosols from Nature. Atmos. Chem. Phys. Discuss. **6**, 107-173 (2006).

Harley, R.A., S.N. Giddings, L.C. Marr, Decadal Trends in Air Pollutant Emissions from Motor Vehicles in Central California. Department of Civil and Environmental Engineering, University of California, Berkeley, CA. Final Report under contract 00-14CCOS to the San Joaquin Valleywide Air Pollution Study Agency and the California Air Resources Board. (2004).

Harley, R.A., L.C. Marr, J.K. Lehner, and Giddings, S.N., Changes in Motor Vehicle Emissions on Diurnal to Decadal Time Scales and Effects on Atmospheric Composition. Environ. Sci. Technol. **39**, 5356-5362, (2005).

Jacobson, M.Z., Fundamentals of Atmospheric Modeling, Section 8.6. Cambridge University Press, (1999).

Lehrman, D., B. Knuth, and D. Fairley, Characterization of the CCOS 2000 Measurement Period. Interim Report under contract 01-2CCOS to the San Joaquin Valleywide Air Pollution Study Agency and the California Air Resources Board. (2001).

Loomis, C., Development of Stack Parameters and Vertical Distributions for Modeling Large Wildfires in the CCOS Domain. Alpine Geophysics Inc., (2003).

Nikolov, N.T., 1-km resolution database of vegetation leaf area index and canopy clumping factor for the western USA. Final Report, USDA Forest Service Agreement NO. PSW-99-001-RJVA, N&T Services Oak Ridge, TN, (1999).

Nowak, D.J.N. et al., Specific leaf weight factor database, publication in preparation, USDA Forest Service – Northeastern Research Station, Syracuse, NY (2000).

Newchurch, M.J. et al., Vertical distribution of ozone at four sites in the United States. J. Geophys. Res. **108(**D1), 4031, (2003). doi: 10.1029/2002JD002059

Scott, K.I. and M.T. Benjamin, Development of a biogenic volatile organic compound emission inventory for the SCOS97-NARSTO domain. Atmos. Environ. **37**(2), S39-S49, (2003).

Tang, Y. et al., Multiscale simulations of tropospheric chemistry in the eastern Pacific and on the U.S. West Coast during spring 2002. J. Geophys. Res. **109**, D23S11 (2004). doi: 10.1029/2004JD004513

Umeda T. and P.T. Martin, Evaluation of data assimiliation technique for a mesoscale meteorological model used for air quality modeling. J. Applied Meteorol. **41**, 12-29, (2002).

Vuilleumier, L., R.A. Harley, and N.J. Brown, First- and Second-Order Sensitivity Analysis of a Photochemically Reactive System (a Green's Function Approach). Environ. Sci. Technol. **31**, 1206-1217 (1997).

Wesely M.L. and B.B. Hicks, A review of the current status of knowledge on dry deposition. Atmos. Environ. **34**(12-14): 2261-2282 (2000).

Appendix A: Analysis Tools and Emissions Processing Software

TCL Interface for Pave Scripting (TIPS)

TIPS is a TCL-based (Tool Control Language) front end to automate and improve the interface of EPA's PAVE analysis utility. This greatly reduces the work and syntax used in running PAVE in script form, which can be a little cumbersome. TIPS makes it simple to look at vertical-layer dependent properties and to focus analysis on pre-defined geographical sub-domains of the output concentration grid file. It has been tested on Red Hat and Centos Linux systems, and can be ported to most OS's since TCL is portable. The only limitation is the availability of PAVE on the desired OS. TIPS is available for download: http://eetd.lbl.gov/AQ/stonse/cmaq/

Physics Analysis Workstation (PAW)

We have chosen to use the PAW software package for post-processing and analysis of CMAQ data. PAW is open-source (and free) software written and maintained at CERN, the European high-energy physics laboratory in Geneva. It has a large user-community. PAW has a powerful, easy, intuitive command line interface allowing plotting and mathematical operations on multiple variables with conditional tests on other variables. Commands can also be concatenated and run automatically as scripts. There is a built-in Fortran interpreter for more complicated tasks. A new user can perform useful tasks in about a day. We find that PAW's better data interrogation capability nicely complements PAVE's (the EPA's graphics and analysis tool) better graphics.

See: http://eetd.lbl.gov/AQ/stonse/paw/ for an introduction, a primer, documentation and downloading information. An application of CMAQ output analysis with PAW in which we look at weekend-weekday ozone differences in the east bay region of the SF Bay area, was presented at the 4th Annual CMAS Conference in Chapel Hill, NC in September with a focus on the use of PAW. http://www.cmascenter.org/html/2005_conference/ppt/6_5.pdf
and http://www.cmascenter.org/html/2005_conference/abstracts/6_5.pdf
The Carolina Environmental Program has expressed interest in PAW as an analysis tool, and are linking to our PAW web page at http://eetd.lbl.gov/AQ/stonse/paw/

IOAPI2AHB

In order to export CMAQ output to PAW or other data analysis software, we have written IOAPI2AHB. IOAPI2AHB is written in Fortran 90 and requires linking only to the IOAPI and Netcdf libraries. IOAPI2AHB is driven by a simple ASCII input file which allows one to select variables from multiple CMAQ input and output files. It consolidates the selected variables by timestep and grid cell coordinates, x,y,z. Thus e.g. a few concentrations, emissions, and temperature are consolidated in this way. For every x,y cell, IOAPI2AHB also performs a layer-weighted column average over z for every variable and indicates that this field is such an average by setting the z index to –1. Similar layer and domain averages are calculated. These averaging capabilities features allow for less congested plotting, while still retaining the capability to quickly check the degree to which an average is representative of the values from which it was constructed. Other features include user-specified limits on x/y/z/timestep range of the output file, PAVE-style alphabetical suffixing of variables, variable name changing, and the option to sum instead of averaging, which is more useful in the case of emissions. For download of a Linux executable and source code: http://eetd.lbl.gov/AQ/stonse/paw/.

Netcdtype12
Seasonal modeling CMAQ input and output files tend to be large, often exceeding the 2Gbyte limit used by normal "type 1" Netcdf files which use 32-bit addressing. This necessitates the use of Netcdf Type 2 format, i.e. 64-bit addressing. Unfortunately PAVE, the graphical analysis tool only supports Netcdf Type 1. Our Fortran 90 software **netcdftype12.f** allows back and forth conversion between the two formats, allowing selection of subsets of timesteps.

Alpine2CMAQ
The Area emission inputs were obtained from CARB, in the CAMx gridded emission file format (described in the CAMx 4.00 Users Guide). Emissions are at ground level, speciated into SAPRC99, spatially allocated to the 190 × 190 4km resolution grid, and temporally resolved to 1 hour. They are day-of-week specific, with differences between weekdays (Monday-Friday) and weekends (Saturday,Sunday). The software program Alpine2cmaq, was written in Fortran 90 to read and convert the files to CMAQ's IOAPI format. Simultaneously, chemical species variables not compatible by the Models-3 SAPRC99 mechanism were either removed or translated.

Laypoint
The Point source emission inputs were obtained from CARB, in the UAM-4 emission file format, useful for describing spatially sparse 3D emission data. Each source is described by location, stack parameters (diameter, height, exit temperature, exit velocity) and hourly emission of pollutant, speciated into SAPRC99. Emissions are day-of-week specific. Smoke 2.1, the EPA's emissions processing package emissions processor was installed at LBNL. We extracted LAYPOINT, the plume-rise algorithm, from Smoke 2.1, and wrote input and output modules for it. The resultant program (in Fortran 90) first performs simple QA, checking for: (1) missing point sources (2) time–ordering of entries (3) missing chemical species (4) reasonable daily total emission values, and then passes the data to LAYPOINT for a plume-rise calculation. LAYPOINT estimates the plume rise, using the temperatures and winds from the meteorological input files. The plume is then allocated to the appropriate vertical layers, and a 3D IOAPI file is created as output in which emissions are spatially allocated to the 4 km resolution grid, and temporally resolved to 1 hour.

Emis_Merge
The software program Emis_Merge was written in Fortran 90, to merge emissions from the five categories and produce an input file for a 15-day CMAQ simulation, stretching from July 24, 2000 to August 8, 2000.

Appendix B: MM5 to CMAQ Mapping of Vertical Layer Structure

MM5 Layer	Top ht (m)	CMAQ Layer
1	20.1	1
2	42.3	2
3	65.8	3
4	90.8	4
5	117	5
6	146	6
7	177	7
8	209	8
9	245	
10	283	9
11	323	
12	366	
13	413	10
14	461	
15	511	11
16	563	
17	618	12
18	674	
19	734	13
20	795	
21	859	14
22	926	
23	996	
24	1068	15
25	1143	
26	1227	
27	1321	16
28	1425	
29	1540	17
30	1669	
31	1812	18
32	1973	
33	2151	19
34	2349	
35	2571	
36	2818	
37	3095	20

38	3418	
39	3798	
40	4242	21
41	4763	
42	5379	
43	6106	22
44	6969	
45	7998	23
46	9233	
47	10920	24
48	12706	25
49	14613	26
50	16668	27

Appendix C: Ozone Time Series Plots

This appendix includes 15-day time series plots for the period July 24 through August 8, 2000 (Julian days 206 to 221). Sundays are flagged on the time axis using red text. Two sets of model predictions are shown: a base case, and an alternate case with cleaner boundary conditions. Observed ozone concentrations are plotted in red on the same plots. The two model simulations are usually quite close together, except at coastal sites where predicted ozone levels are lower using the clean BC inputs, leading to better agreement with ozone observations.

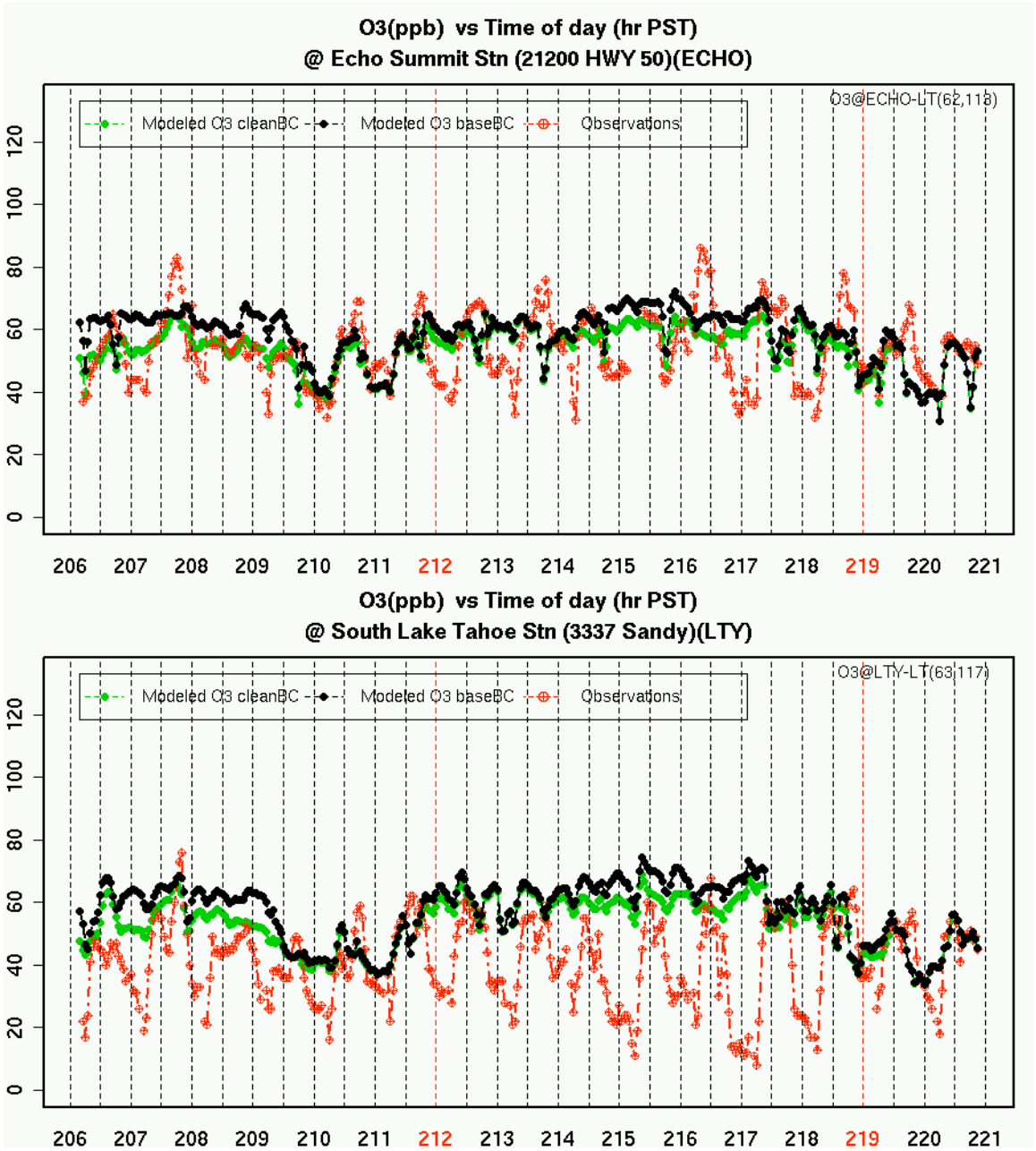
O3(ppb) vs Time of day (hr PST)
@ Echo Summit Stn (21200 HWY 50)(ECHO)
O3@ECHO-LT(62,118)
Modeled O3 cleanBC
Modeled O3 baseBC
Observations
0
20
40
60
80
100
120
206
207
208
209
210
211
212
213
214
215
216
217
218
219
220
221
O3(ppb) vs Time of day (hr PST)
@ South Lake Tahoe Stn (3337 Sandy)(LTY)
O3@LTY-LT(63,117)
Modeled O3 cleanBC
Modeled O3 baseBC
Observations
0
20
40
60
80
100
120
206
207
208
209
210
211
212
213
214
215
216
217
218
219
220
221

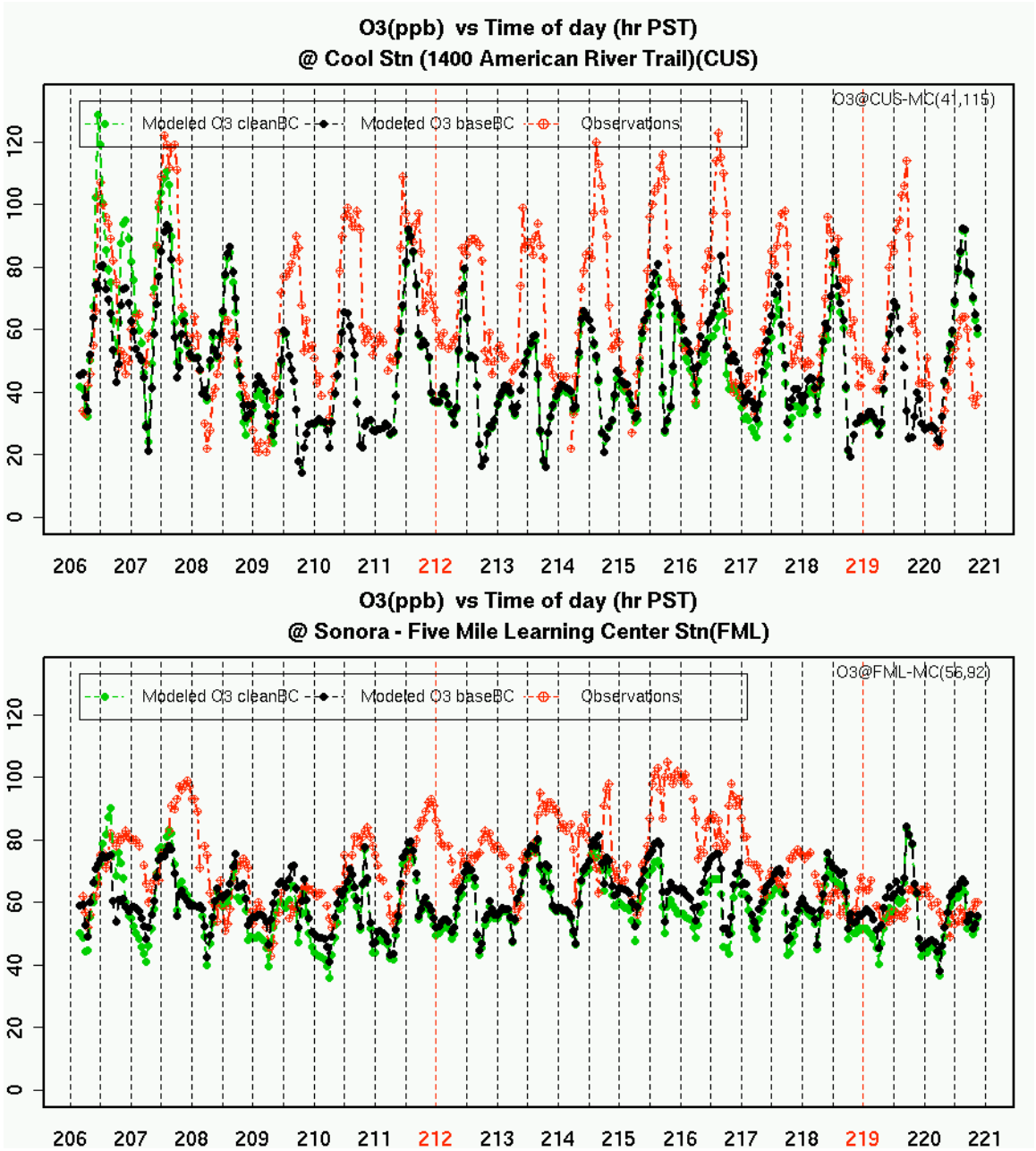
O3(ppb) vs Time of day (hr PST)
@ Cool Stn (1400 American River Trail)(CUS)
O3@CUS-MC(41,115)
Modeled O3 cleanBC
Modeled O3 baseBC
Observations
0
20
40
60
80
100
120
206
207
208
209
210
211
212
213
214
215
216
217
218
219
220
221
O3(ppb) vs Time of day (hr PST)
@ Sonora - Five Mile Learning Center Stn(FML)
O3@FML-MC(56,92)
Modeled O3 cleanBC
Modeled O3 baseBC
Observations
0
20
40
60
80
100
120
206
207
208
209
210
211
212
213
214
215
216
217
218
219
220
221

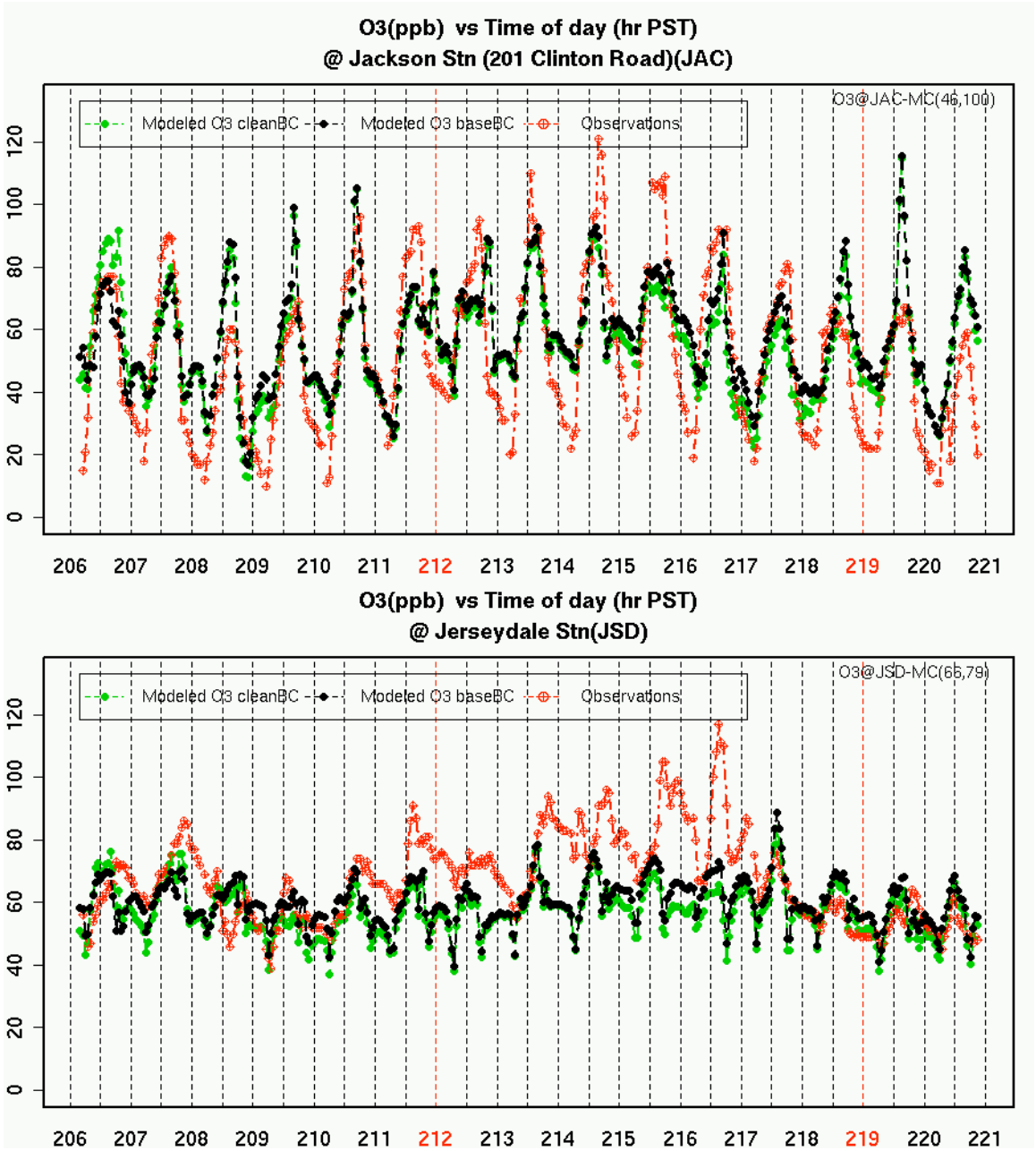
O3(ppb) vs Time of day (hr PST)
@ Jackson Stn (201 Clinton Road)(JAC)
O3@JAC-MC(46,100)
Modeled O3 cleanBC
Modeled O3 baseBC
Observations
0
20
40
60
80
100
120
206
207
208
209
210
211
212
213
214
215
216
217
218
219
220
221
O3(ppb) vs Time of day (hr PST)
@ Jerseydale Stn(JSD)
O3@JSD-MC(66,79)
Modeled O3 cleanBC
Modeled O3 baseBC
Observations
0
20
40
60
80
100
120
206
207
208
209
210
211
212
213
214
215
216
217
218
219
220
221

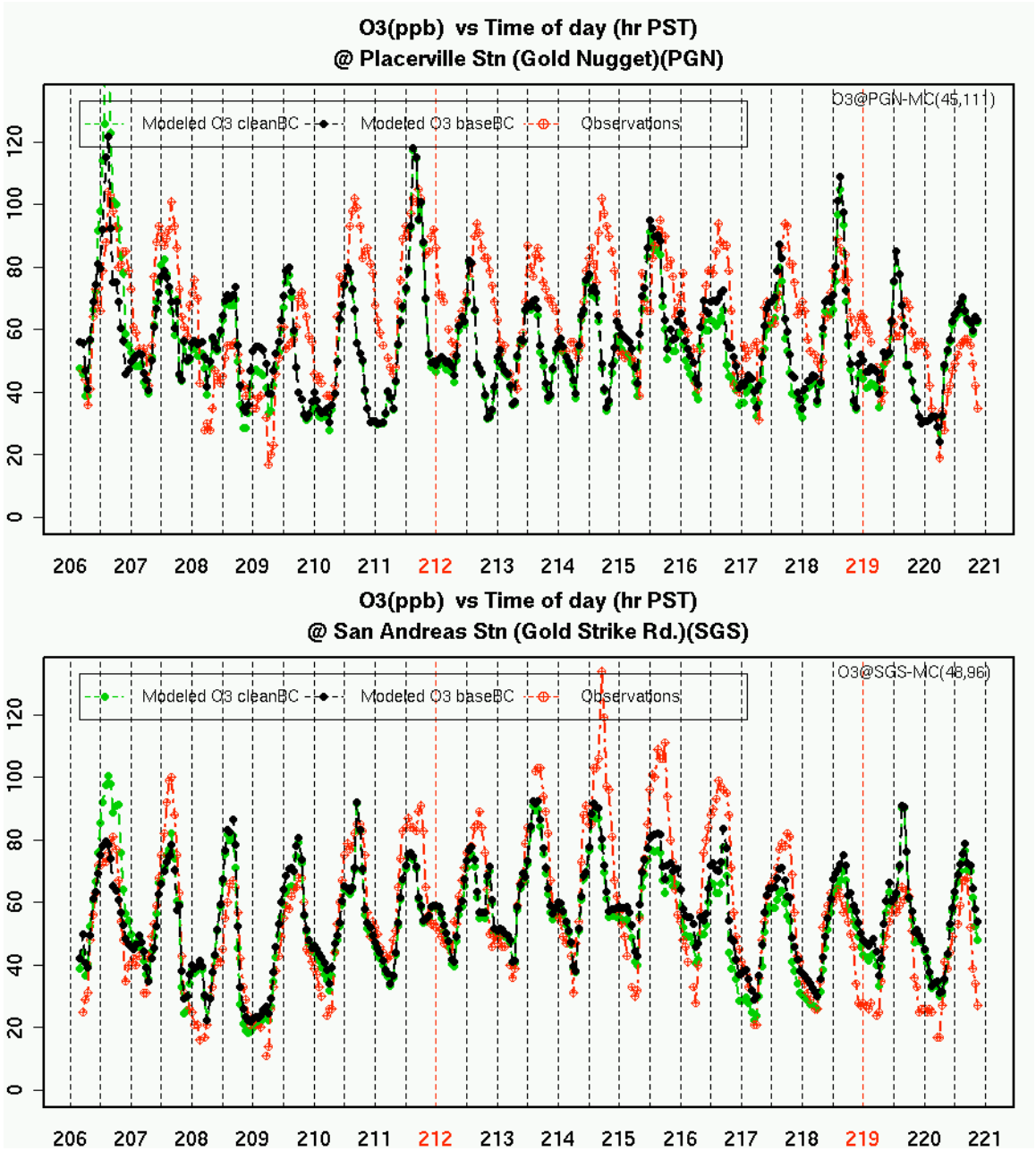
O3(ppb) vs Time of day (hr PST)
@ Placerville Stn (Gold Nugget)(PGN)
O3@PGN-MC(45,111)
Modeled O3 cleanBC
Modeled O3 baseBC
Observations
0
20
40
60
80
100
120
206
207
208
209
210
211
212
213
214
215
216
217
218
219
220
221
O3(ppb) vs Time of day (hr PST)
@ San Andreas Stn (Gold Strike Rd.)(SGS)
O3@SGS-MC(48,96)
Modeled O3 cleanBC
Modeled O3 baseBC
Observations
0
20
40
60
80
100
120
206
207
208
209
210
211
212
213
214
215
216
217
218
219
220
221

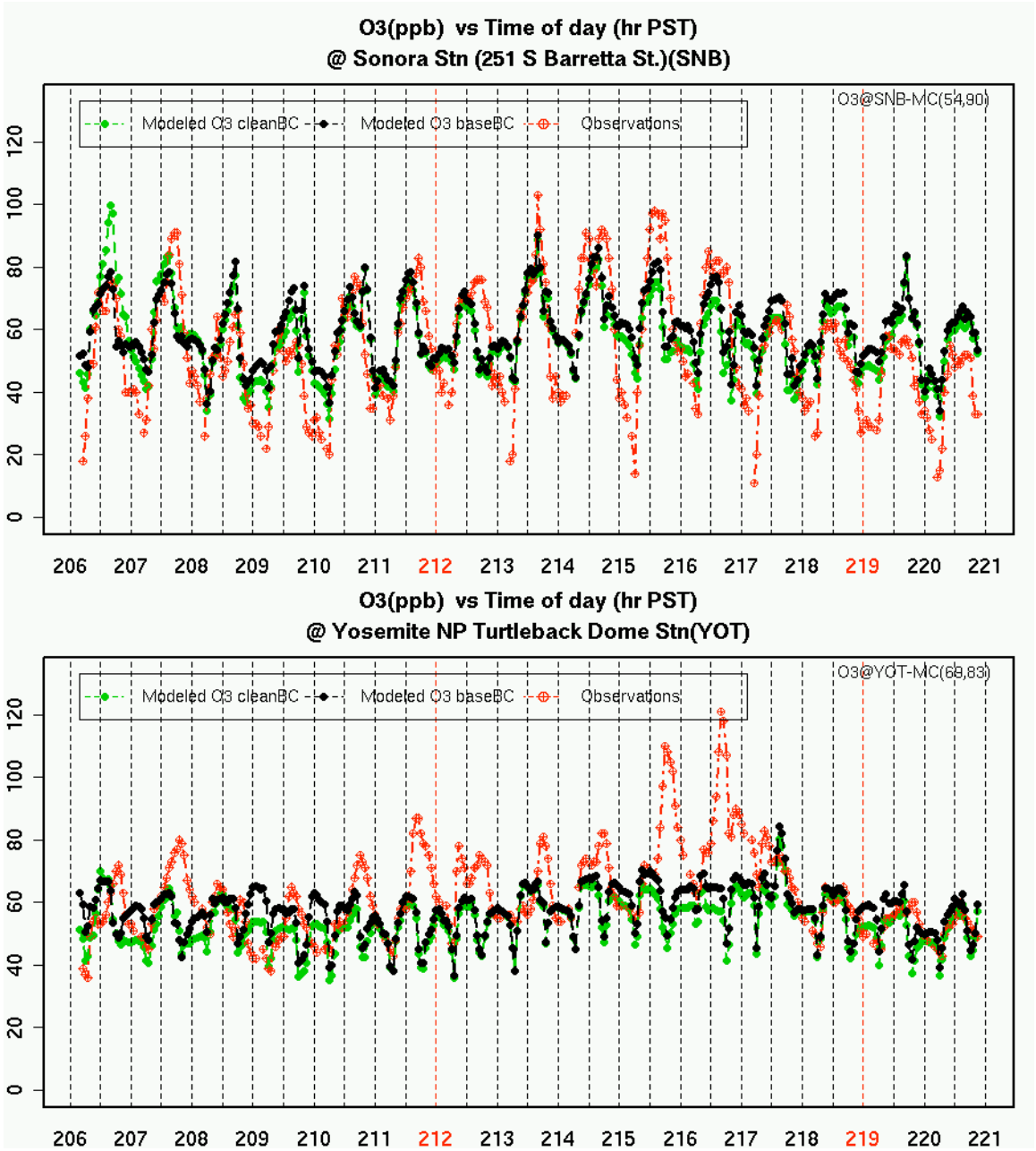
O3(ppb) vs Time of day (hr PST)
@ Sonora Stn (251 S Barretta St.)(SNB)
O3@SNB-MC(54,90)
Modeled O3 cleanBC
Modeled O3 baseBC
Observations
0
20
40
60
80
100
120
206
207
208
209
210
211
212
213
214
215
216
217
218
219
220
221
O3(ppb) vs Time of day (hr PST)
@ Yosemite NP Turtleback Dome Stn(YOT)
O3@YOT-MC(68,83)
Modeled O3 cleanBC
Modeled O3 baseBC
Observations
0
20
40
60
80
100
120
206
207
208
209
210
211
212
213
214
215
216
217
218
219
220
221

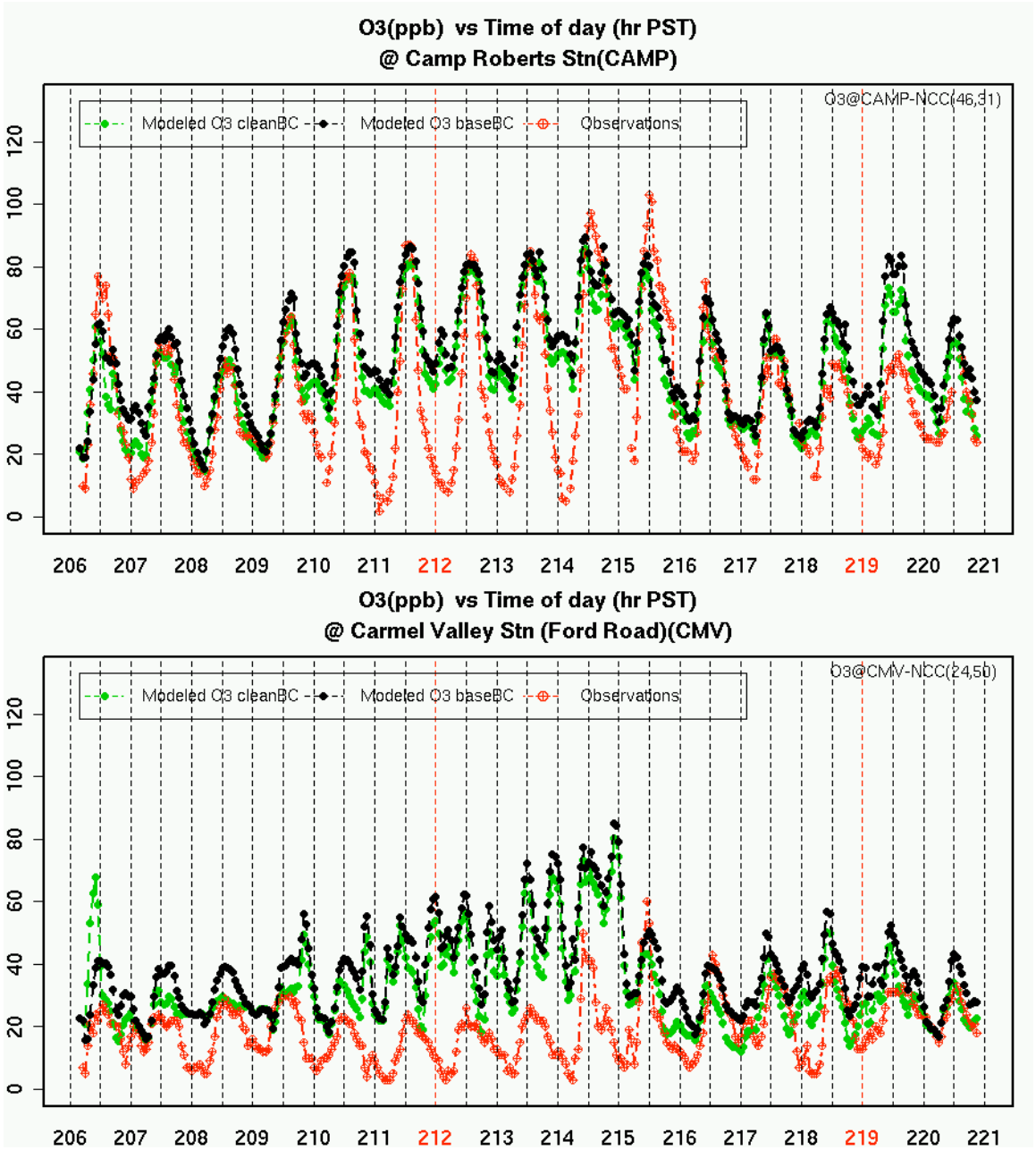
O3(ppb) vs Time of day (hr PST)
@ Camp Roberts Stn(CAMP)
O3@CAMP-NCC(46,31)
Modeled O3 cleanBC
Modeled O3 baseBC
Observations
0
20
40
60
80
100
120
206
207
208
209
210
211
212
213
214
215
216
217
218
219
220
221
O3(ppb) vs Time of day (hr PST)
@ Carmel Valley Stn (Ford Road)(CMV)
O3@CMV-NCC(24,50)
Modeled O3 cleanBC
Modeled O3 baseBC
Observations
0
20
40
60
80
100
120
206
207
208
209
210
211
212
213
214
215
216
217
218
219
220
221

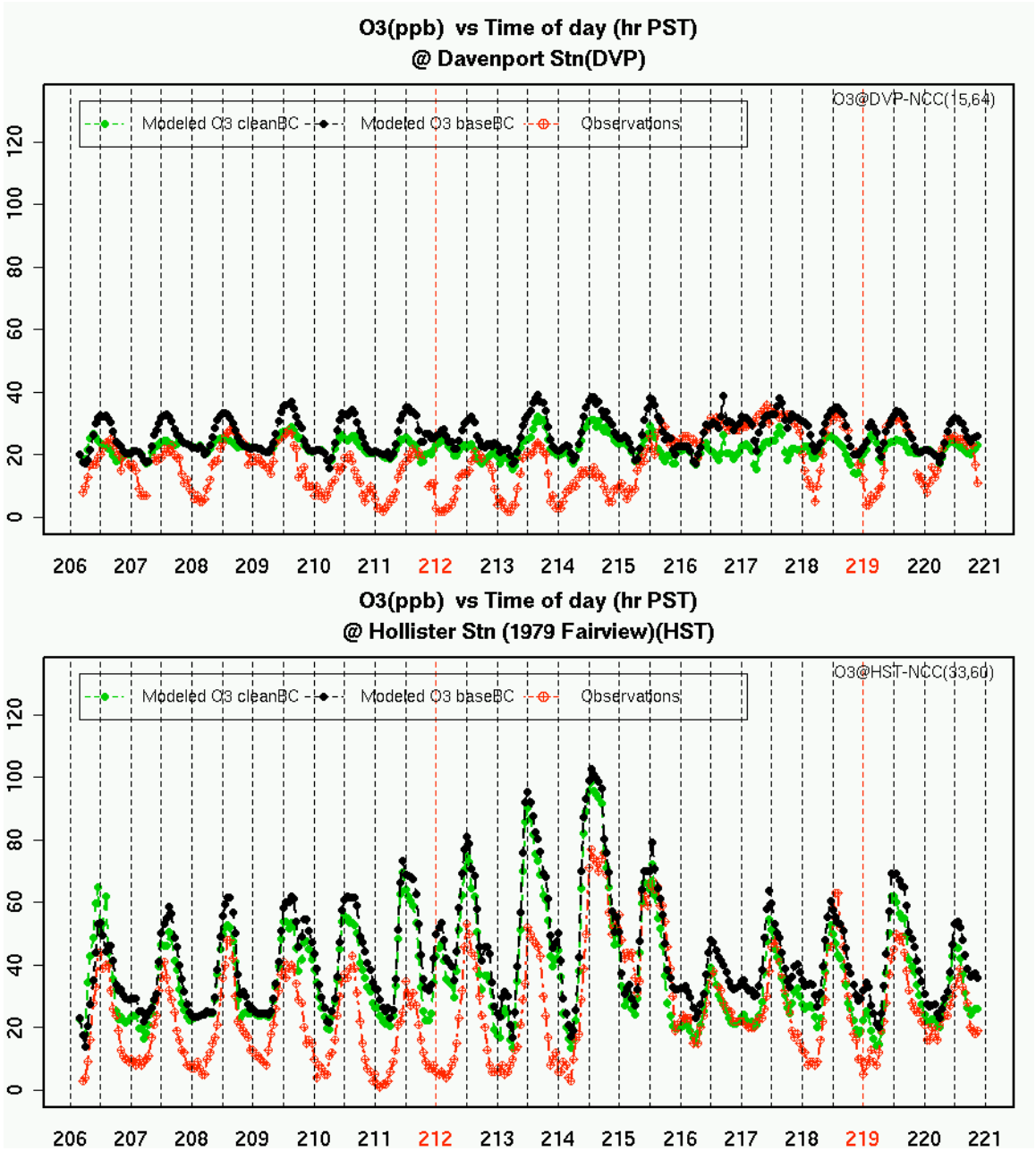
O3(ppb) vs Time of day (hr PST)
@ Davenport Stn(DVP)
O3@DVP-NCC(15,64)
Modeled O3 cleanBC
Modeled O3 baseBC
Observations
0
20
40
60
80
100
120
206
207
208
209
210
211
212
213
214
215
216
217
218
219
220
221
O3(ppb) vs Time of day (hr PST)
@ Hollister Stn (1979 Fairview)(HST)
O3@HST-NCC(33,60)
Modeled O3 cleanBC
Modeled O3 baseBC
Observations
0
20
40
60
80
100
120
206
207
208
209
210
211
212
213
214
215
216
217
218
219
220
221

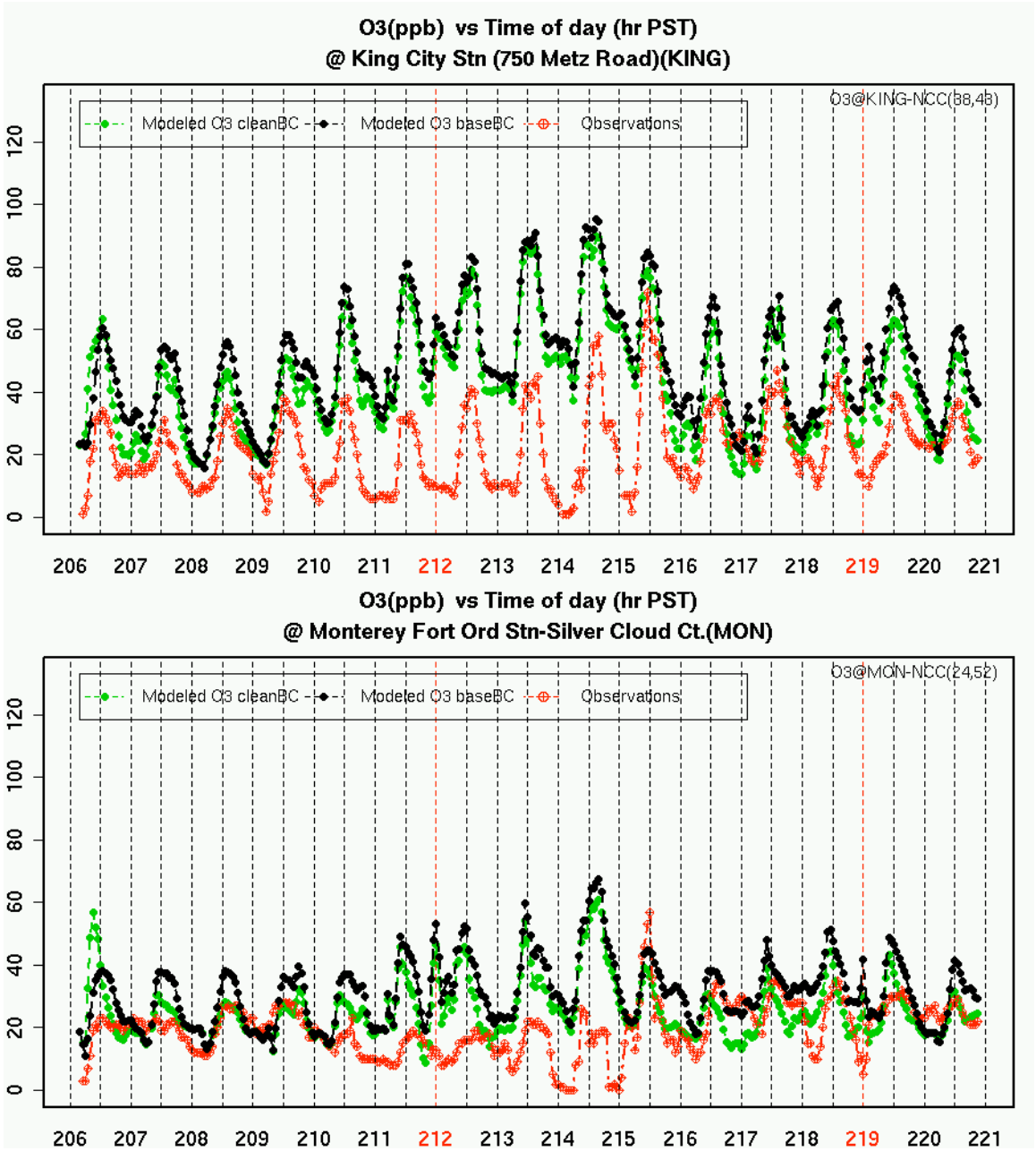
O3(ppb) vs Time of day (hr PST)
@ King City Stn (750 Metz Road)(KING)
O3@KING-NCC(38,48)
Modeled O3 cleanBC
Modeled O3 baseBC
Observations
0
20
40
60
80
100
120
206
207
208
209
210
211
212
213
214
215
216
217
218
219
220
221
O3(ppb) vs Time of day (hr PST)
@ Monterey Fort Ord Stn-Silver Cloud Ct.(MON)
O3@MON-NCC(24,52)
Modeled O3 cleanBC
Modeled O3 baseBC
Observations
0
20
40
60
80
100
120
206
207
208
209
210
211
212
213
214
215
216
217
218
219
220
221

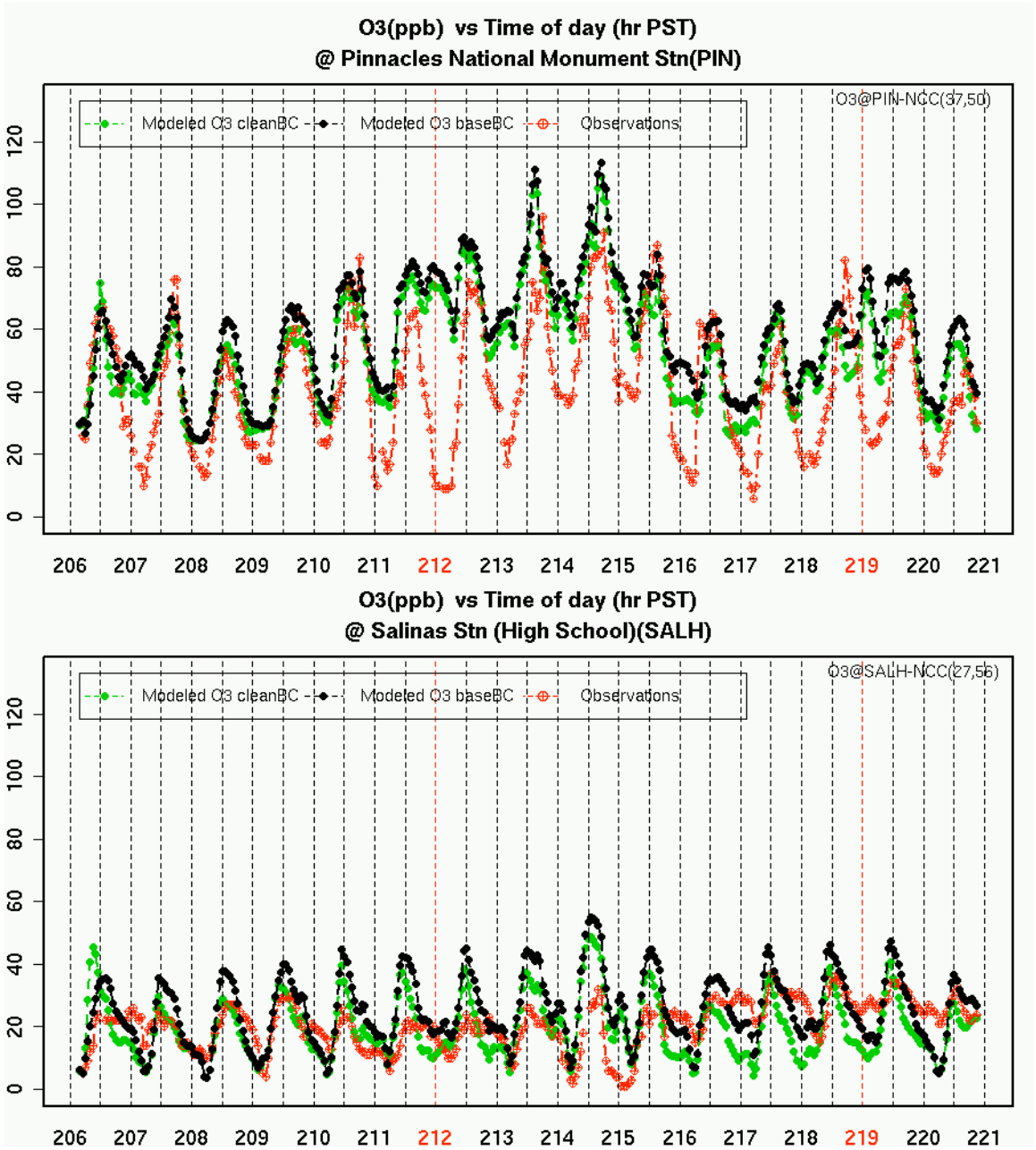
O3(ppb) vs Time of day (hr PST)
@ Pinnacles National Monument Stn(PIN)
O3@PIN-NCC(37,50)
Modeled O3 cleanBC
Modeled O3 baseBC
Observations
0
20
40
60
80
100
120
206
207
208
209
210
211
212
213
214
215
216
217
218
219
220
221
O3(ppb) vs Time of day (hr PST)
@ Salinas Stn (High School)(SALH)
O3@SALH-NCC(27,56)
Modeled O3 cleanBC
Modeled O3 baseBC
Observations
0
20
40
60
80
100
120
206
207
208
209
210
211
212
213
214
215
216
217
218
219
220
221

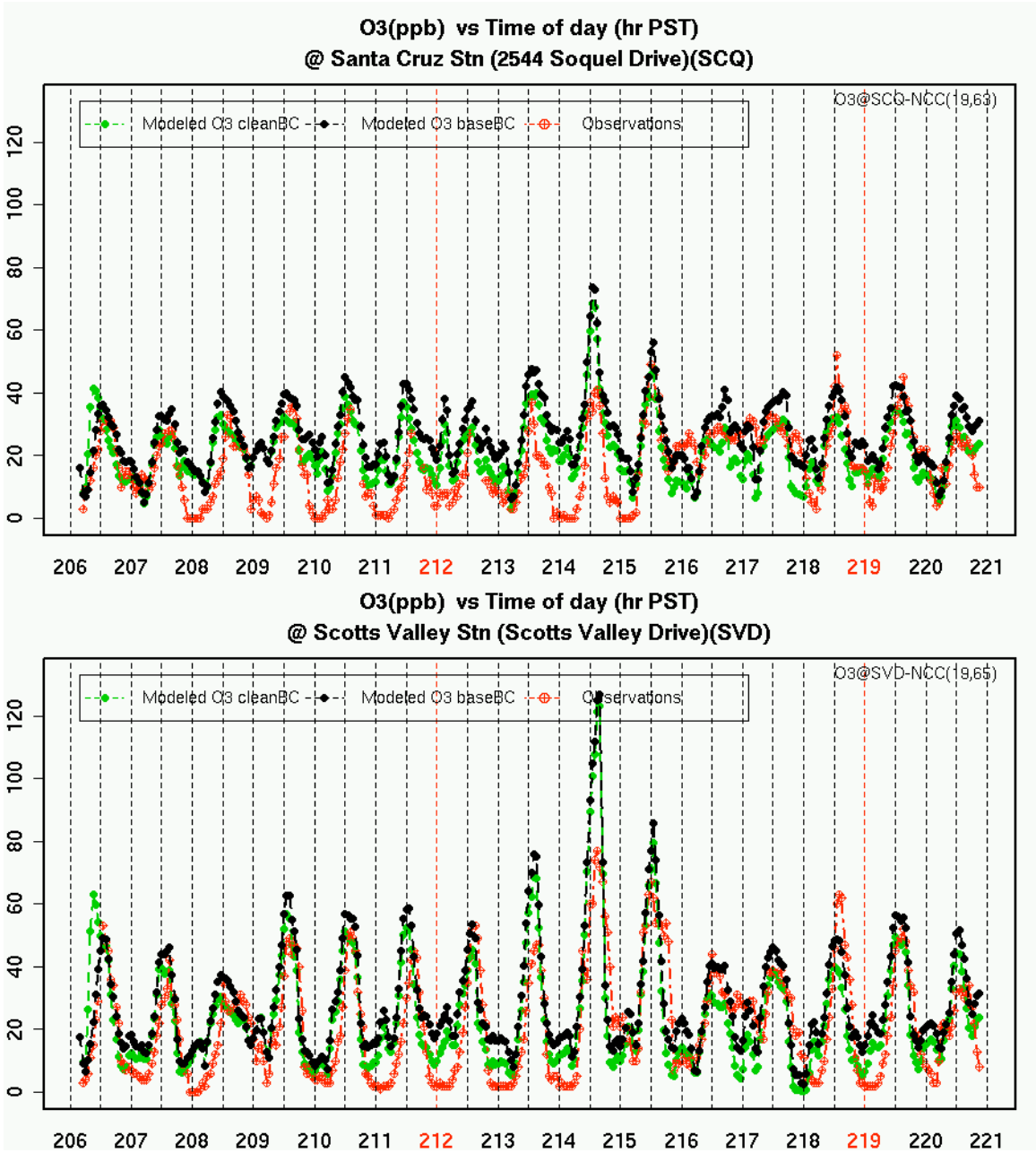
O3(ppb) vs Time of day (hr PST)
@ Santa Cruz Stn (2544 Soquel Drive)(SCQ)
O3@SCQ-NCC(19,63)
Modeled O3 cleanBC
Modeled O3 baseBC
Observations
0
20
40
60
80
100
120
206
207
208
209
210
211
212
213
214
215
216
217
218
219
220
221
O3(ppb) vs Time of day (hr PST)
@ Scotts Valley Stn (Scotts Valley Drive)(SVD)
O3@SVD-NCC(19,65)
Modeled O3 cleanBC
Modeled O3 baseBC
Observations
0
20
40
60
80
100
120
206
207
208
209
210
211
212
213
214
215
216
217
218
219
220
221

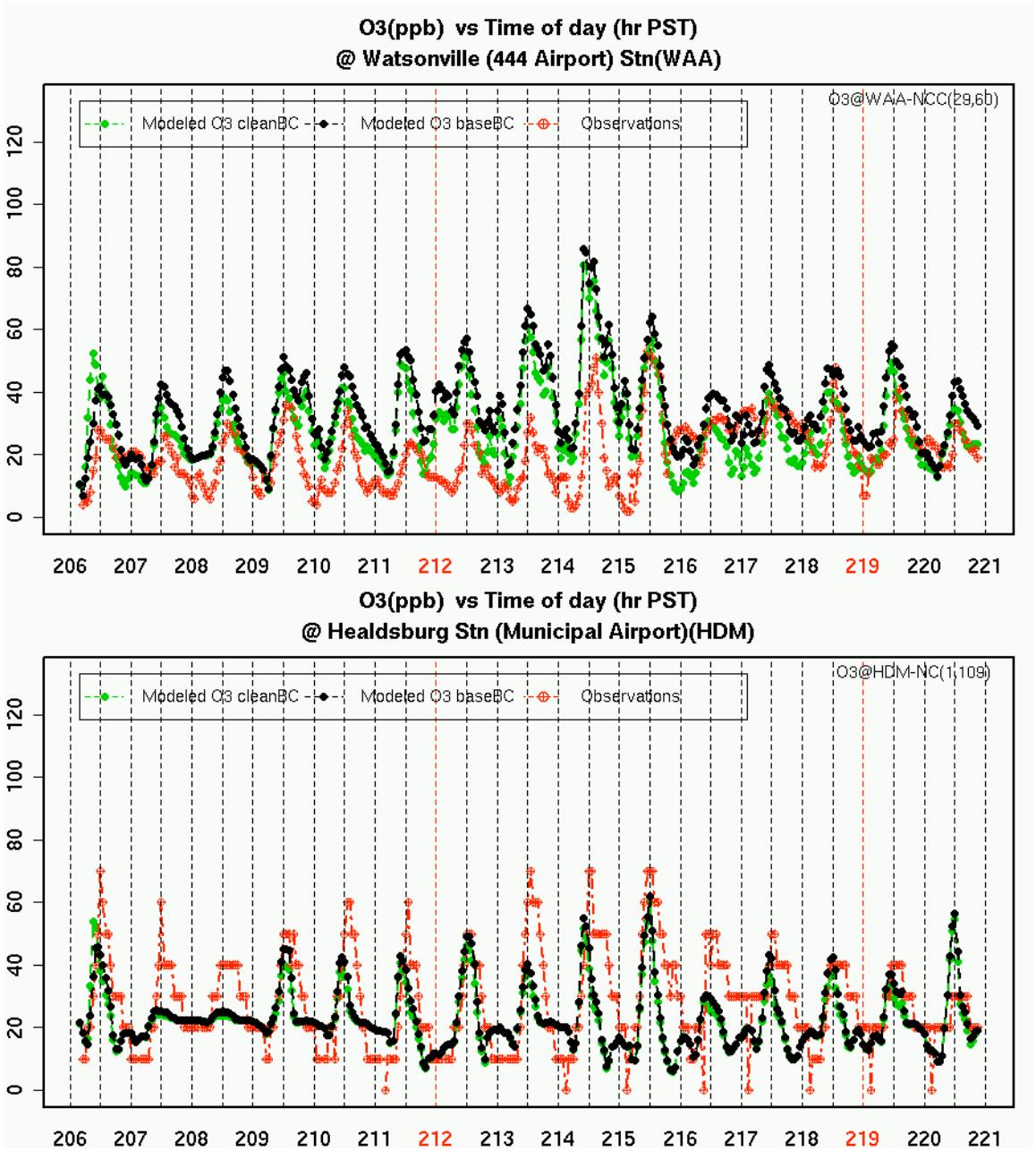
O3(ppb) vs Time of day (hr PST)
@ Watsonville (444 Airport) Stn(WAA)
O3@WAA-NCC(29,60)
Modeled O3 cleanBC
Modeled O3 baseBC
Observations
0
20
40
60
80
100
120
206
207
208
209
210
211
212
213
214
215
216
217
218
219
220
221
O3(ppb) vs Time of day (hr PST)
@ Healdsburg Stn (Municipal Airport)(HDM)
O3@HDM-NC(1,109)
Modeled O3 cleanBC
Modeled O3 baseBC
Observations
0
20
40
60
80
100
120
206
207
208
209
210
211
212
213
214
215
216
217
218
219
220
221

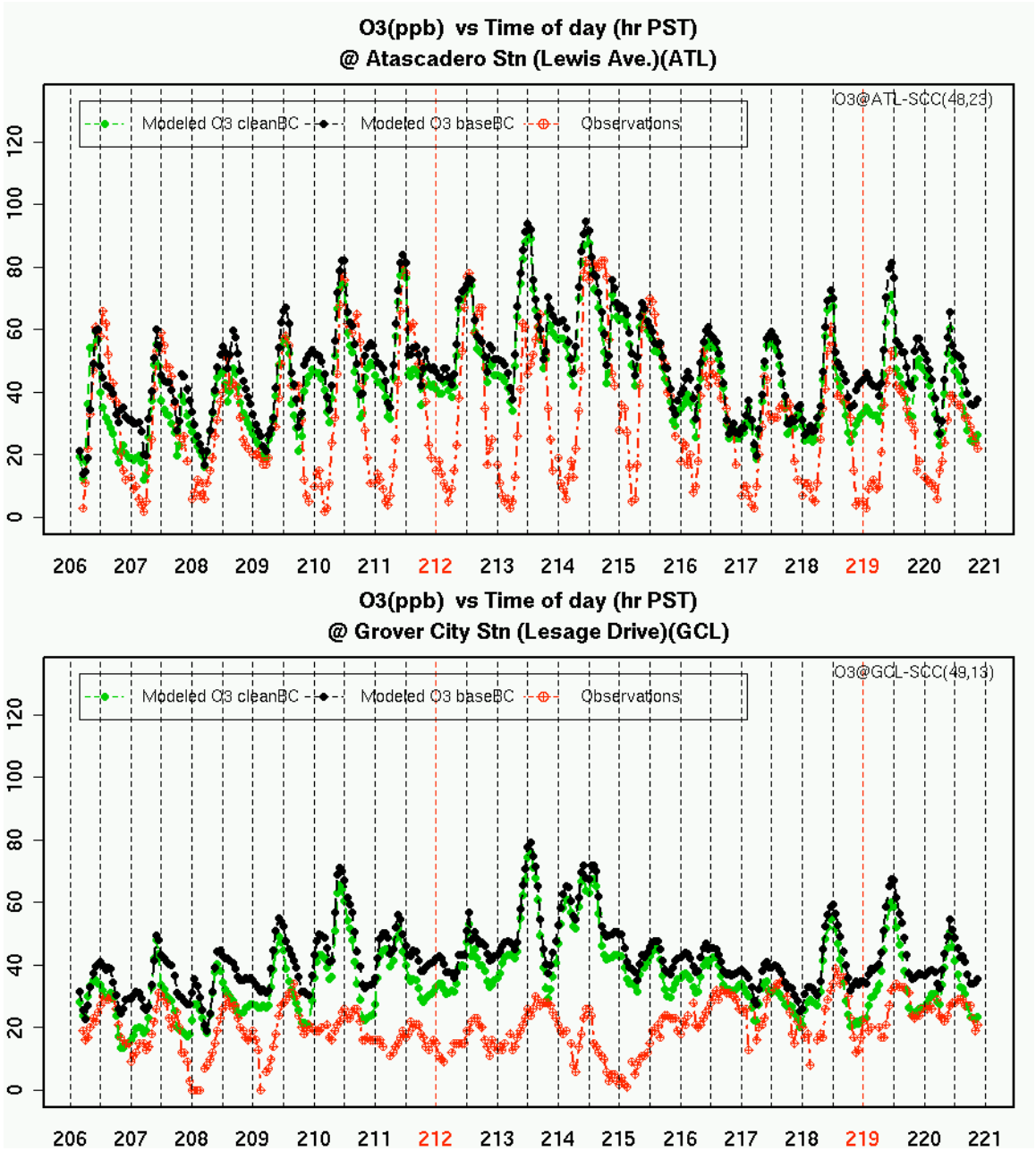
O3(ppb) vs Time of day (hr PST)
@ Atascadero Stn (Lewis Ave.)(ATL)
O3@ATL-SCC(48,23)
Modeled O3 cleanBC
Modeled O3 baseBC
Observations
0
20
40
60
80
100
120
206
207
208
209
210
211
212
213
214
215
216
217
218
219
220
221
O3(ppb) vs Time of day (hr PST)
@ Grover City Stn (Lesage Drive)(GCL)
O3@GCL-SCC(49,13)
Modeled O3 cleanBC
Modeled O3 baseBC
Observations
0
20
40
60
80
100
120
206
207
208
209
210
211
212
213
214
215
216
217
218
219
220
221

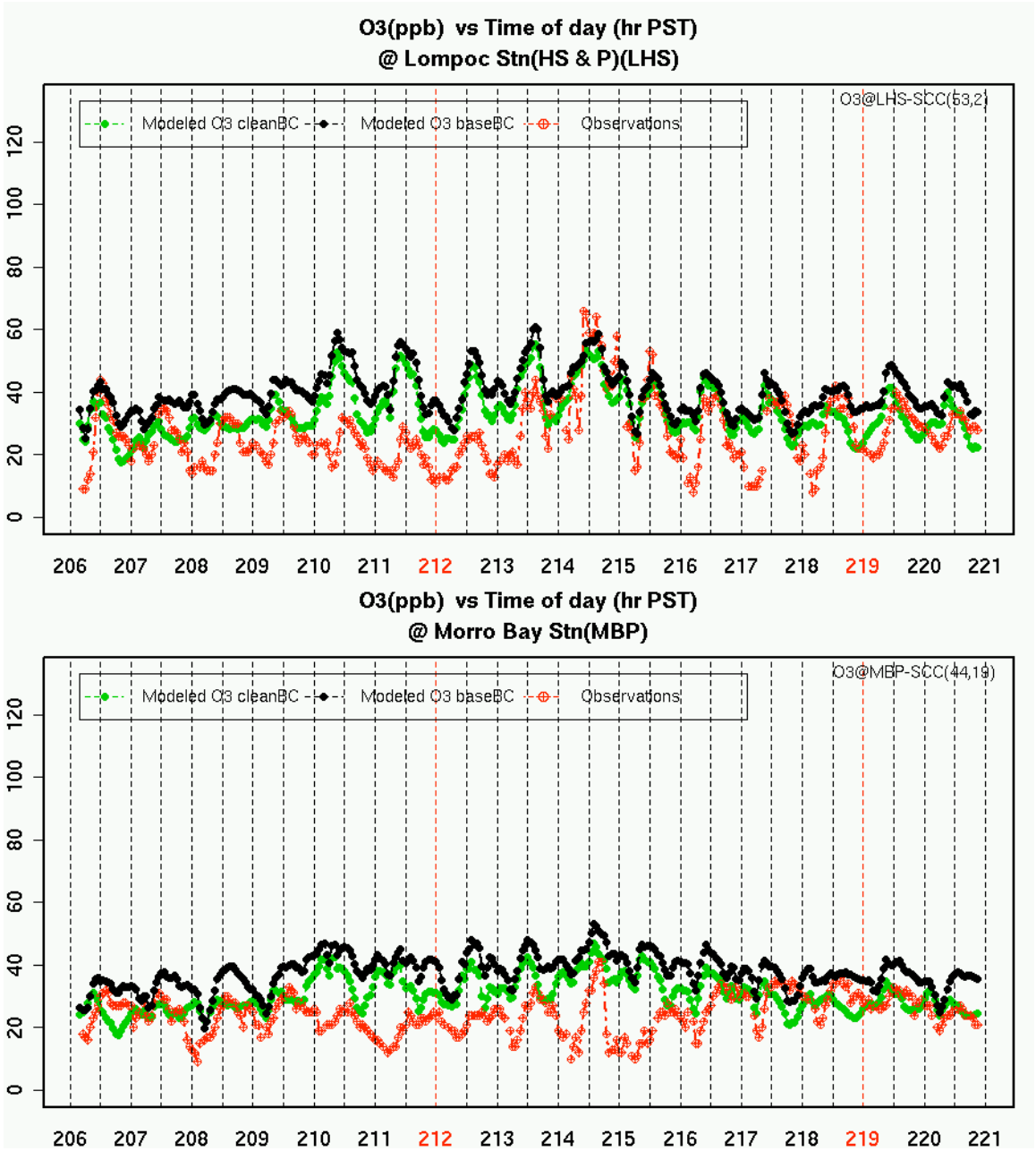
O3(ppb) vs Time of day (hr PST)
@ Lompoc Stn(HS & P)(LHS)
O3@LHS-SCC(53,2)
Modeled O3 cleanBC
Modeled O3 baseBC
Observations
0
20
40
60
80
100
120
206
207
208
209
210
211
212
213
214
215
216
217
218
219
220
221
O3(ppb) vs Time of day (hr PST)
@ Morro Bay Stn(MBP)
O3@MBP-SCC(44,19)
Modeled O3 cleanBC
Modeled O3 baseBC
Observations
0
20
40
60
80
100
120
206
207
208
209
210
211
212
213
214
215
216
217
218
219
220
221

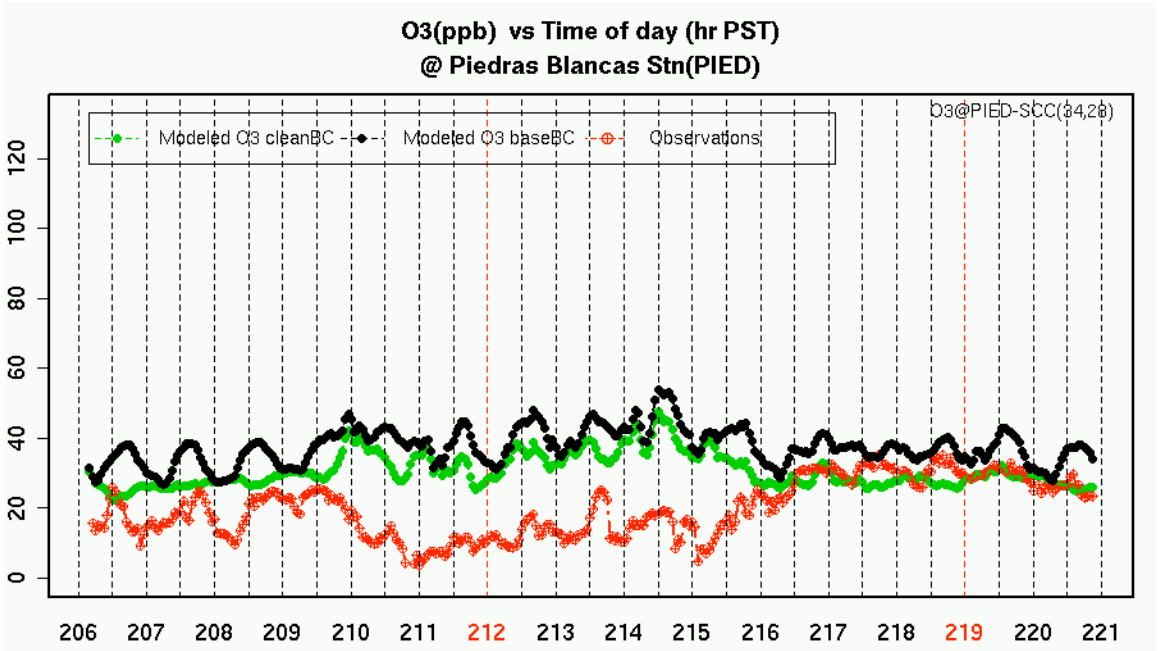
O3(ppb) vs Time of day (hr PST)
@ Piedras Blancas Stn(PIED)
O3@PIED-SCC(34,28)
Modeled O3 cleanBC
Modeled O3 baseBC
Observations
0
20
40
60
80
100
120
206
207
208
209
210
211
212
213
214
215
216
217
218
219
220
221

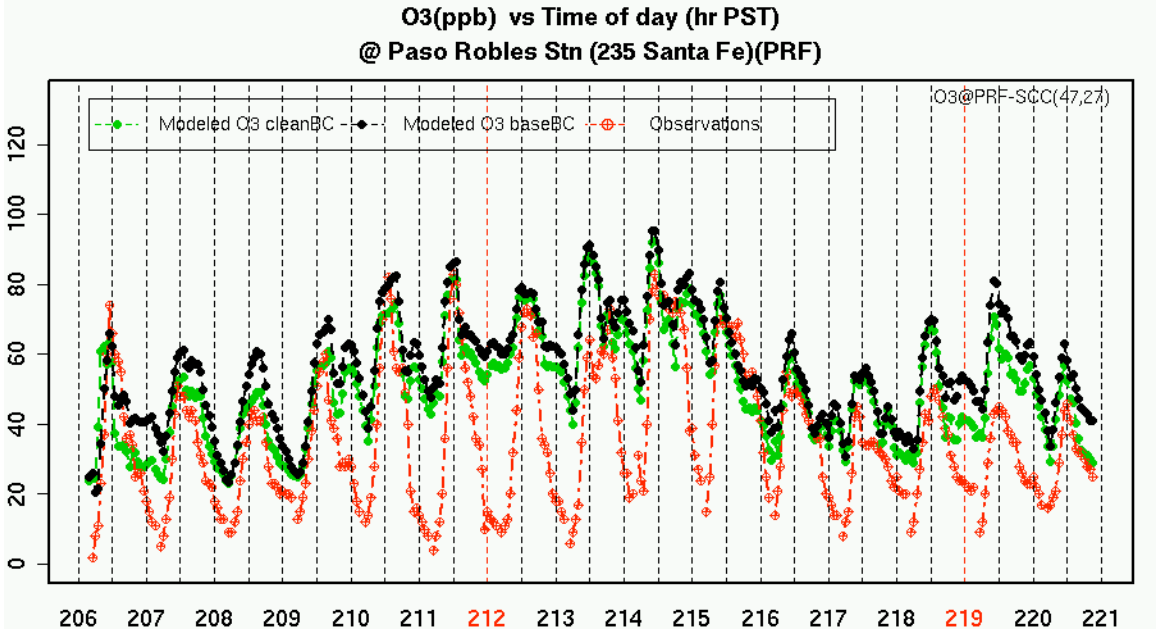
O3(ppb) vs Time of day (hr PST)
@ Paso Robles Stn (235 Santa Fe)(PRF)
O3@PRF-SCC(47,27)
Modeled O3 cleanBC
Modeled O3 baseBC
Observations
0
20
40
60
80
100
120
206
207
208
209
210
211
212
213
214
215
216
217
218
219
220
221

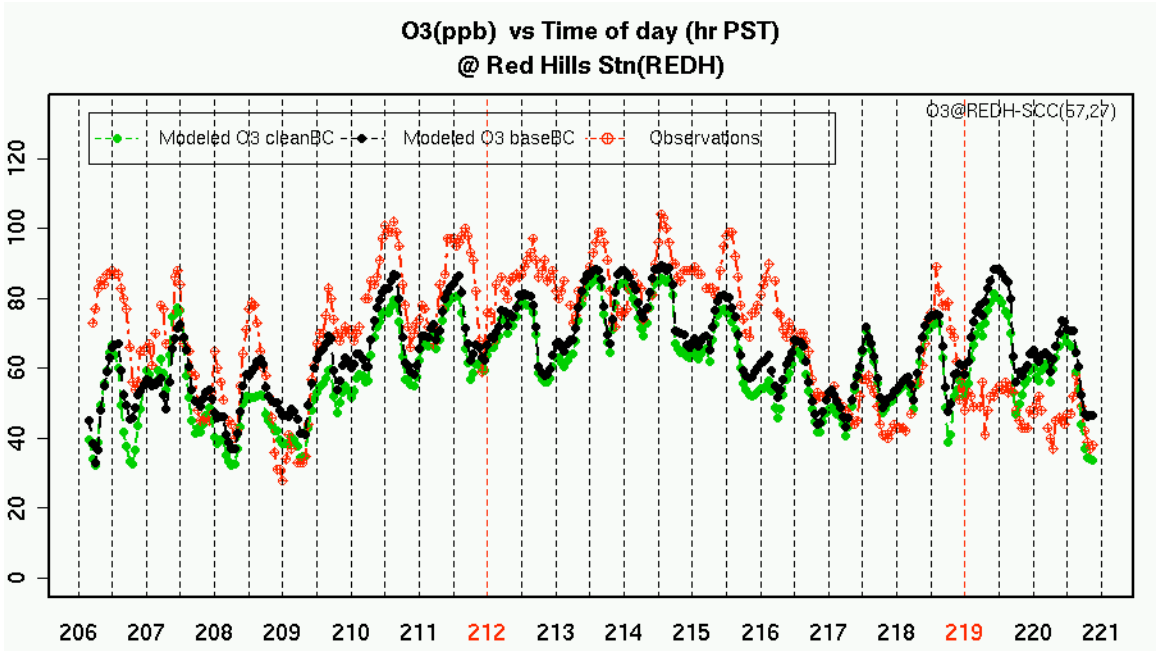
O3(ppb) vs Time of day (hr PST)
@ Red Hills Stn(REDH)
O3@REDH-SCC(57,27)
Modeled O3 cleanBC
Modeled O3 baseBC
Observations
0
20
40
60
80
100
120
206
207
208
209
210
211
212
213
214
215
216
217
218
219
220
221

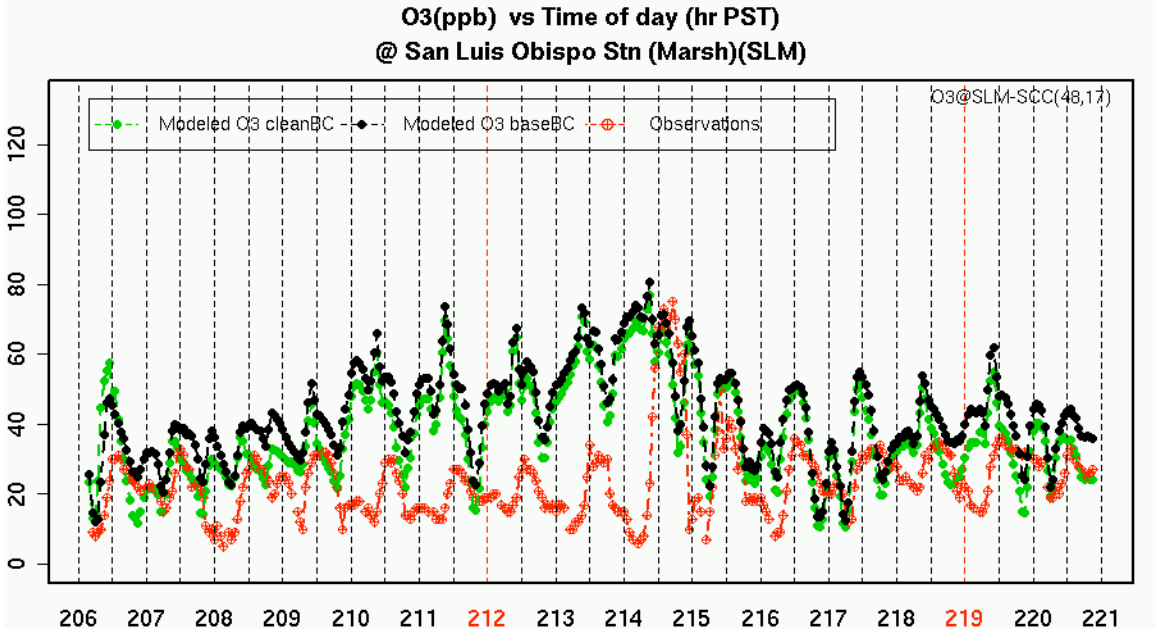
O3(ppb) vs Time of day (hr PST)
@ San Luis Obispo Stn (Marsh)(SLM)
O3@SLM-SCC(48,17)
Modeled O3 cleanBC
Modeled O3 baseBC
Observations
0
20
40
60
80
100
120
206
207
208
209
210
211
212
213
214
215
216
217
218
219
220
221

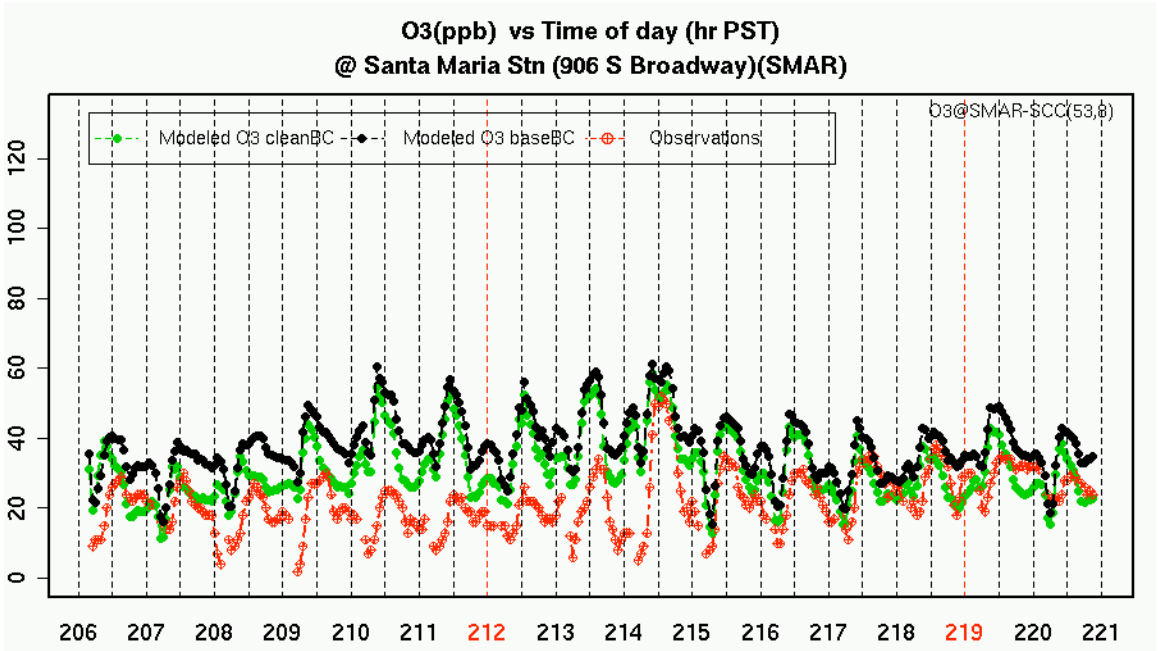
O3(ppb) vs Time of day (hr PST)
@ Santa Maria Stn (906 S Broadway)(SMAR)
O3@SMAR-SCC(53,8)
Modeled O3 cleanBC
Modeled O3 baseBC
Observations
0
20
40
60
80
100
120
206
207
208
209
210
211
212
213
214
215
216
217
218
219
220
221

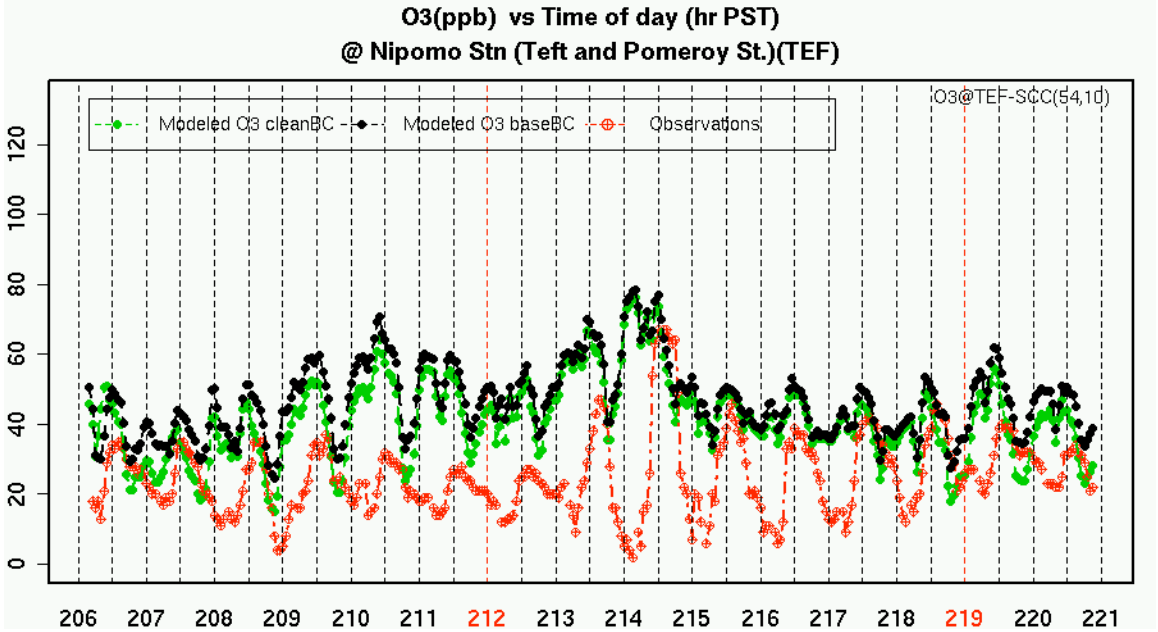
O3(ppb) vs Time of day (hr PST)
@ Nipomo Stn (Teft and Pomeroy St.)(TEF)
O3@TEF-SCC(54,10)
Modeled O3 cleanBC
Modeled O3 baseBC
Observations
0
20
40
60
80
100
120
206
207
208
209
210
211
212
213
214
215
216
217
218
219
220
221

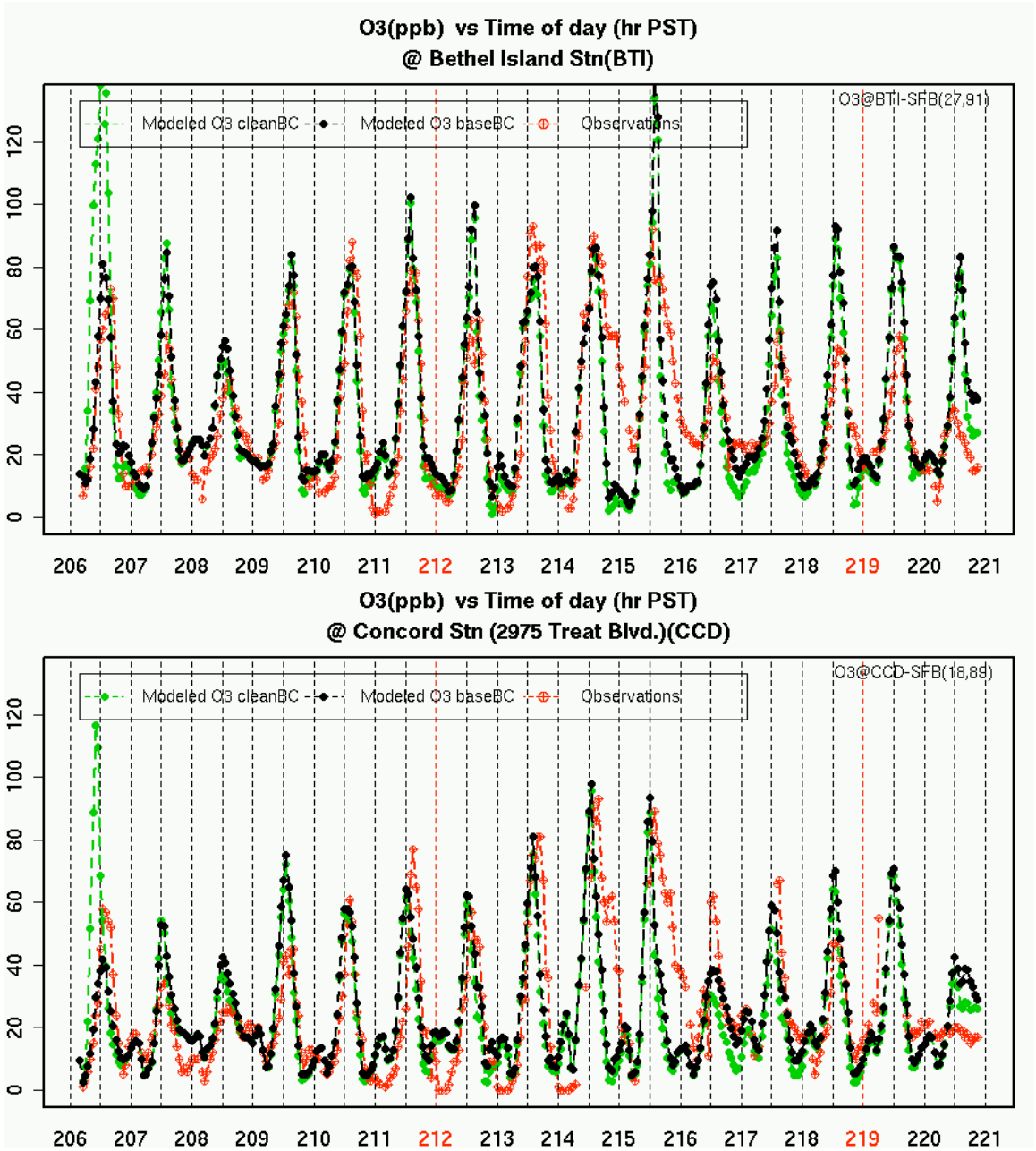
O3(ppb) vs Time of day (hr PST)
@ Bethel Island Stn(BTI)
O3@BTI-SFB(27,91)
Modeled O3 cleanBC
Modeled O3 baseBC
Observations
0
20
40
60
80
100
120
206
207
208
209
210
211
212
213
214
215
216
217
218
219
220
221
O3(ppb) vs Time of day (hr PST)
@ Concord Stn (2975 Treat Blvd.)(CCD)
O3@CCD-SFB(18,89)
Modeled O3 cleanBC
Modeled O3 baseBC
Observations
0
20
40
60
80
100
120
206
207
208
209
210
211
212
213
214
215
216
217
218
219
220
221

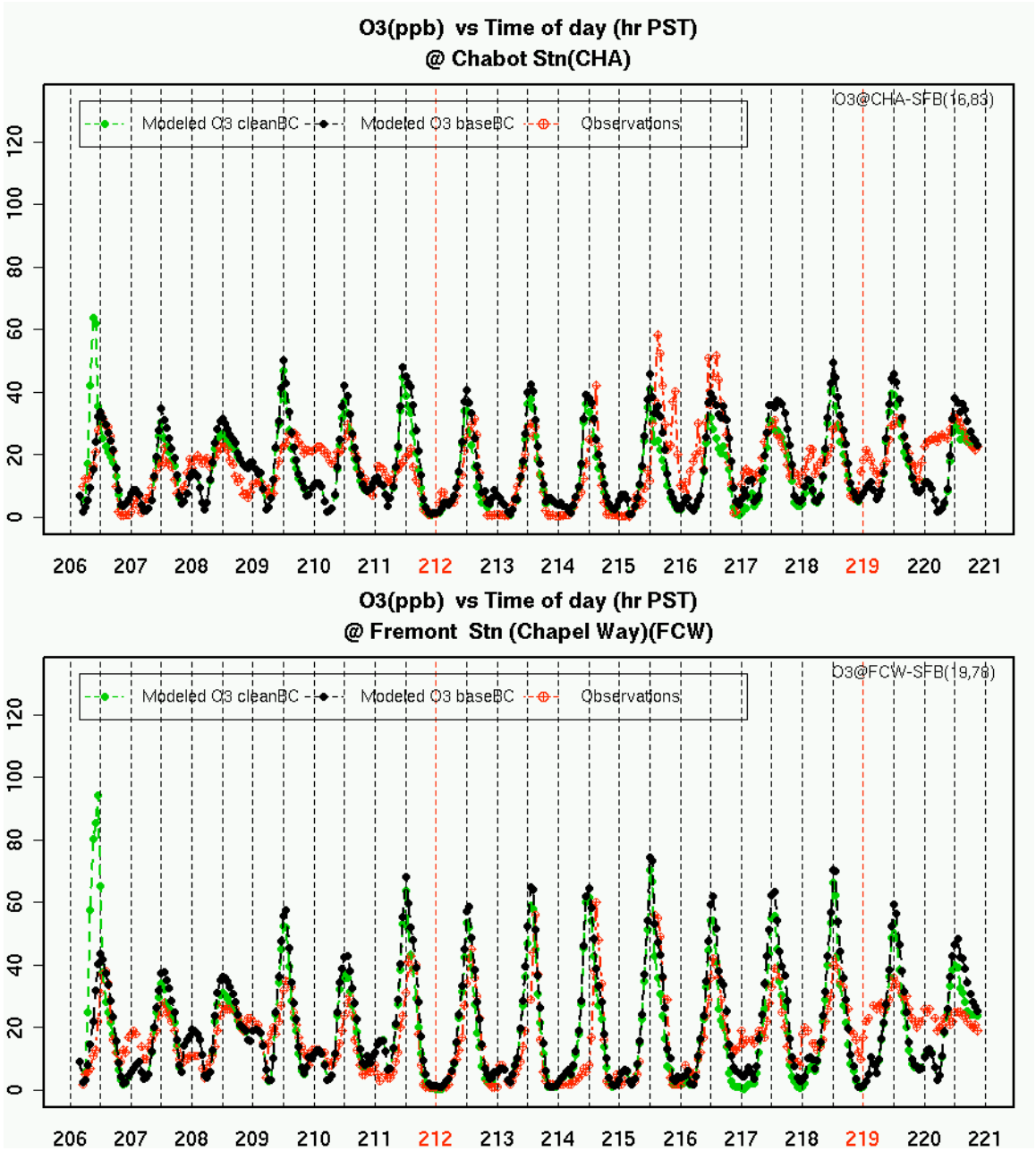
O3(ppb) vs Time of day (hr PST)
@ Chabot Stn(CHA)
O3@CHA-SFB(16,83)
Modeled O3 cleanBC
Modeled O3 baseBC
Observations
0
20
40
60
80
100
120
206
207
208
209
210
211
212
213
214
215
216
217
218
219
220
221
O3(ppb) vs Time of day (hr PST)
@ Fremont Stn (Chapel Way)(FCW)
O3@FCW-SFB(19,78)
Modeled O3 cleanBC
Modeled O3 baseBC
Observations
0
20
40
60
80
100
120
206
207
208
209
210
211
212
213
214
215
216
217
218
219
220
221

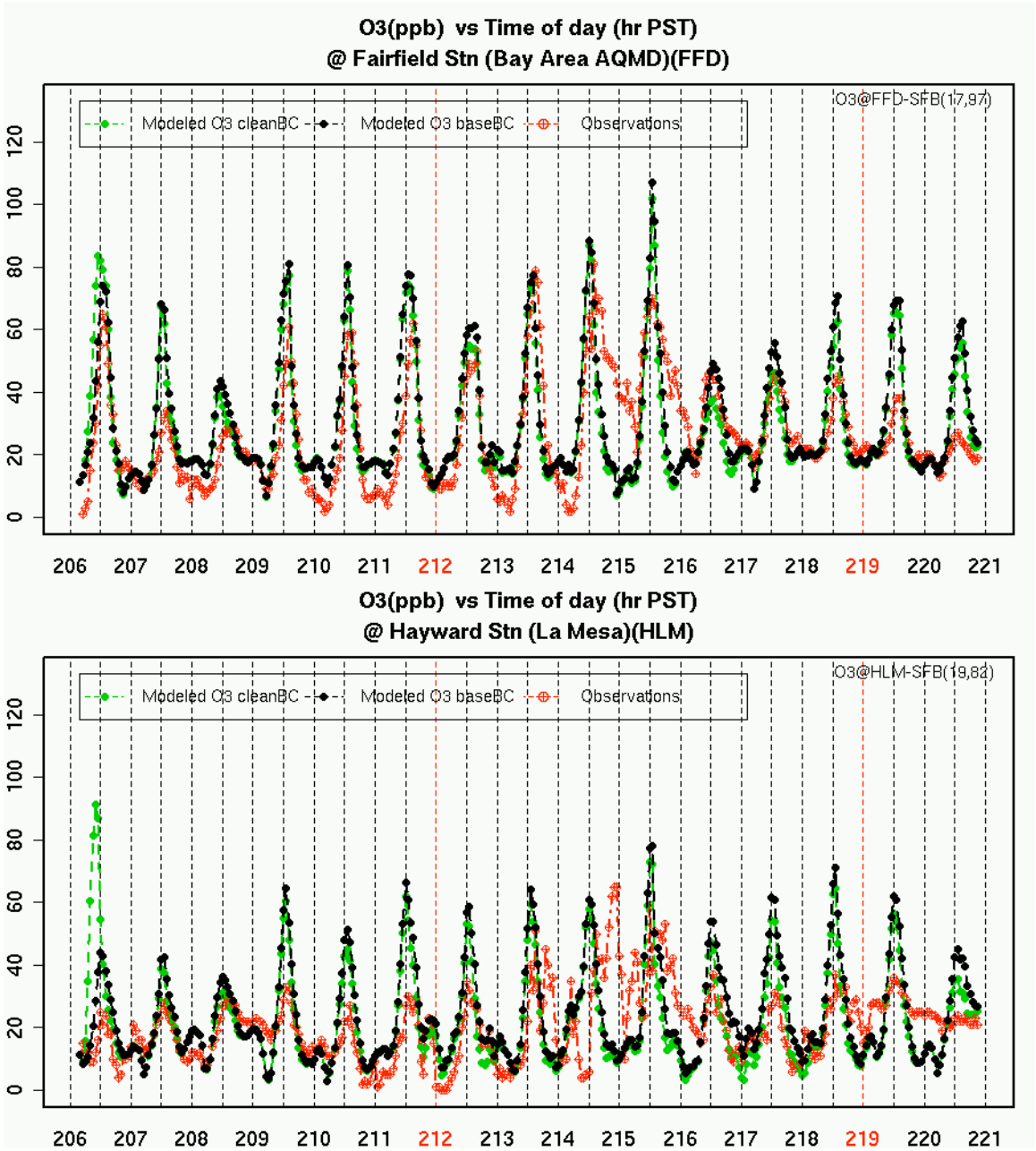
O3(ppb) vs Time of day (hr PST)
@ Fairfield Stn (Bay Area AQMD)(FFD)
O3@FFD-SFB(17,97)
Modeled O3 cleanBC
Modeled O3 baseBC
Observations
0
20
40
60
80
100
120
206
207
208
209
210
211
212
213
214
215
216
217
218
219
220
221
O3(ppb) vs Time of day (hr PST)
@ Hayward Stn (La Mesa)(HLM)
O3@HLM-SFB(19,82)
Modeled O3 cleanBC
Modeled O3 baseBC
Observations
0
20
40
60
80
100
120
206
207
208
209
210
211
212
213
214
215
216
217
218
219
220
221

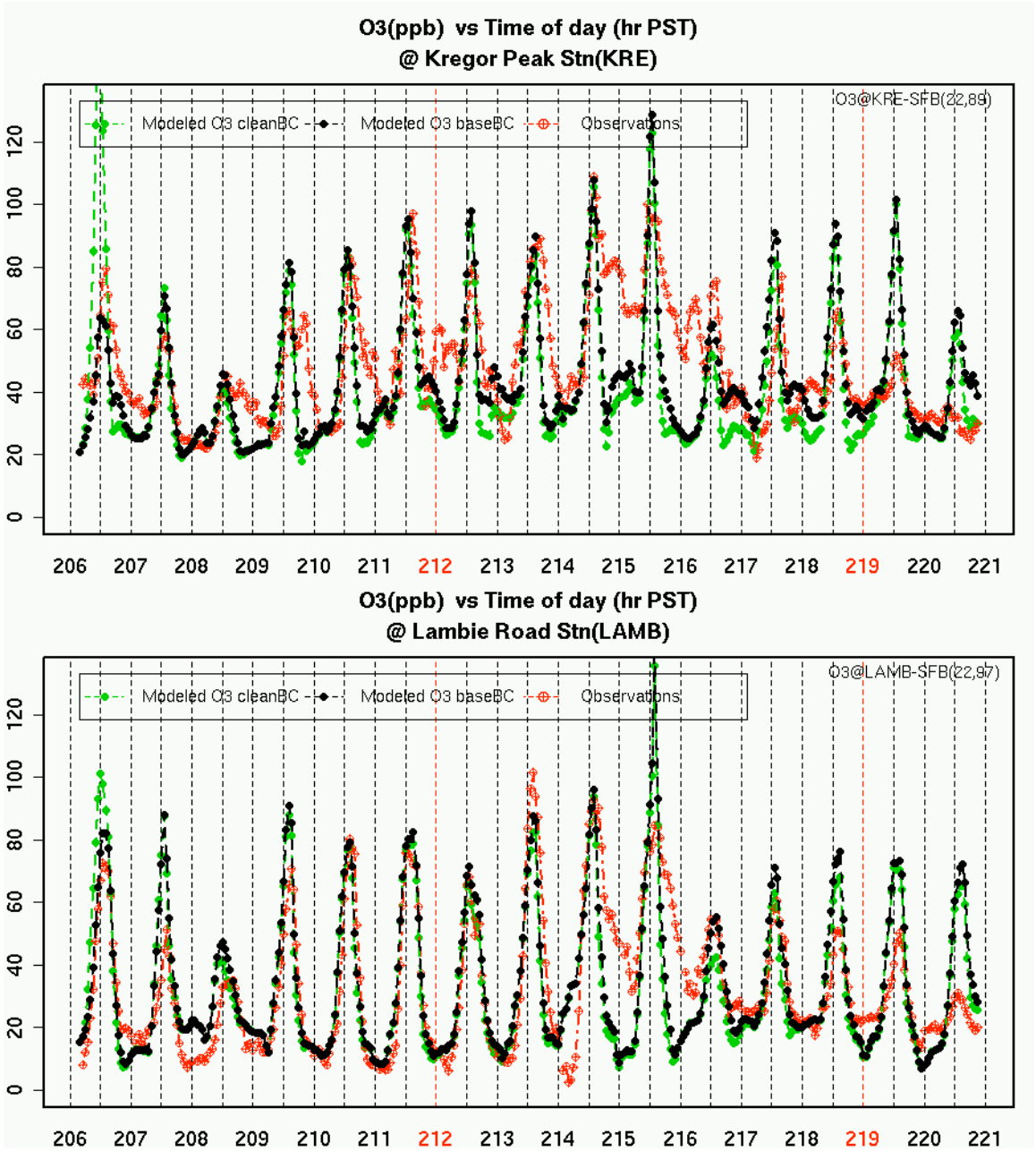
O3(ppb) vs Time of day (hr PST)
@ Kregor Peak Stn(KRE)
O3@KRE-SFB(22,89)
Modeled O3 cleanBC
Modeled O3 baseBC
Observations
0
20
40
60
80
100
120
206
207
208
209
210
211
212
213
214
215
216
217
218
219
220
221
O3(ppb) vs Time of day (hr PST)
@ Lambie Road Stn(LAMB)
O3@LAMB-SFB(22,97)
Modeled O3 cleanBC
Modeled O3 baseBC
Observations
0
20
40
60
80
100
120
206
207
208
209
210
211
212
213
214
215
216
217
218
219
220
221

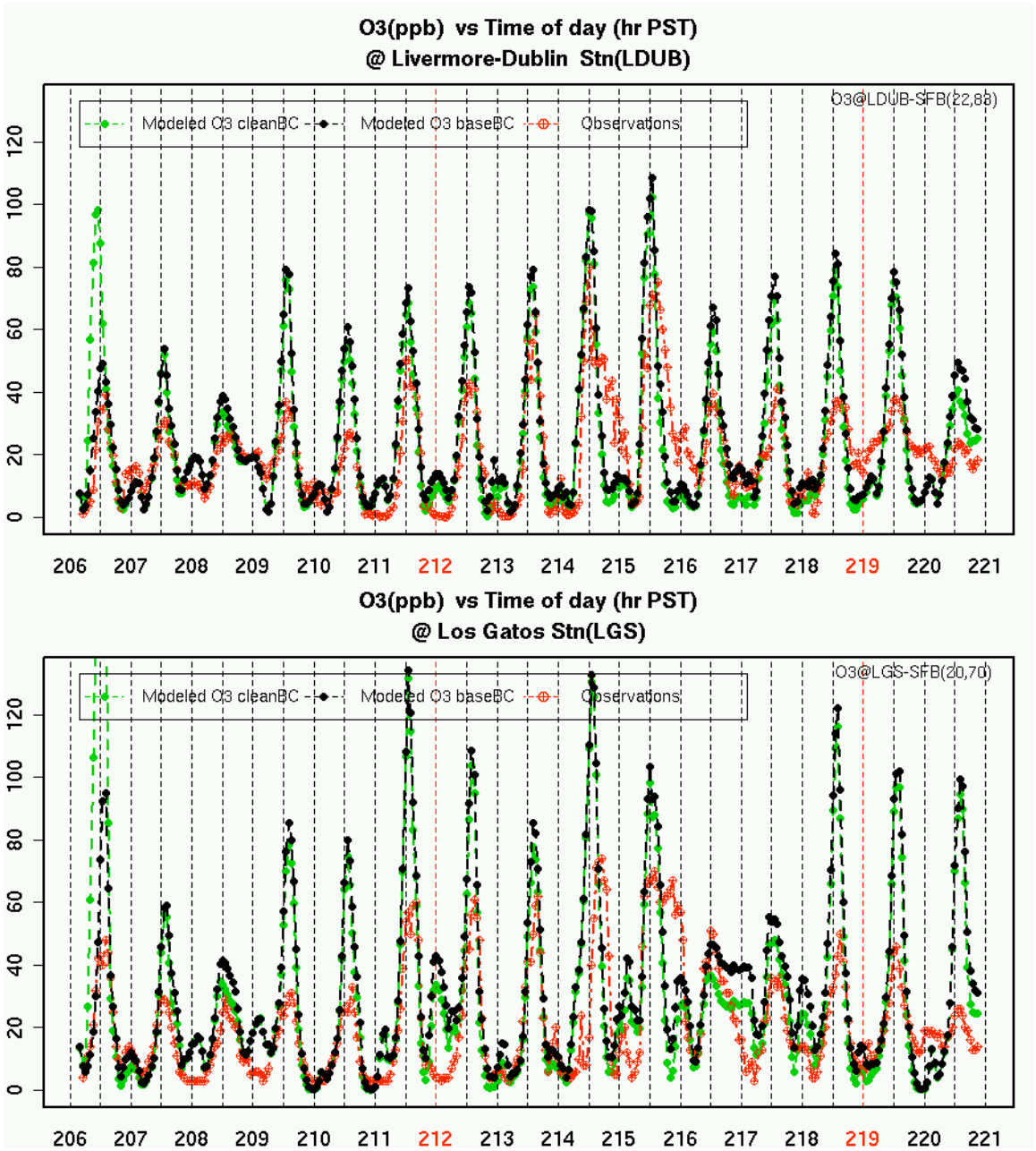
O3(ppb) vs Time of day (hr PST)
@ Livermore-Dublin Stn(LDUB)
O3@LDUB-SFB(22,88)
Modeled O3 cleanBC
Modeled O3 baseBC
Observations
0
20
40
60
80
100
120
206
207
208
209
210
211
212
213
214
215
216
217
218
219
220
221
O3(ppb) vs Time of day (hr PST)
@ Los Gatos Stn(LGS)
O3@LGS-SFB(20,70)
Modeled O3 cleanBC
Modeled O3 baseBC
Observations
0
20
40
60
80
100
120
206
207
208
209
210
211
212
213
214
215
216
217
218
219
220
221

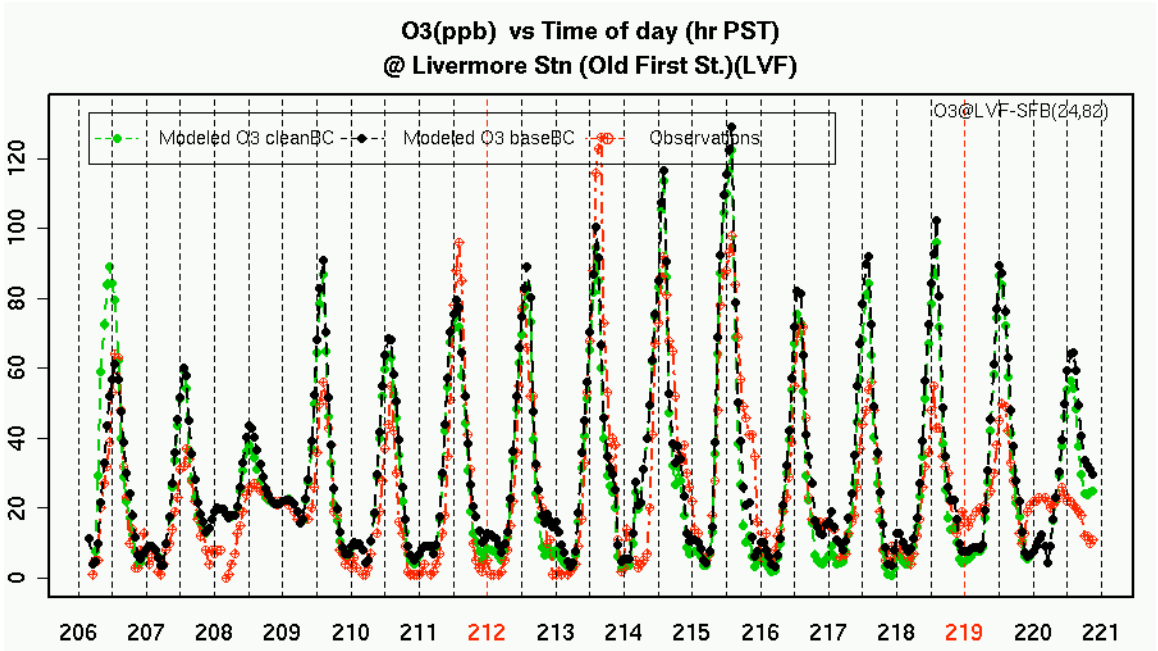
O3(ppb) vs Time of day (hr PST)
@ Livermore Stn (Old First St.)(LVF)
O3@LVF-SFB(24,82)
Modeled O3 cleanBC
Modeled O3 baseBC
Observations
0
20
40
60
80
100
120
206
207
208
209
210
211
212
213
214
215
216
217
218
219
220
221

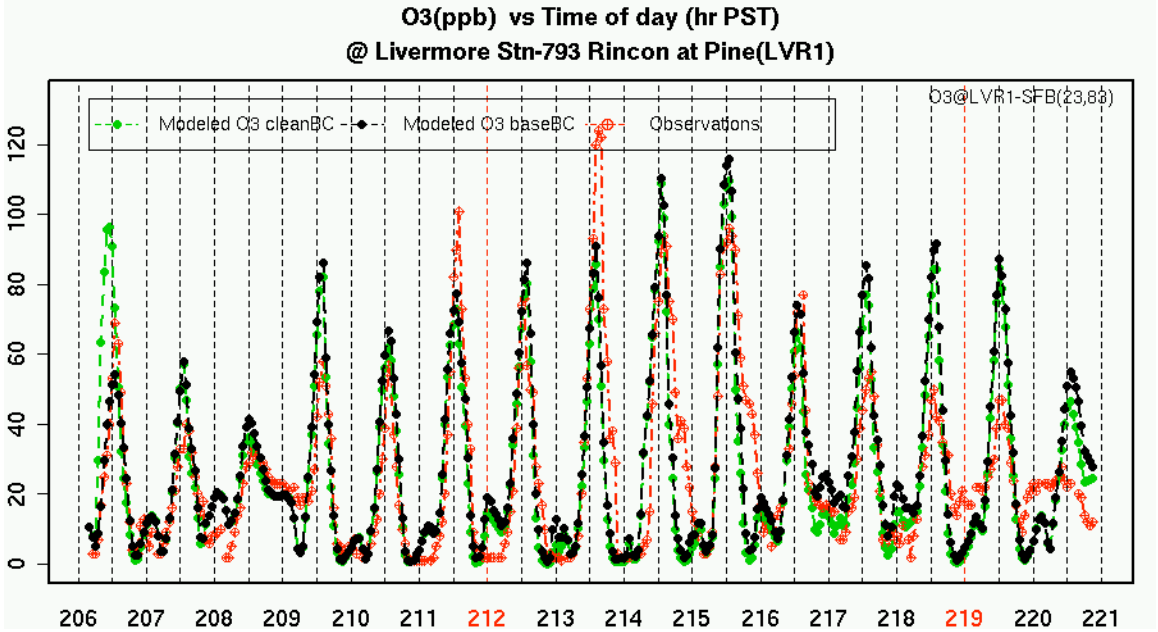
O3(ppb) vs Time of day (hr PST)
@ Livermore Stn-793 Rincon at Pine(LVR1)
O3@LVR1-SFB(23,83)
Modeled O3 cleanBC
Modeled O3 baseBC
Observations
0
20
40
60
80
100
120
206
207
208
209
210
211
212
213
214
215
216
217
218
219
220
221

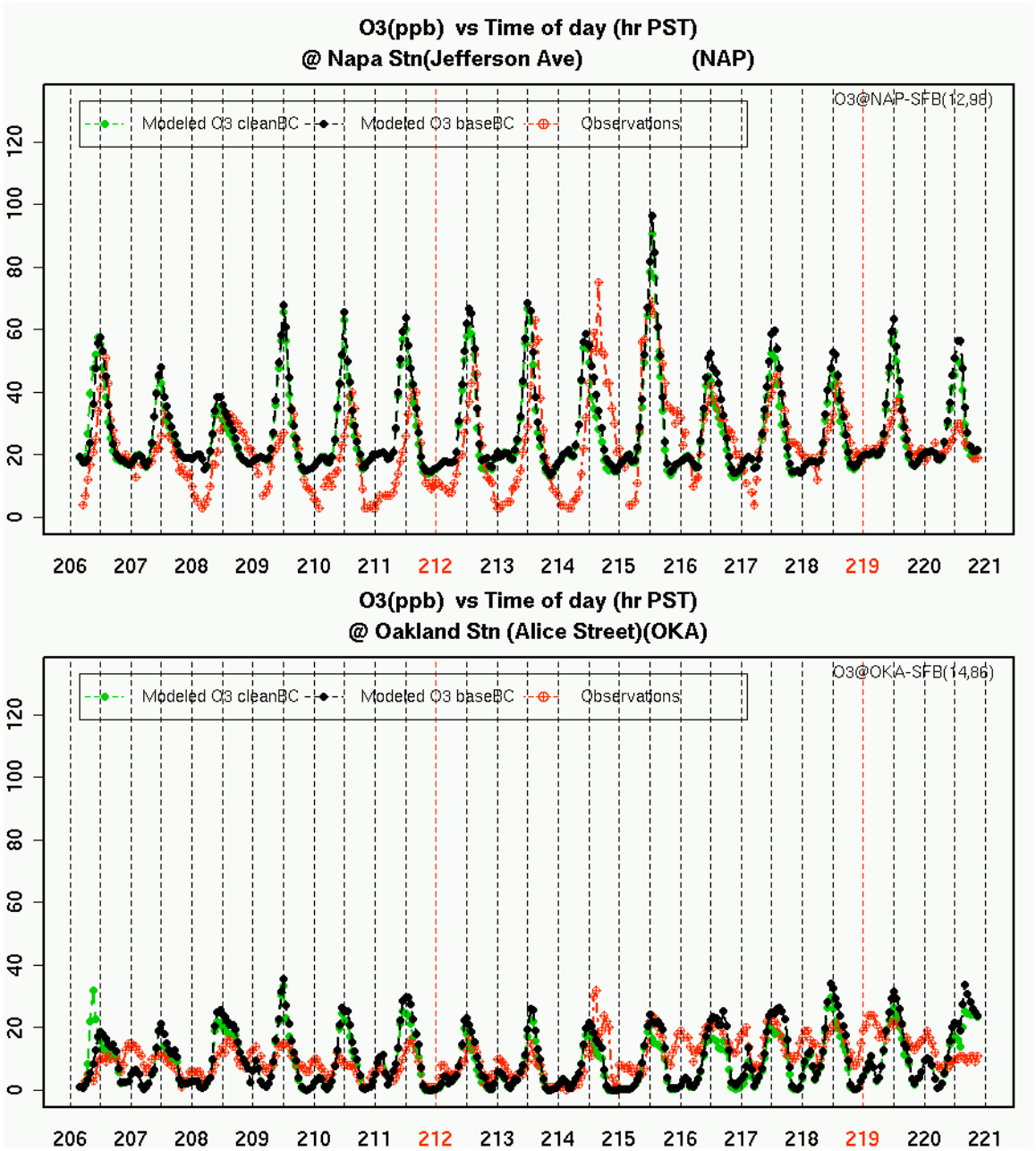
O3(ppb) vs Time of day (hr PST)
@ Napa Stn(Jefferson Ave) (NAP)
O3@NAP-SFB(12,98)
Modeled O3 cleanBC
Modeled O3 baseBC
Observations
0
20
40
60
80
100
120
206
207
208
209
210
211
212
213
214
215
216
217
218
219
220
221
O3(ppb) vs Time of day (hr PST)
@ Oakland Stn (Alice Street)(OKA)
O3@OKA-SFB(14,86)
Modeled O3 cleanBC
Modeled O3 baseBC
Observations
0
20
40
60
80
100
120
206
207
208
209
210
211
212
213
214
215
216
217
218
219
220
221

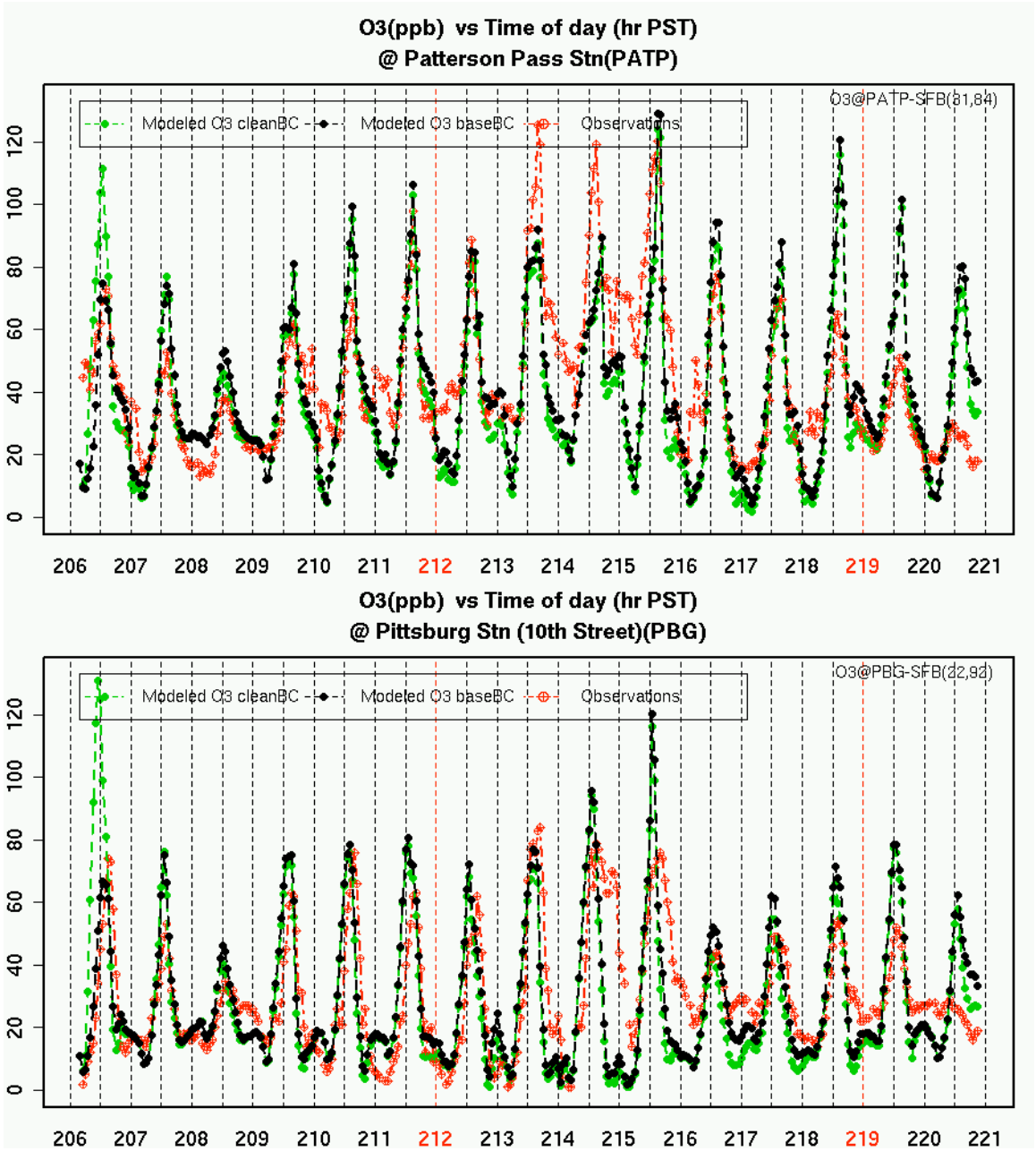
O3(ppb) vs Time of day (hr PST)
@ Patterson Pass Stn(PATP)
O3@PATP-SFB(81,84)
Modeled O3 cleanBC
Modeled O3 baseBC
Observations
0
20
40
60
80
100
120
206
207
208
209
210
211
212
213
214
215
216
217
218
219
220
221
O3(ppb) vs Time of day (hr PST)
@ Pittsburg Stn (10th Street)(PBG)
O3@PBG-SFB(22,92)
Modeled O3 cleanBC
Modeled O3 baseBC
Observations
0
20
40
60
80
100
120
206
207
208
209
210
211
212
213
214
215
216
217
218
219
220
221

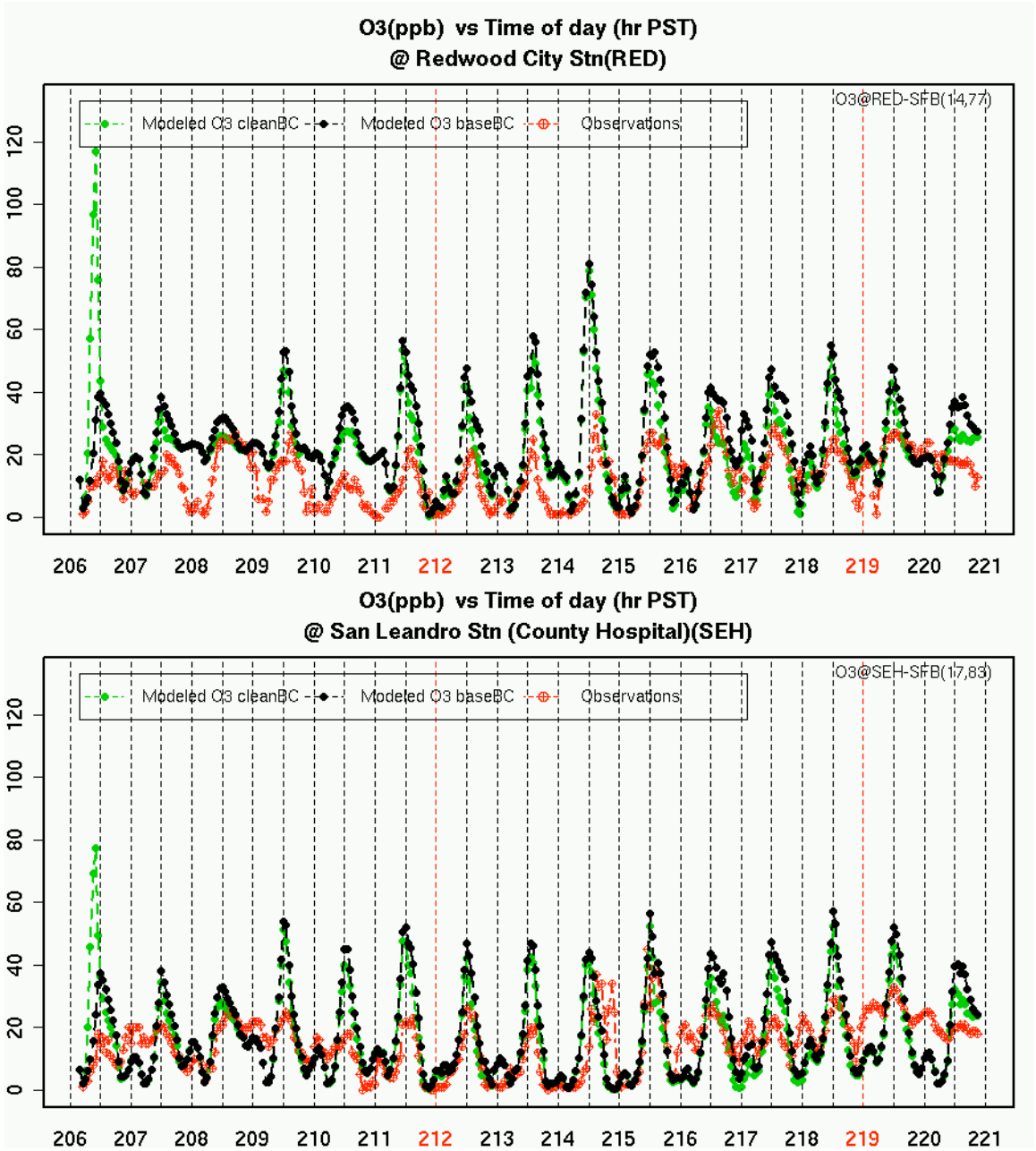
O3(ppb) vs Time of day (hr PST)
@ Redwood City Stn(RED)
O3@RED-SFB(14,77)
Modeled O3 cleanBC
Modeled O3 baseBC
Observations
0
20
40
60
80
100
120
206
207
208
209
210
211
212
213
214
215
216
217
218
219
220
221
O3(ppb) vs Time of day (hr PST)
@ San Leandro Stn (County Hospital)(SEH)
O3@SEH-SFB(17,83)
Modeled O3 cleanBC
Modeled O3 baseBC
Observations
0
20
40
60
80
100
120
206
207
208
209
210
211
212
213
214
215
216
217
218
219
220
221

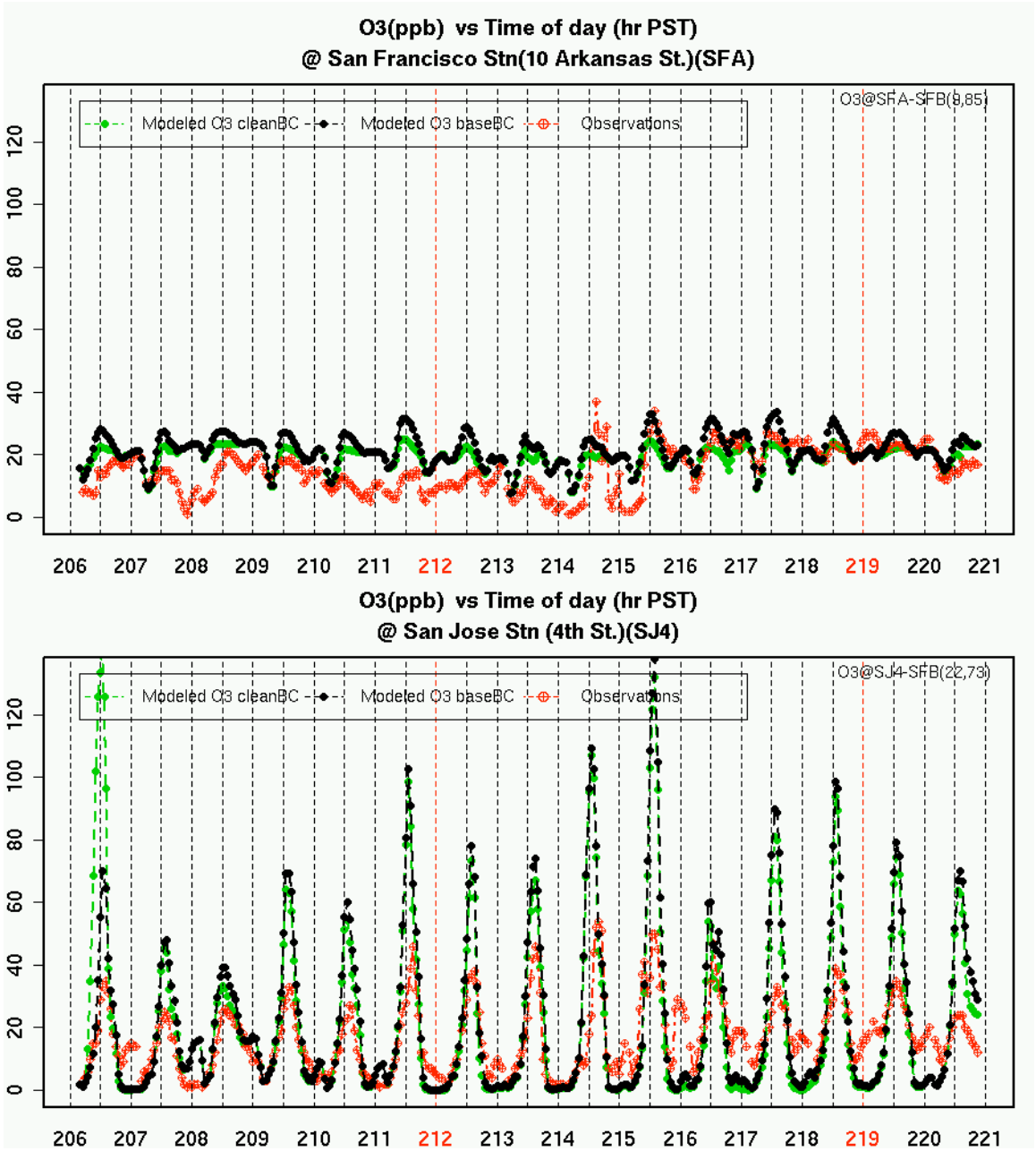
O3(ppb) vs Time of day (hr PST)
@ San Francisco Stn(10 Arkansas St.)(SFA)
O3@SFA-SFB(9,85)
Modeled O3 cleanBC
Modeled O3 baseBC
Observations
0
20
40
60
80
100
120
206
207
208
209
210
211
212
213
214
215
216
217
218
219
220
221
O3(ppb) vs Time of day (hr PST)
@ San Jose Stn (4th St.)(SJ4)
O3@SJ4-SFB(22,73)
Modeled O3 cleanBC
Modeled O3 baseBC
Observations
0
20
40
60
80
100
120
206
207
208
209
210
211
212
213
214
215
216
217
218
219
220
221

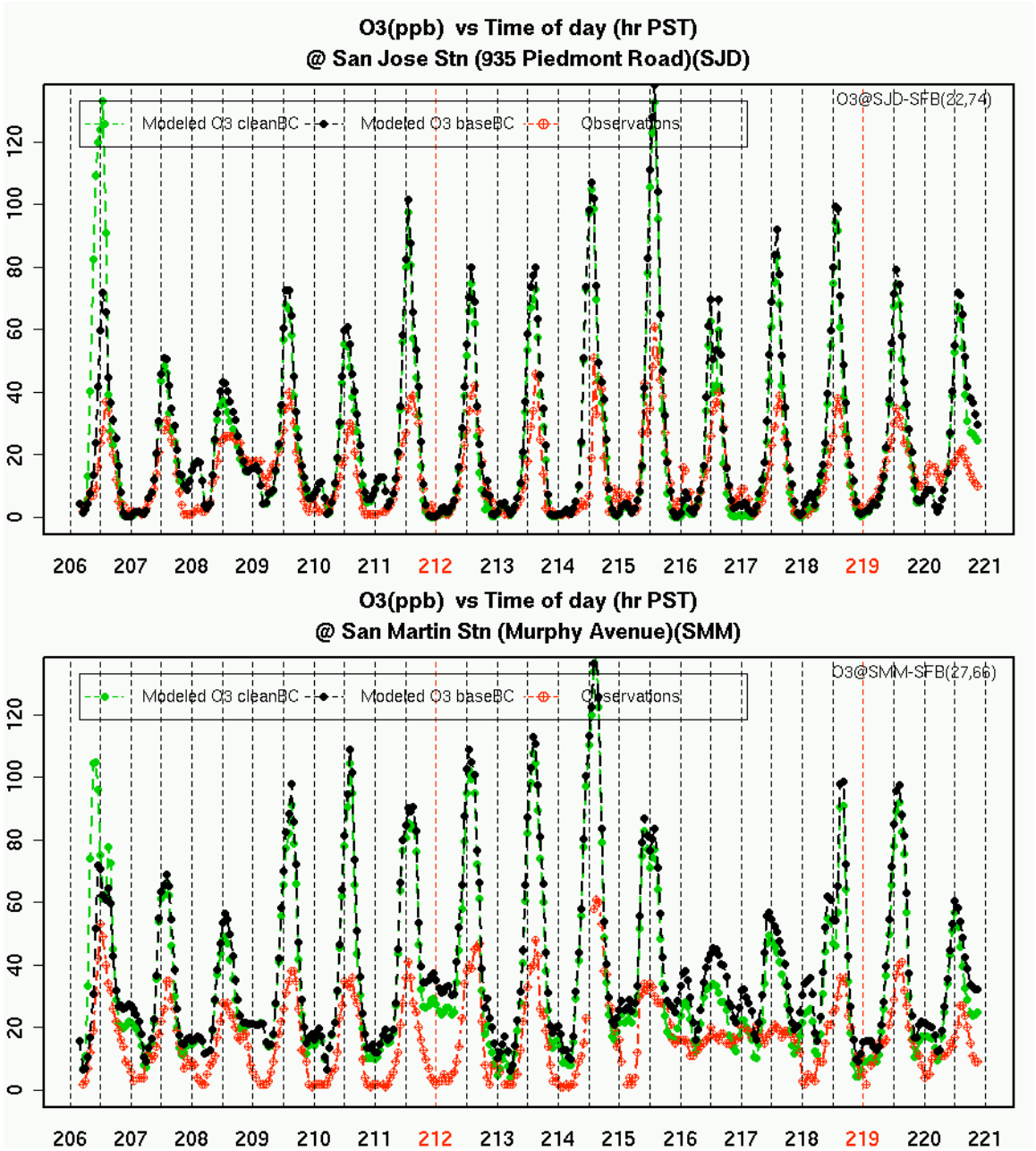
O3(ppb) vs Time of day (hr PST)
@ San Jose Stn (935 Piedmont Road)(SJD)
O3@SJD-SFB(22,74)
Modeled O3 cleanBC
Modeled O3 baseBC
Observations
0
20
40
60
80
100
120
206
207
208
209
210
211
212
213
214
215
216
217
218
219
220
221
O3(ppb) vs Time of day (hr PST)
@ San Martin Stn (Murphy Avenue)(SMM)
O3@SMM-SFB(27,66)
Modeled O3 cleanBC
Modeled O3 baseBC
Observations
0
20
40
60
80
100
120
206
207
208
209
210
211
212
213
214
215
216
217
218
219
220
221

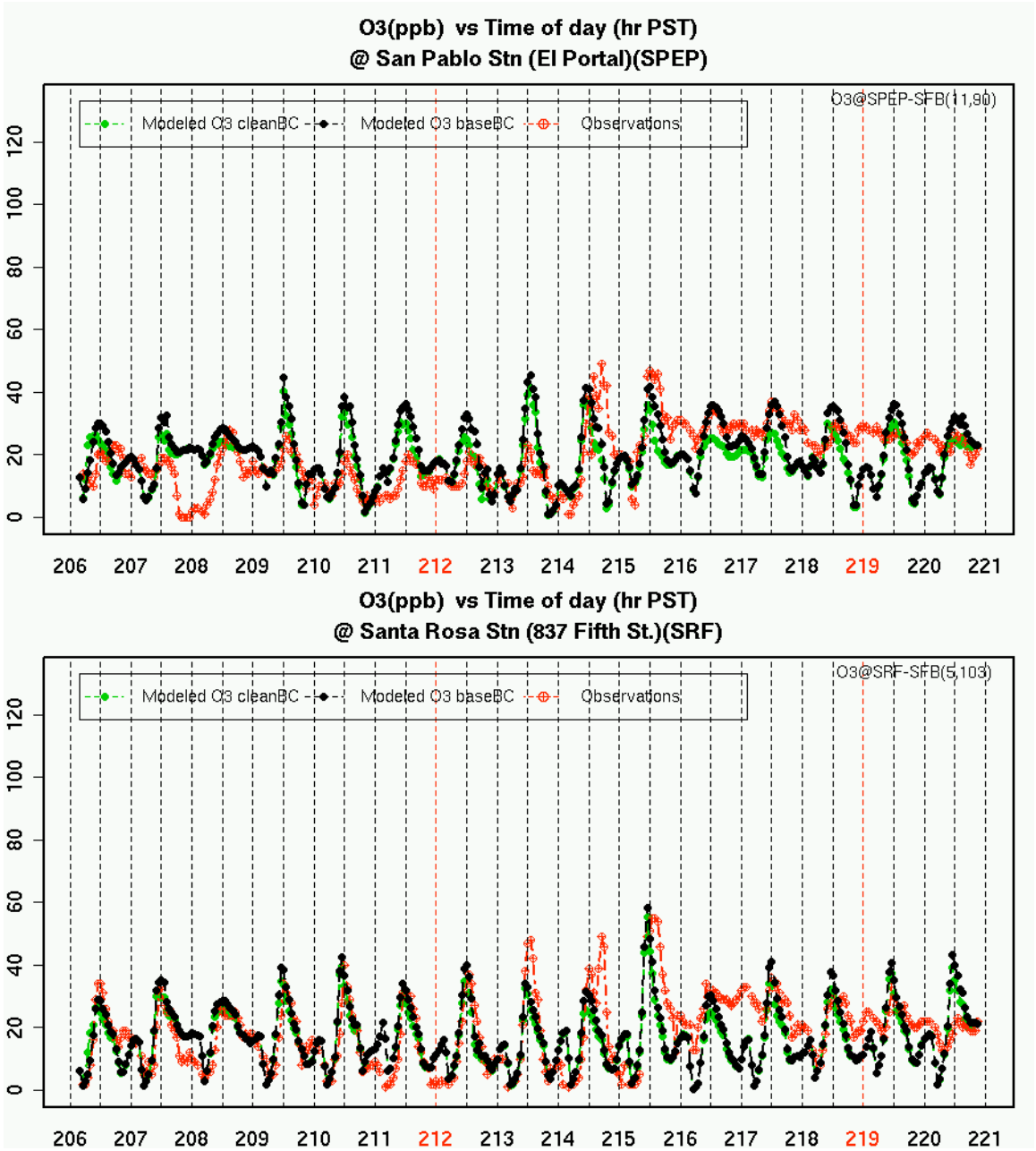
O3(ppb) vs Time of day (hr PST)
@ San Pablo Stn (El Portal)(SPEP)
O3@SPEP-SFB(11,90)
Modeled O3 cleanBC
Modeled O3 baseBC
Observations
0
20
40
60
80
100
120
206
207
208
209
210
211
212
213
214
215
216
217
218
219
220
221
O3(ppb) vs Time of day (hr PST)
@ Santa Rosa Stn (837 Fifth St.)(SRF)
O3@SRF-SFB(5,103)
Modeled O3 cleanBC
Modeled O3 baseBC
Observations
0
20
40
60
80
100
120
206
207
208
209
210
211
212
213
214
215
216
217
218
219
220
221

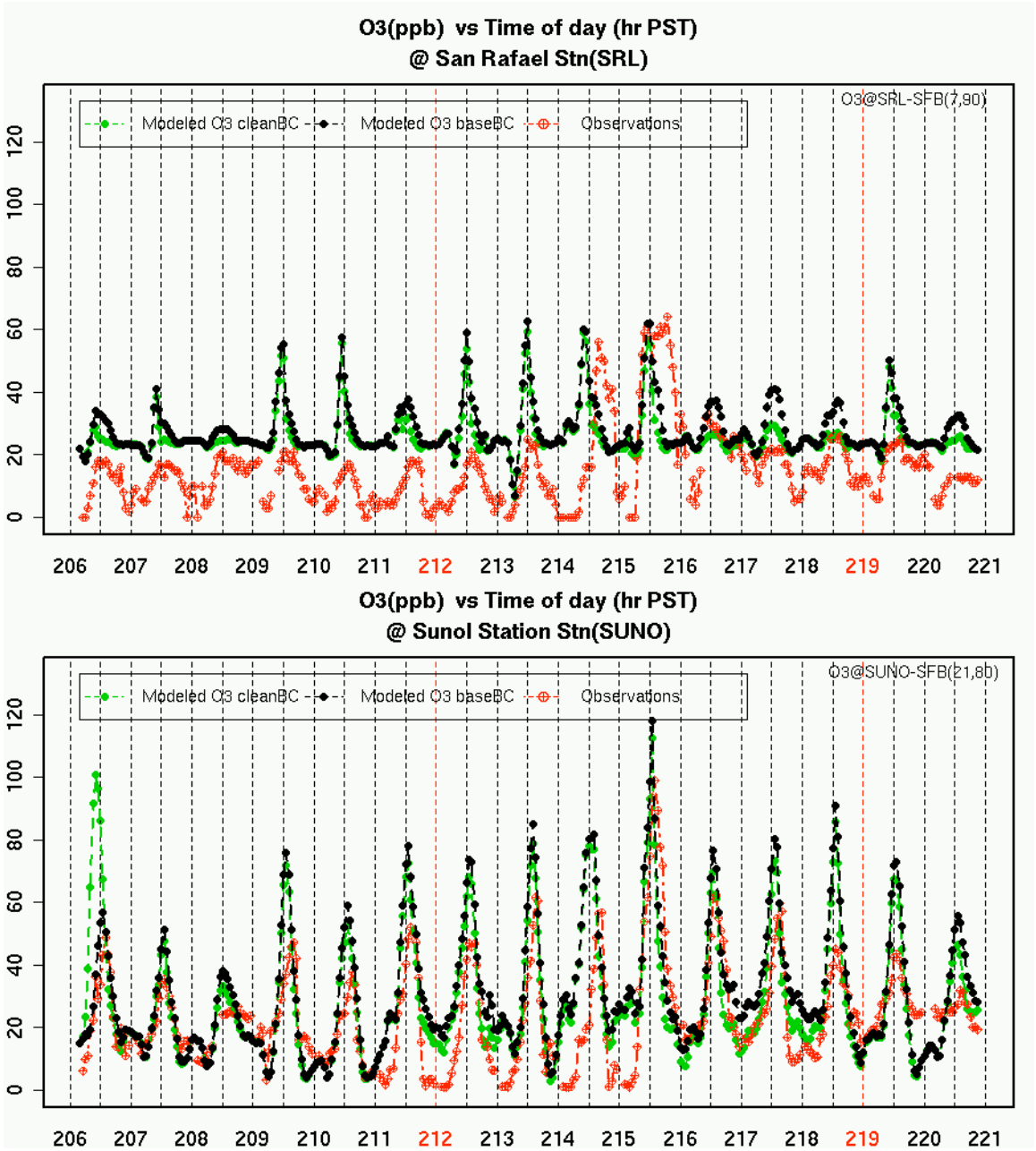
O3(ppb) vs Time of day (hr PST)
@ San Rafael Stn(SRL)
O3@SRL-SFB(7,90)
Modeled O3 cleanBC
Modeled O3 baseBC
Observations
0
20
40
60
80
100
120
206
207
208
209
210
211
212
213
214
215
216
217
218
219
220
221
O3(ppb) vs Time of day (hr PST)
@ Sunol Station Stn(SUNO)
O3@SUNO-SFB(21,80)
Modeled O3 cleanBC
Modeled O3 baseBC
Observations
0
20
40
60
80
100
120
206
207
208
209
210
211
212
213
214
215
216
217
218
219
220
221

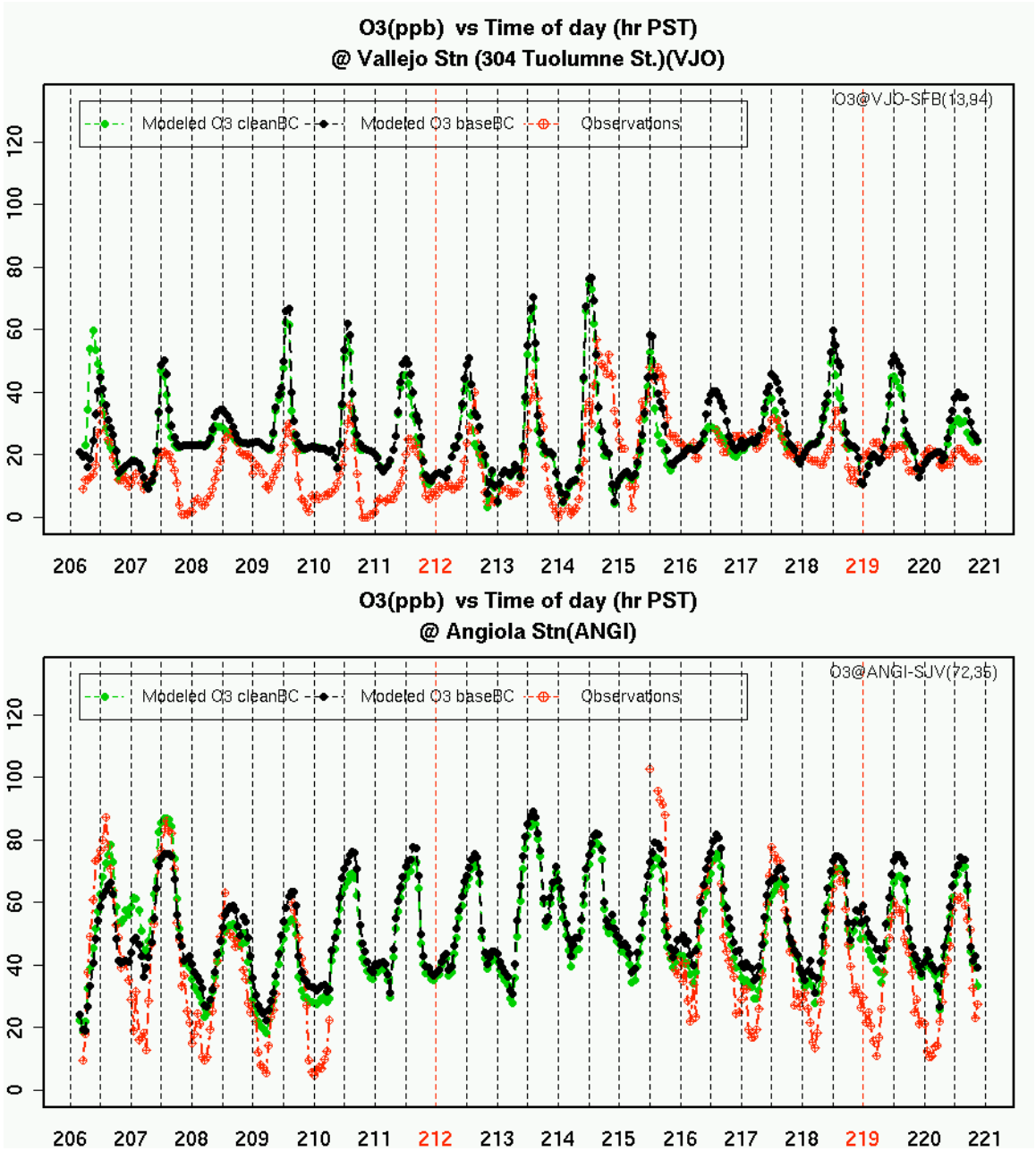
O3(ppb) vs Time of day (hr PST)
@ Vallejo Stn (304 Tuolumne St.)(VJO)
O3@VJO-SFB(13,94)
Modeled O3 cleanBC
Modeled O3 baseBC
Observations
0
20
40
60
80
100
120
206
207
208
209
210
211
212
213
214
215
216
217
218
219
220
221
O3(ppb) vs Time of day (hr PST)
@ Angiola Stn(ANGI)
O3@ANGI-SJV(72,35)
Modeled O3 cleanBC
Modeled O3 baseBC
Observations
0
20
40
60
80
100
120
206
207
208
209
210
211
212
213
214
215
216
217
218
219
220
221

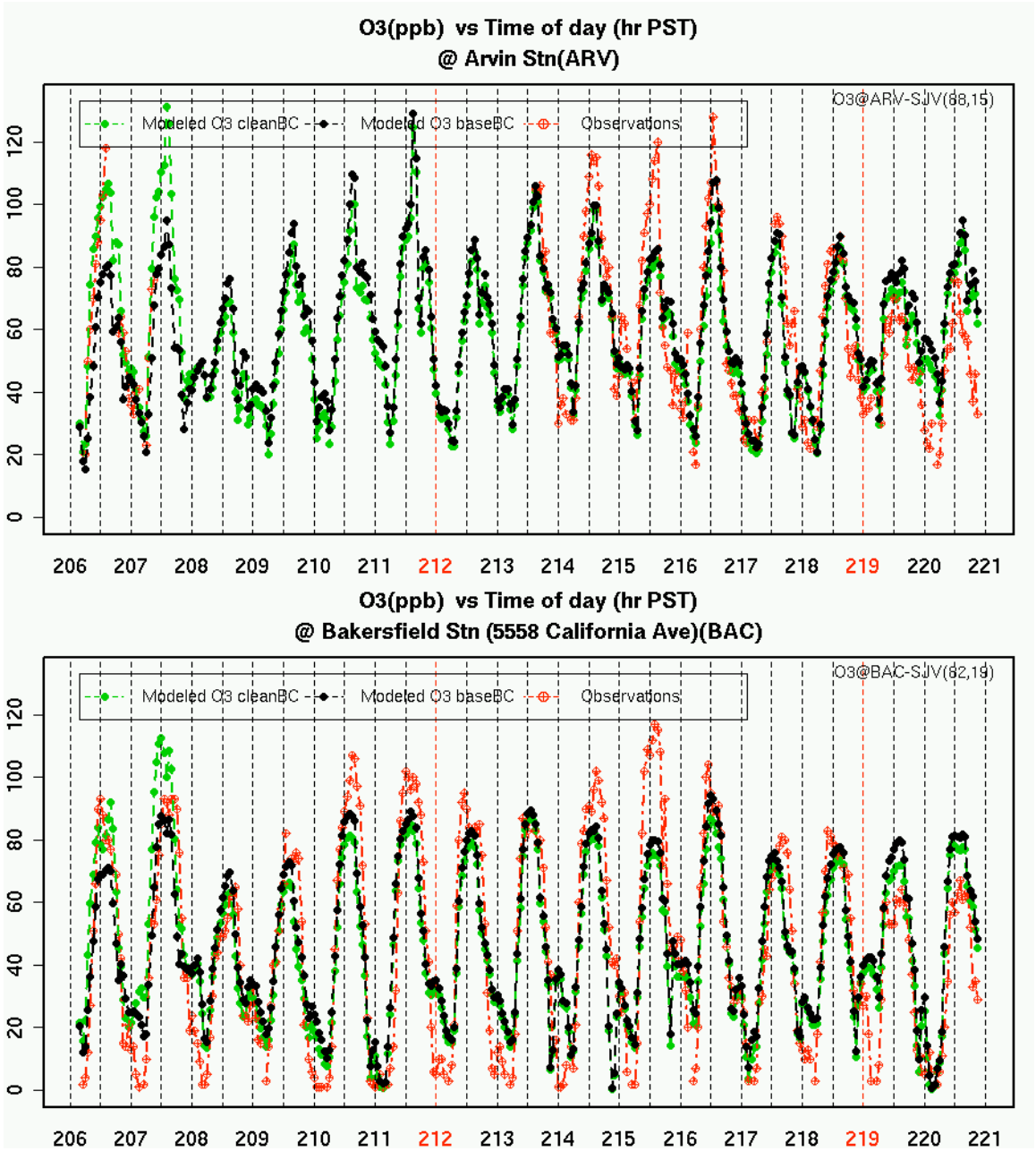
O3(ppb) vs Time of day (hr PST)
@ Arvin Stn(ARV)
O3@ARV-SJV(88,15)
Modeled O3 cleanBC
Modeled O3 baseBC
Observations
0
20
40
60
80
100
120
206
207
208
209
210
211
212
213
214
215
216
217
218
219
220
221
O3(ppb) vs Time of day (hr PST)
@ Bakersfield Stn (5558 California Ave)(BAC)
O3@BAC-SJV(82,19)
Modeled O3 cleanBC
Modeled O3 baseBC
Observations
0
20
40
60
80
100
120
206
207
208
209
210
211
212
213
214
215
216
217
218
219
220
221

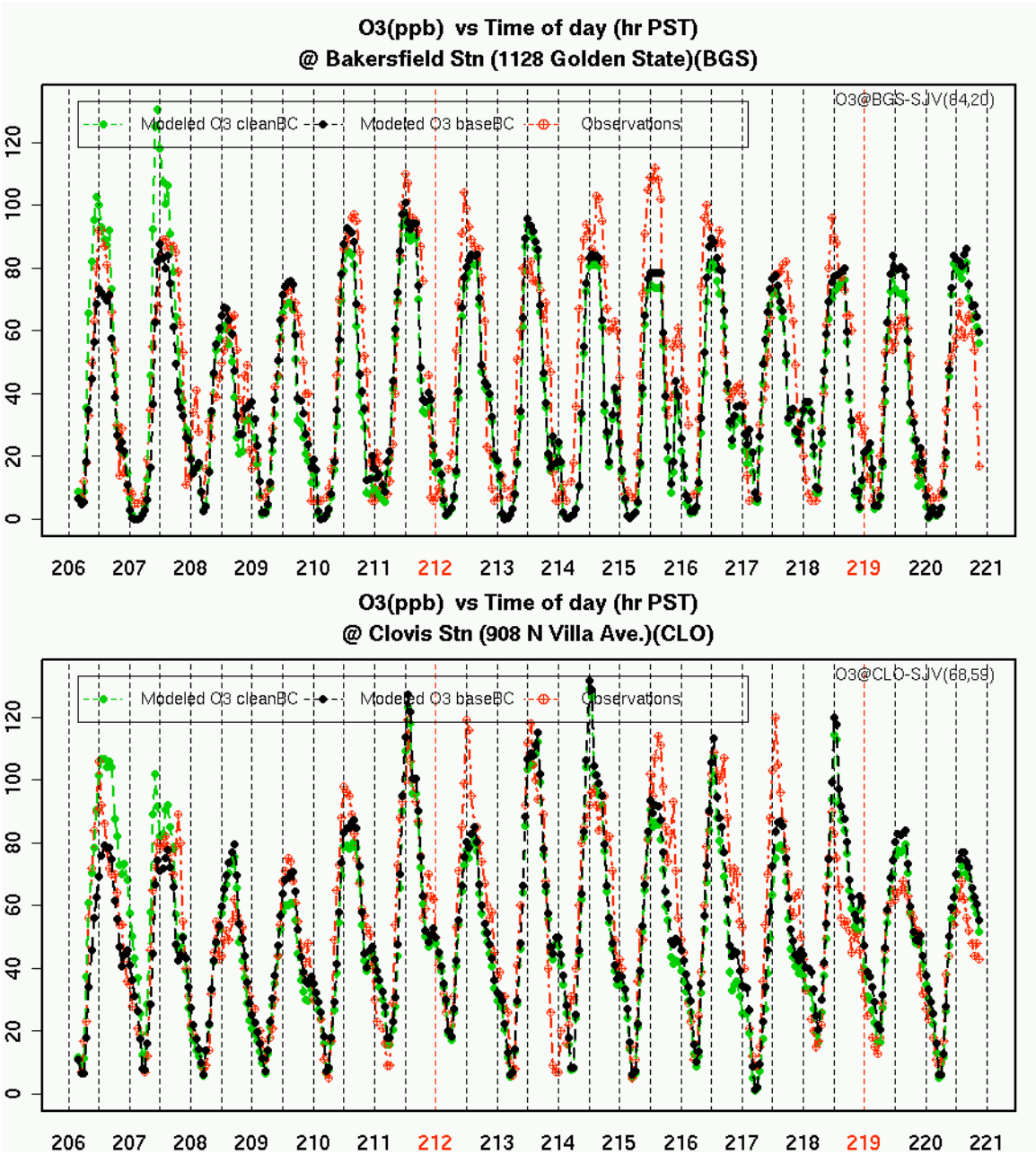
O3(ppb) vs Time of day (hr PST)
@ Bakersfield Stn (1128 Golden State)(BGS)
O3@BGS-SJV(64,20)
Modeled O3 cleanBC
Modeled O3 baseBC
Observations
0
20
40
60
80
100
120
206
207
208
209
210
211
212
213
214
215
216
217
218
219
220
221
O3(ppb) vs Time of day (hr PST)
@ Clovis Stn (908 N Villa Ave.)(CLO)
O3@CLO-SJV(68,59)
Modeled O3 cleanBC
Modeled O3 baseBC
Observations
0
20
40
60
80
100
120
206
207
208
209
210
211
212
213
214
215
216
217
218
219
220
221

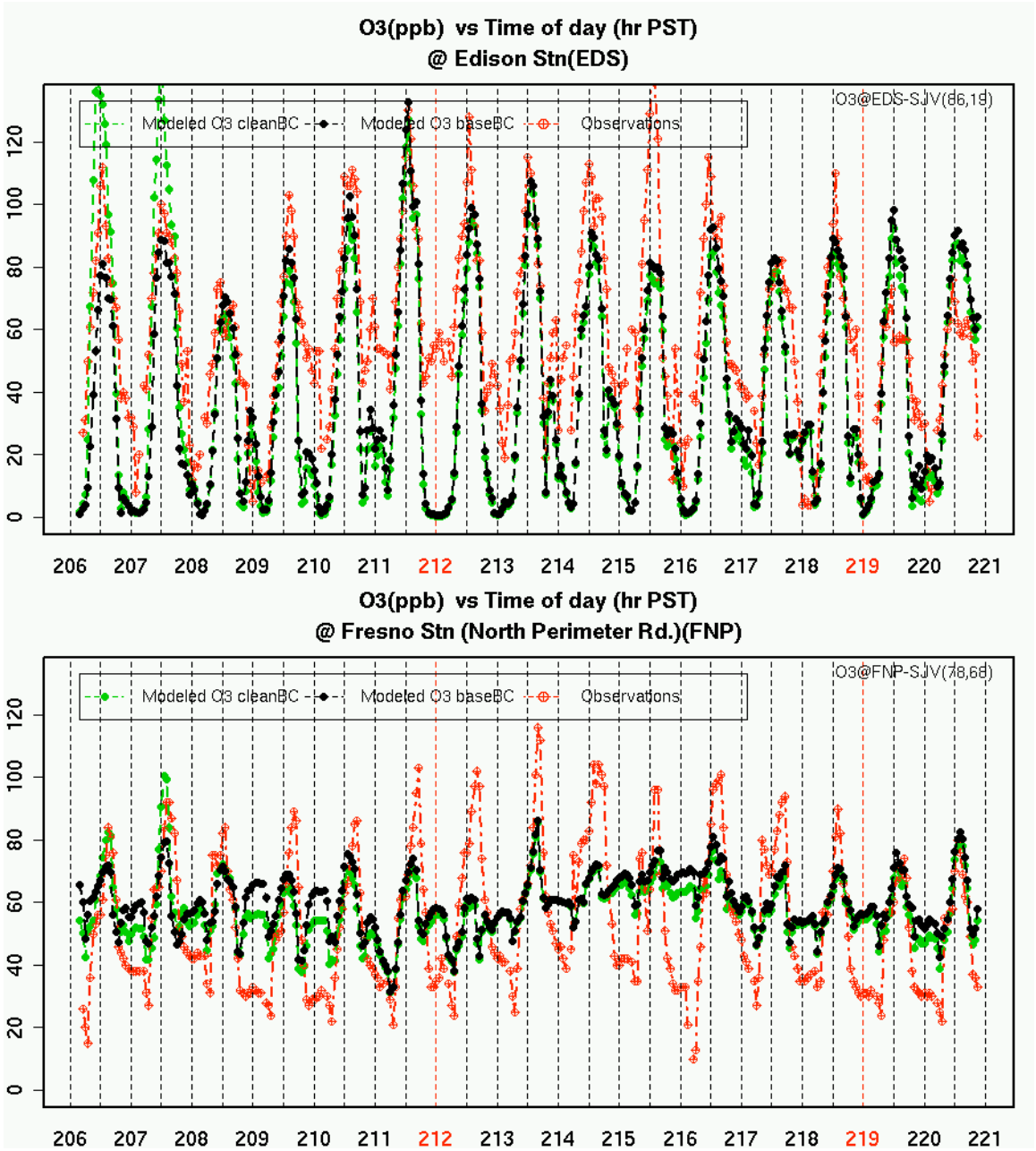
O3(ppb) vs Time of day (hr PST)
@ Edison Stn(EDS)
O3@EDS-SJV(86,19)
Modeled O3 cleanBC
Modeled O3 baseBC
Observations
0
20
40
60
80
100
120
206
207
208
209
210
211
212
213
214
215
216
217
218
219
220
221
O3(ppb) vs Time of day (hr PST)
@ Fresno Stn (North Perimeter Rd.)(FNP)
O3@FNP-SJV(78,68)
Modeled O3 cleanBC
Modeled O3 baseBC
Observations
0
20
40
60
80
100
120
206
207
208
209
210
211
212
213
214
215
216
217
218
219
220
221

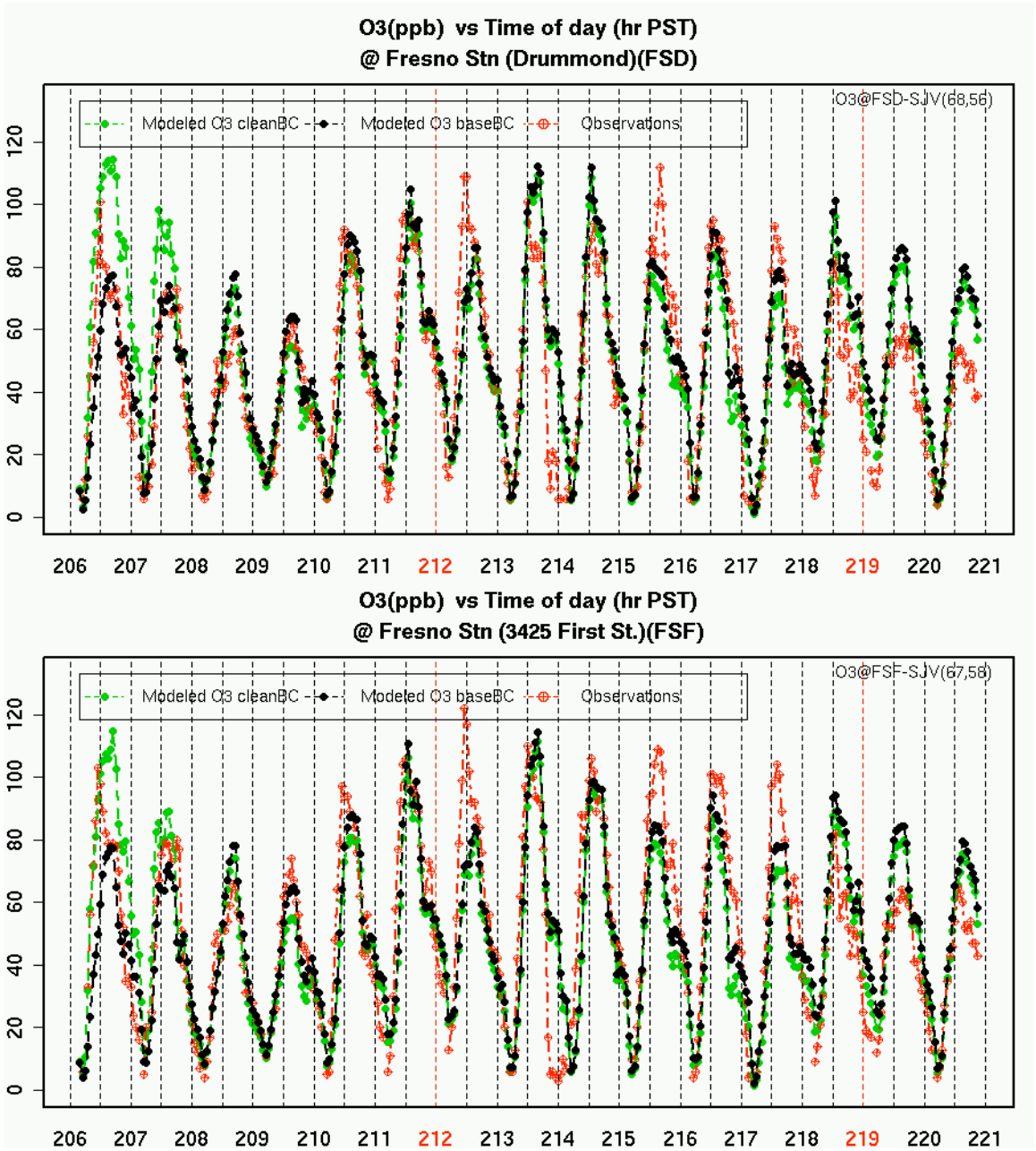
O3(ppb) vs Time of day (hr PST)
@ Fresno Stn (Drummond)(FSD)
O3@FSD-SJV(68,56)
Modeled O3 cleanBC
Modeled O3 baseBC
Observations
0
20
40
60
80
100
120
206
207
208
209
210
211
212
213
214
215
216
217
218
219
220
221
O3(ppb) vs Time of day (hr PST)
@ Fresno Stn (3425 First St.)(FSF)
O3@FSF-SJV(67,58)
Modeled O3 cleanBC
Modeled O3 baseBC
Observations
0
20
40
60
80
100
120
206
207
208
209
210
211
212
213
214
215
216
217
218
219
220
221

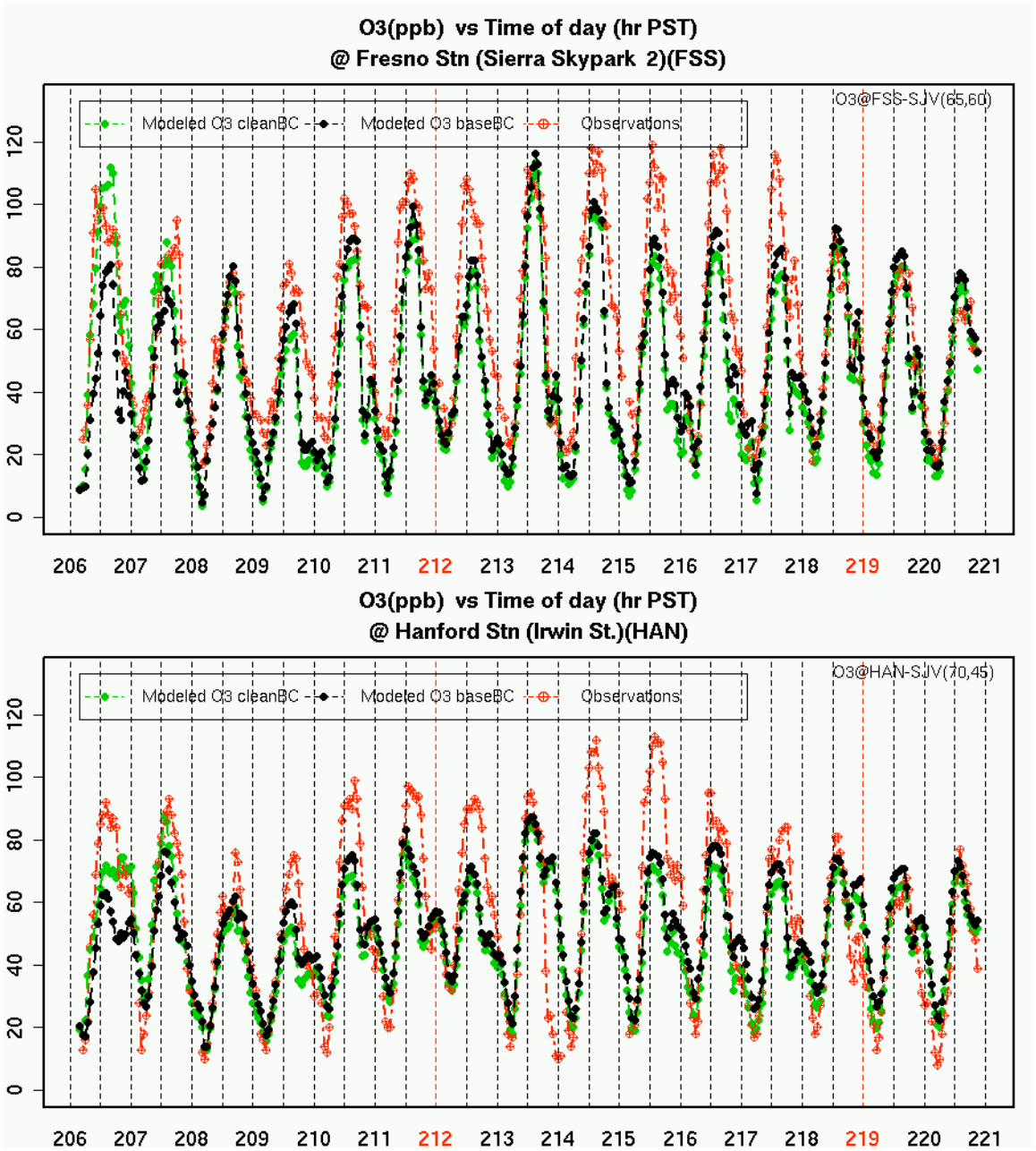
O3(ppb) vs Time of day (hr PST)
@ Fresno Stn (Sierra Skypark 2)(FSS)
O3@FSS-SJV(65,60)
Modeled O3 cleanBC
Modeled O3 baseBC
Observations
0
20
40
60
80
100
120
206
207
208
209
210
211
212
213
214
215
216
217
218
219
220
221
O3(ppb) vs Time of day (hr PST)
@ Hanford Stn (Irwin St.)(HAN)
O3@HAN-SJV(70,45)
Modeled O3 cleanBC
Modeled O3 baseBC
Observations
0
20
40
60
80
100
120
206
207
208
209
210
211
212
213
214
215
216
217
218
219
220
221

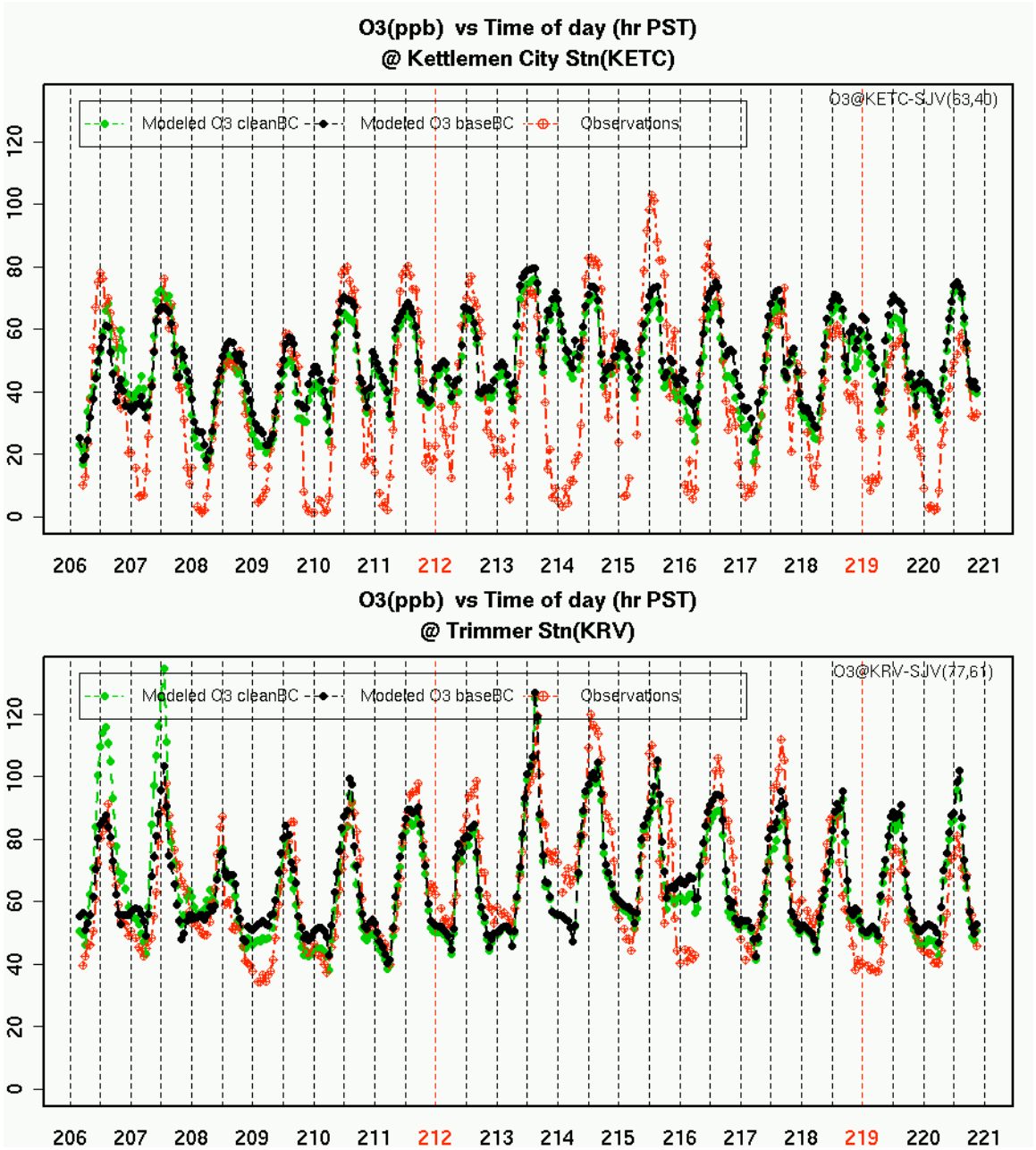
O3(ppb) vs Time of day (hr PST)
@ Kettlemen City Stn(KETC)
O3@KETC-SJV(63,40)
Modeled O3 cleanBC
Modeled O3 baseBC
Observations
0
20
40
60
80
100
120
206
207
208
209
210
211
212
213
214
215
216
217
218
219
220
221
O3(ppb) vs Time of day (hr PST)
@ Trimmer Stn(KRV)
O3@KRV-SJV(77,61)
Modeled O3 cleanBC
Modeled O3 baseBC
Observations
0
20
40
60
80
100
120
206
207
208
209
210
211
212
213
214
215
216
217
218
219
220
221

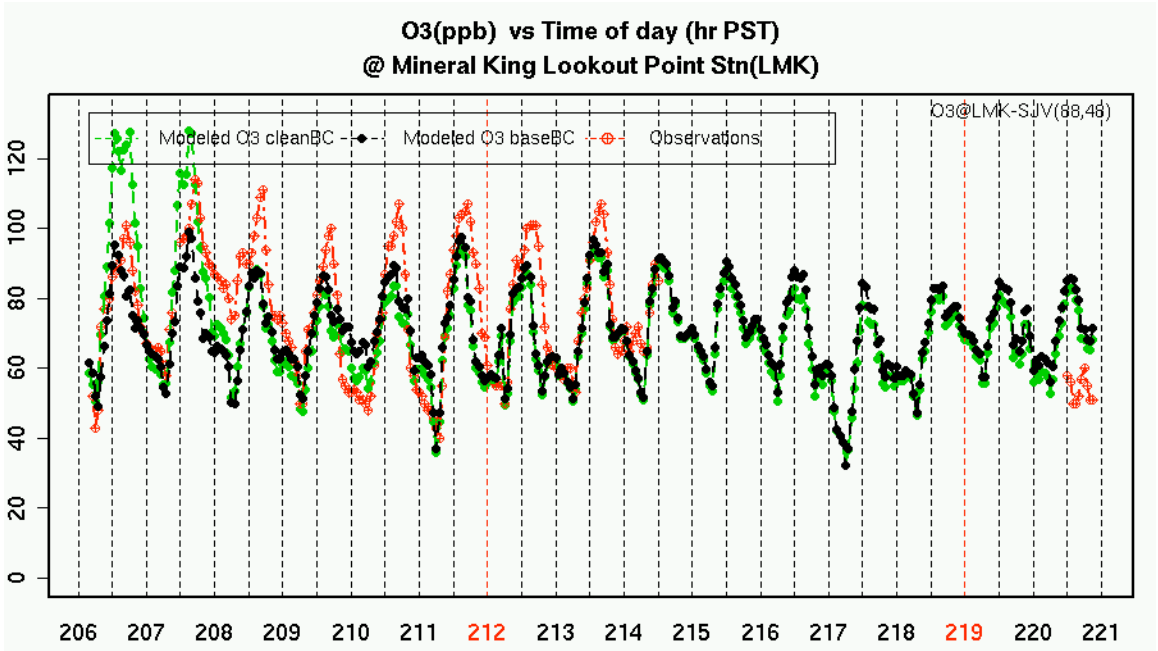
O3(ppb) vs Time of day (hr PST)
@ Mineral King Lookout Point Stn(LMK)
O3@LMK-SJV(68,48)
Modeled O3 cleanBC
Modeled O3 baseBC
Observations
0
20
40
60
80
100
120
206
207
208
209
210
211
212
213
214
215
216
217
218
219
220
221

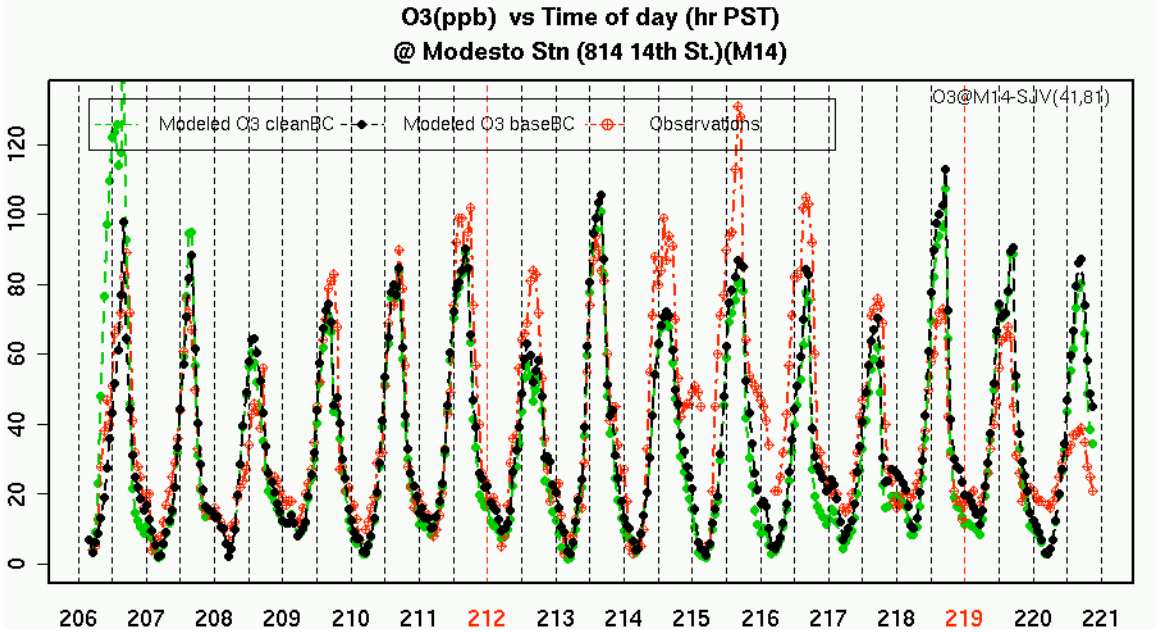
O3(ppb) vs Time of day (hr PST)
@ Modesto Stn (814 14th St.)(M14)
O3@M14-SJV(41,81)
Modeled O3 cleanBC
Modeled O3 baseBC
Observations
0
20
40
60
80
100
120
206
207
208
209
210
211
212
213
214
215
216
217
218
219
220
221

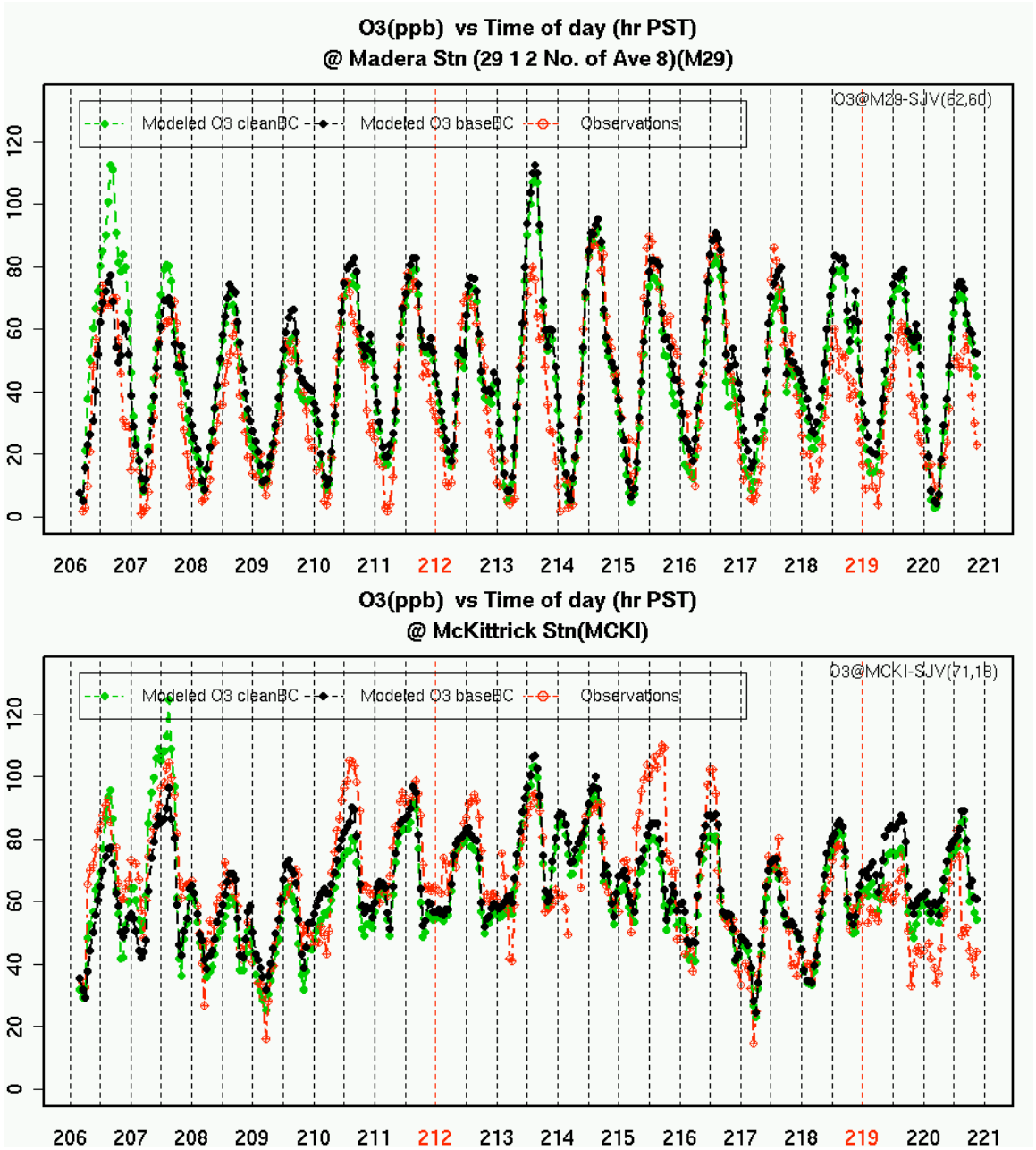
O3(ppb) vs Time of day (hr PST)
@ Madera Stn (29 1 2 No. of Ave 8)(M29)
O3@M29-SJV(62,60)
Modeled O3 cleanBC
Modeled O3 baseBC
Observations
0
20
40
60
80
100
120
206
207
208
209
210
211
212
213
214
215
216
217
218
219
220
221
O3(ppb) vs Time of day (hr PST)
@ McKittrick Stn(MCKI)
O3@MCKI-SJV(71,18)
Modeled O3 cleanBC
Modeled O3 baseBC
Observations
0
20
40
60
80
100
120
206
207
208
209
210
211
212
213
214
215
216
217
218
219
220
221

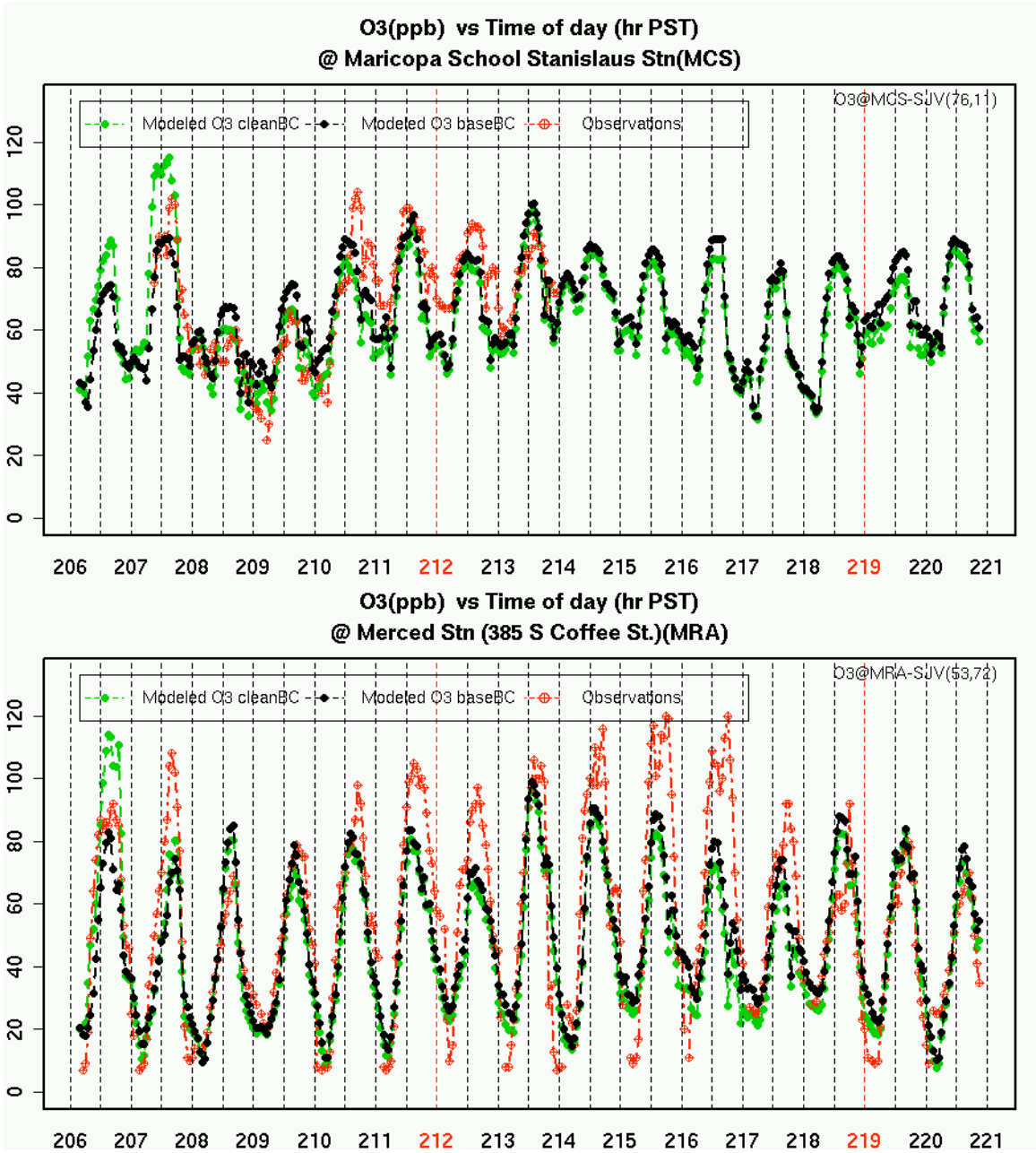
O3(ppb) vs Time of day (hr PST)
@ Maricopa School Stanislaus Stn(MCS)
O3@MCS-SJV(76,11)
Modeled O3 cleanBC
Modeled O3 baseBC
Observations
0
20
40
60
80
100
120
206
207
208
209
210
211
212
213
214
215
216
217
218
219
220
221
O3(ppb) vs Time of day (hr PST)
@ Merced Stn (385 S Coffee St.)(MRA)
O3@MRA-SJV(53,72)
Modeled O3 cleanBC
Modeled O3 baseBC
Observations
0
20
40
60
80
100
120
206
207
208
209
210
211
212
213
214
215
216
217
218
219
220
221

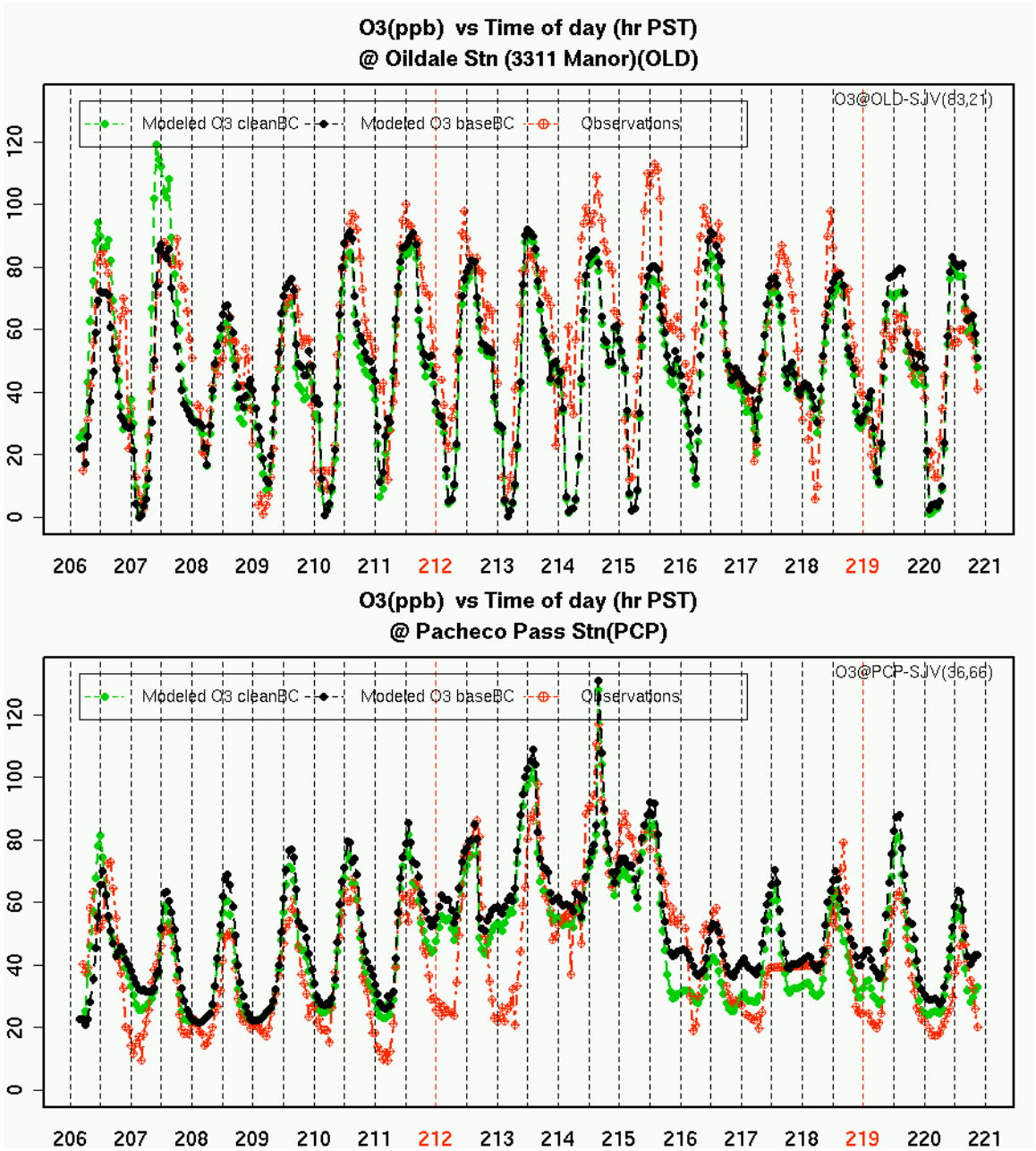
O3(ppb) vs Time of day (hr PST)
@ Oildale Stn (3311 Manor)(OLD)
O3@OLD-SJV(83,21)
Modeled O3 cleanBC
Modeled O3 baseBC
Observations
0
20
40
60
80
100
120
206
207
208
209
210
211
212
213
214
215
216
217
218
219
220
221
O3(ppb) vs Time of day (hr PST)
@ Pacheco Pass Stn(PCP)
O3@PCP-SJV(36,66)
Modeled O3 cleanBC
Modeled O3 baseBC
Observations
0
20
40
60
80
100
120
206
207
208
209
210
211
212
213
214
215
216
217
218
219
220
221

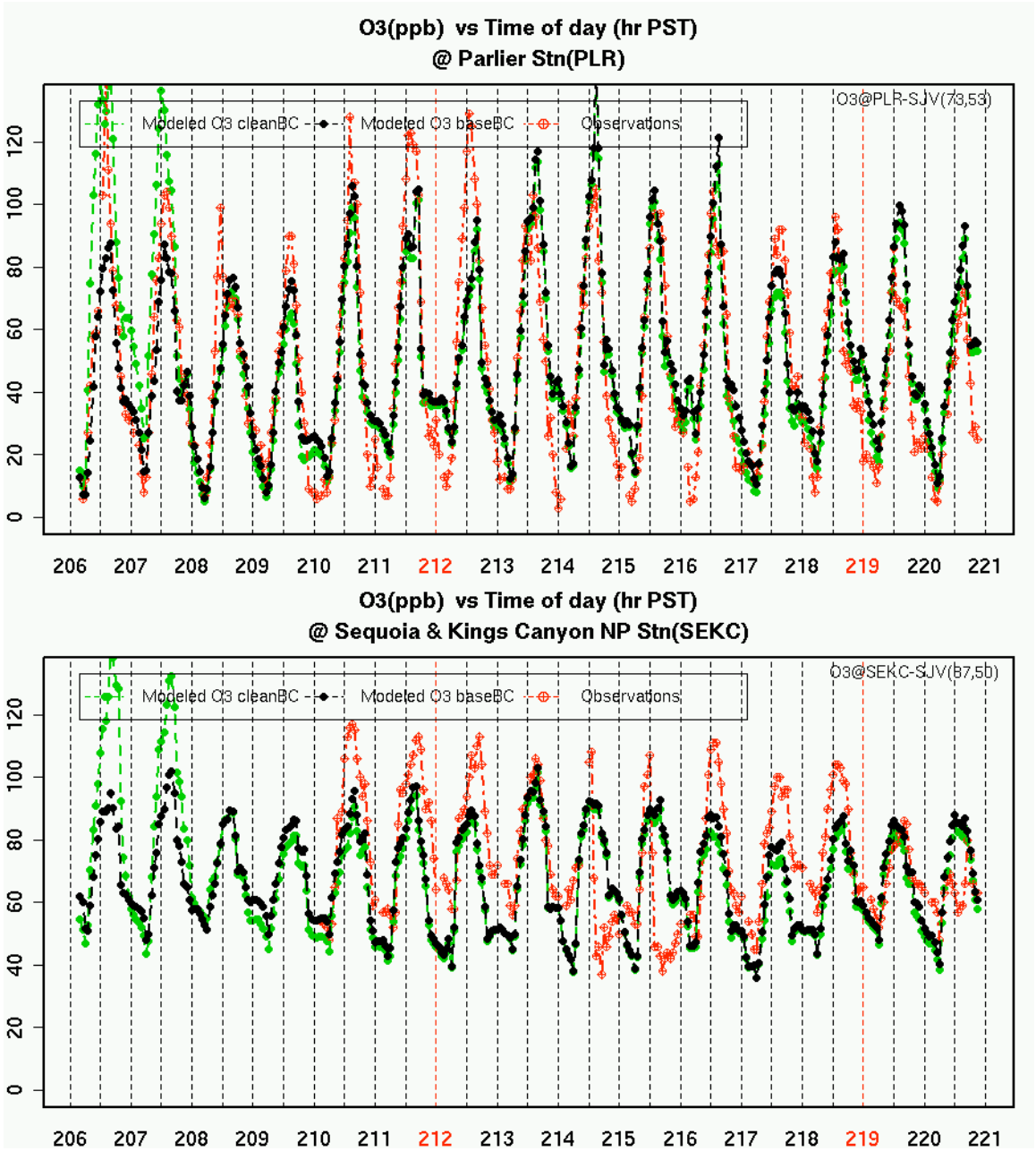
O3(ppb) vs Time of day (hr PST)
@ Parlier Stn(PLR)
O3@PLR-SJV(73,53)
Modeled O3 cleanBC
Modeled O3 baseBC
Observations
0
20
40
60
80
100
120
206
207
208
209
210
211
212
213
214
215
216
217
218
219
220
221
O3(ppb) vs Time of day (hr PST)
@ Sequoia & Kings Canyon NP Stn(SEKC)
O3@SEKC-SJV(87,50)
Modeled O3 cleanBC
Modeled O3 baseBC
Observations
0
20
40
60
80
100
120
206
207
208
209
210
211
212
213
214
215
216
217
218
219
220
221

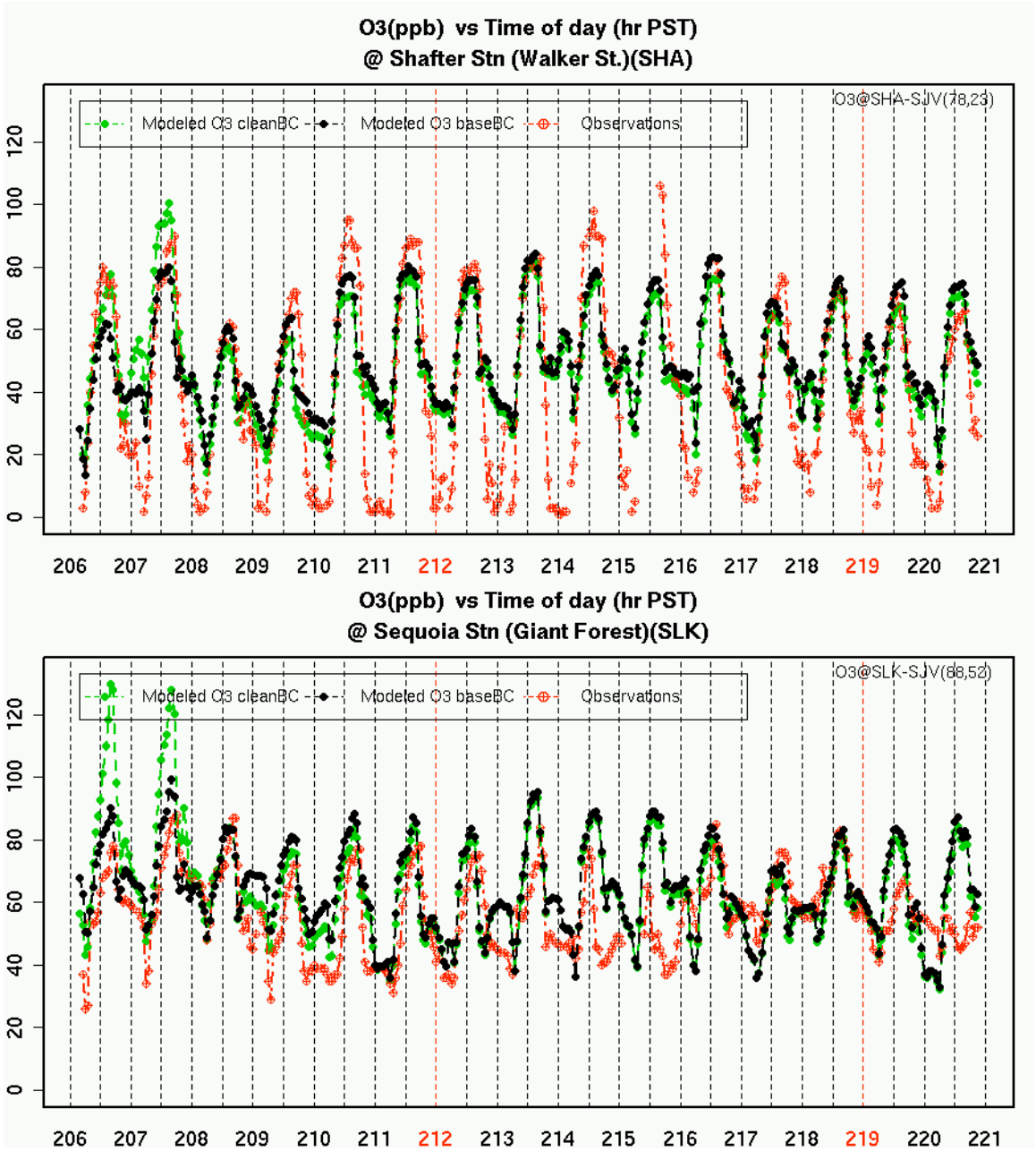
O3(ppb) vs Time of day (hr PST)
@ Shafter Stn (Walker St.)(SHA)
O3@SHA-SJV(78,23)
Modeled O3 cleanBC
Modeled O3 baseBC
Observations
0
20
40
60
80
100
120
206
207
208
209
210
211
212
213
214
215
216
217
218
219
220
221
O3(ppb) vs Time of day (hr PST)
@ Sequoia Stn (Giant Forest)(SLK)
O3@SLK-SJV(88,52)
Modeled O3 cleanBC
Modeled O3 baseBC
Observations
0
20
40
60
80
100
120
206
207
208
209
210
211
212
213
214
215
216
217
218
219
220
221

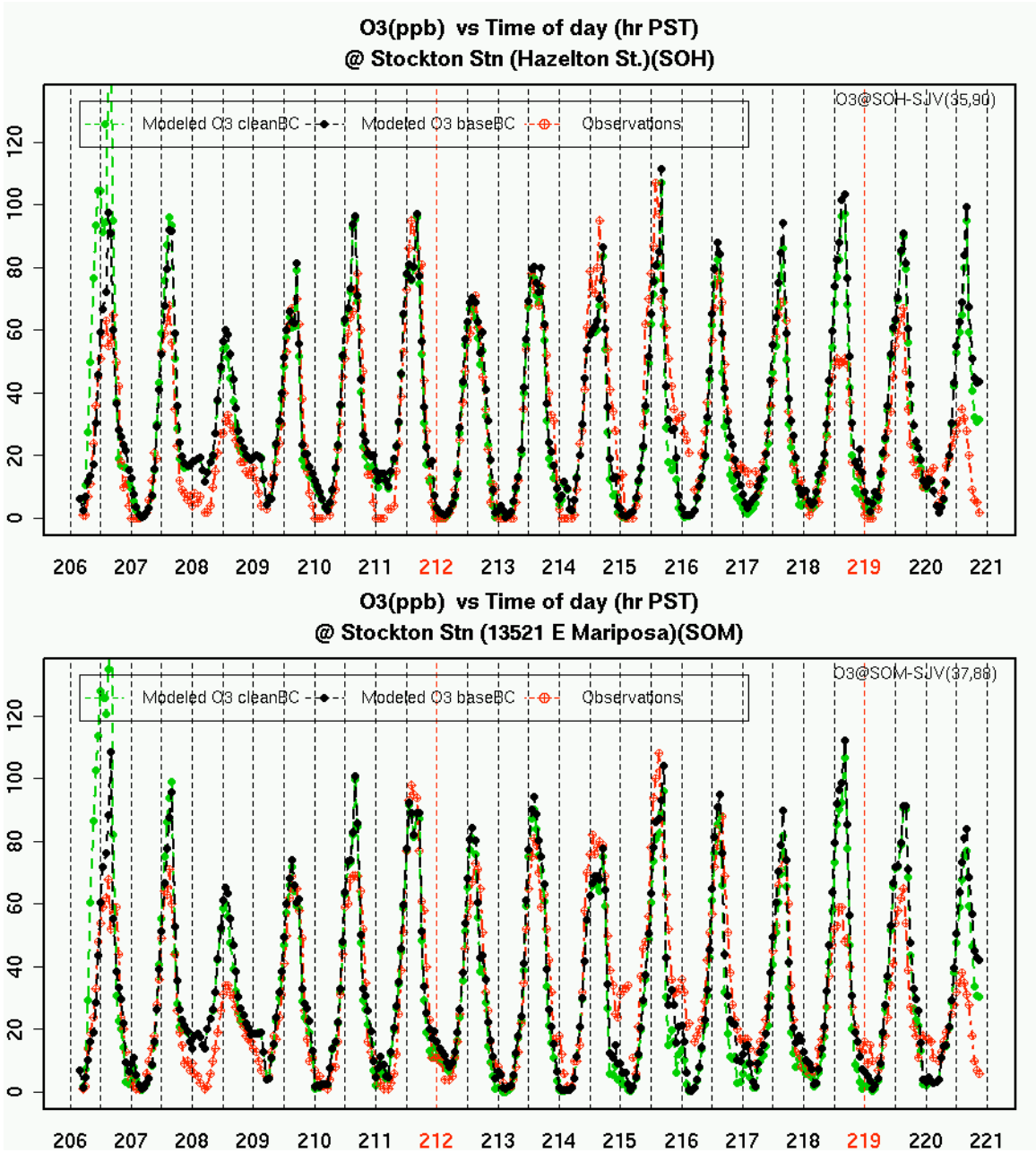
O3(ppb) vs Time of day (hr PST)
@ Stockton Stn (Hazelton St.)(SOH)
O3@SOH-SJV(35,90)
Modeled O3 cleanBC
Modeled O3 baseBC
Observations
0
20
40
60
80
100
120
206
207
208
209
210
211
212
213
214
215
216
217
218
219
220
221
O3(ppb) vs Time of day (hr PST)
@ Stockton Stn (13521 E Mariposa)(SOM)
O3@SOM-SJV(37,88)
Modeled O3 cleanBC
Modeled O3 baseBC
Observations
0
20
40
60
80
100
120
206
207
208
209
210
211
212
213
214
215
216
217
218
219
220
221

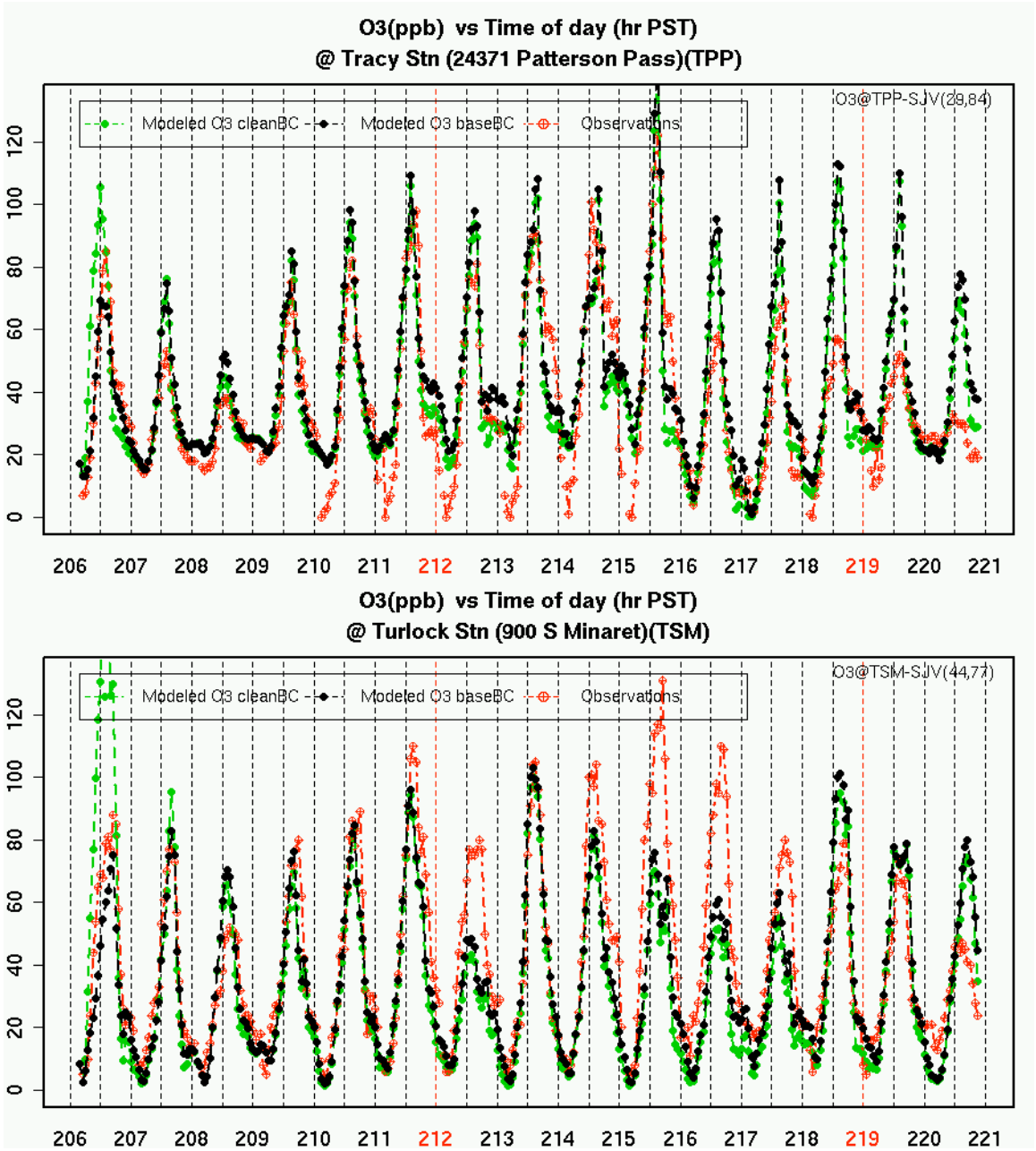
O3(ppb) vs Time of day (hr PST)
@ Tracy Stn (24371 Patterson Pass)(TPP)
O3@TPP-SJV(28,84)
Modeled O3 cleanBC
Modeled O3 baseBC
Observations
0
20
40
60
80
100
120
206
207
208
209
210
211
212
213
214
215
216
217
218
219
220
221
O3(ppb) vs Time of day (hr PST)
@ Turlock Stn (900 S Minaret)(TSM)
O3@TSM-SJV(44,77)
Modeled O3 cleanBC
Modeled O3 baseBC
Observations
0
20
40
60
80
100
120
206
207
208
209
210
211
212
213
214
215
216
217
218
219
220
221

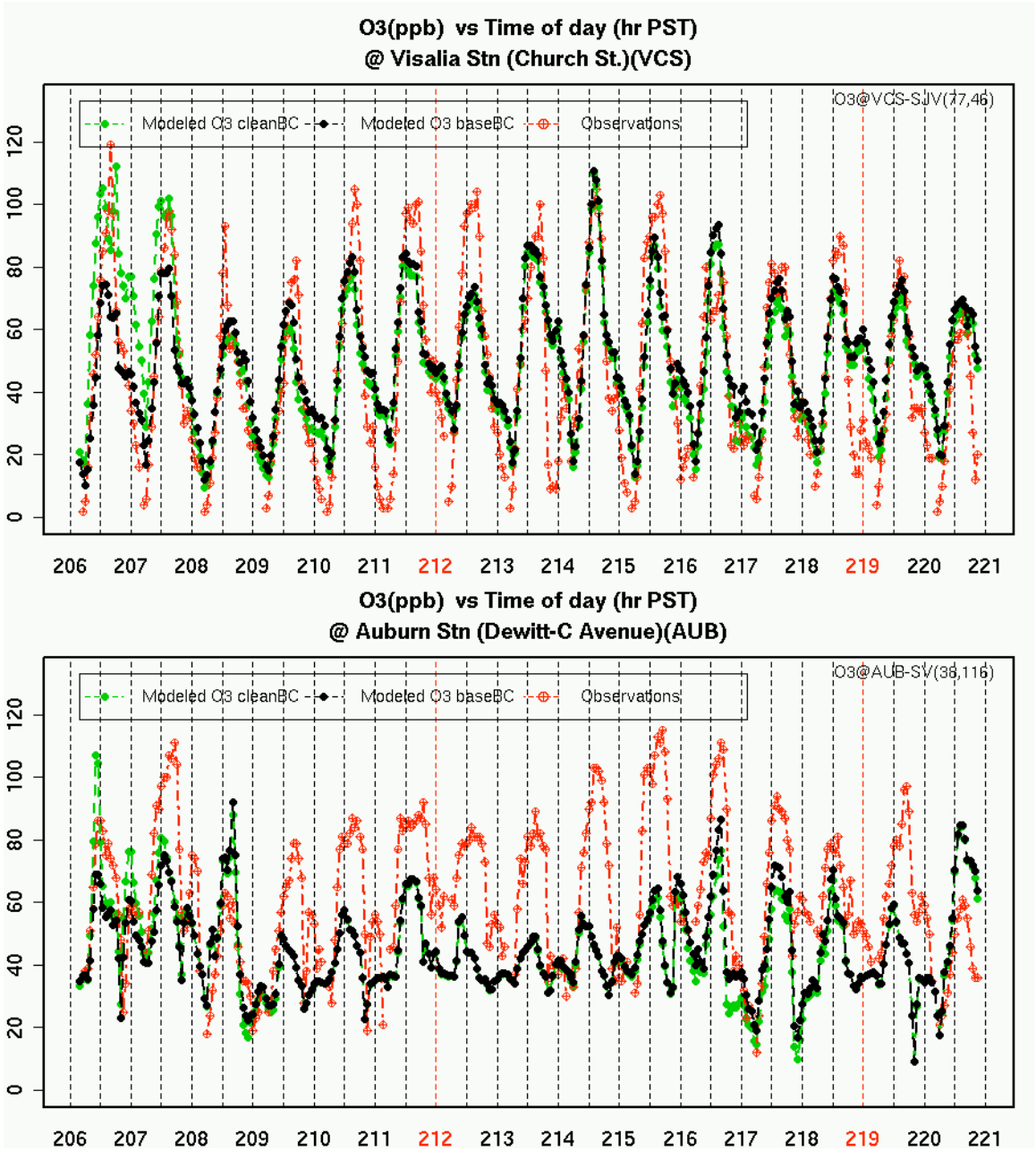
O3(ppb) vs Time of day (hr PST)
@ Visalia Stn (Church St.)(VCS)
O3@VCS-SJV(77,46)
Modeled O3 cleanBC
Modeled O3 baseBC
Observations
0
20
40
60
80
100
120
206
207
208
209
210
211
212
213
214
215
216
217
218
219
220
221
O3(ppb) vs Time of day (hr PST)
@ Auburn Stn (Dewitt-C Avenue)(AUB)
O3@AUB-SV(38,116)
Modeled O3 cleanBC
Modeled O3 baseBC
Observations
0
20
40
60
80
100
120
206
207
208
209
210
211
212
213
214
215
216
217
218
219
220
221

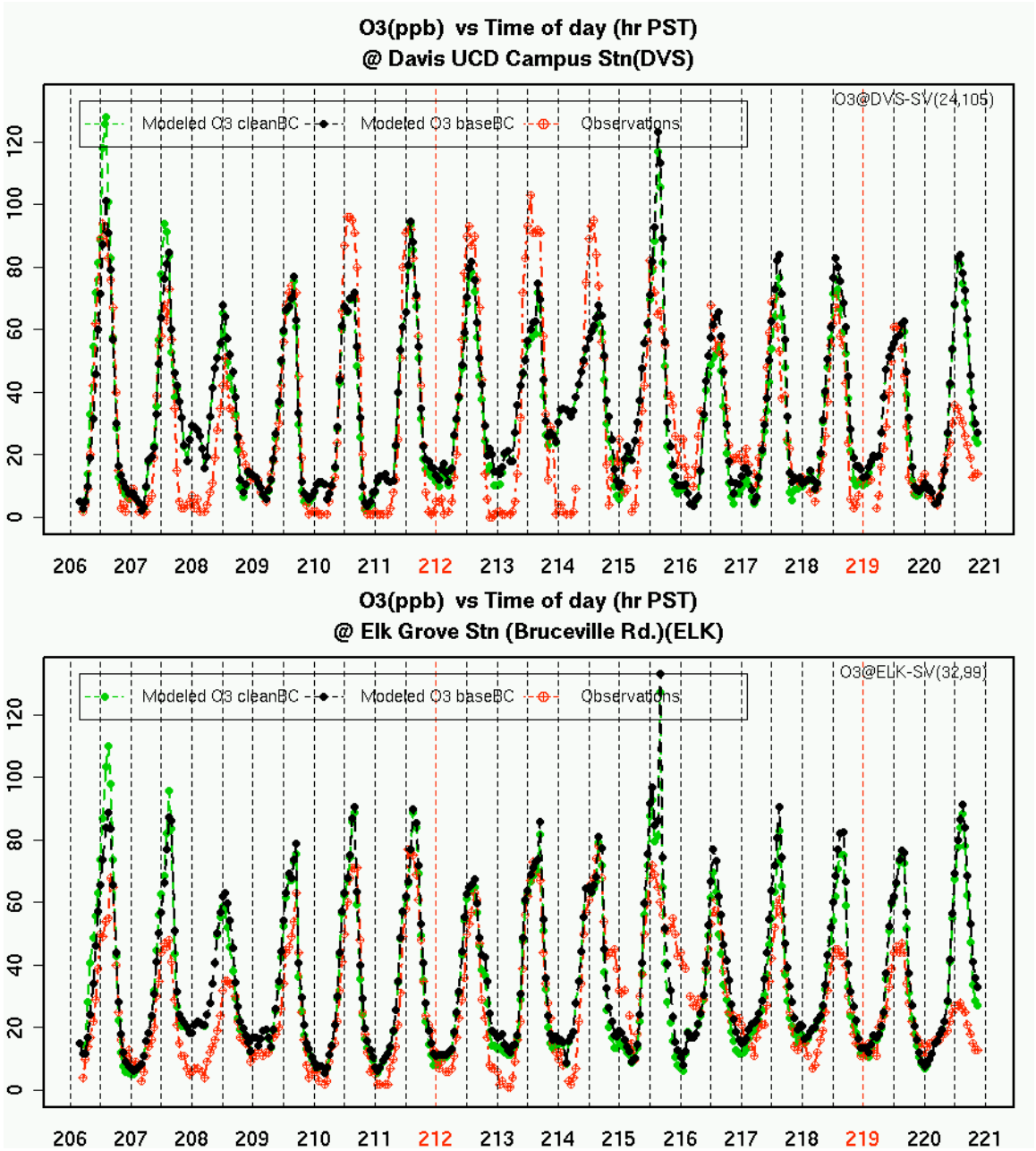
O3(ppb) vs Time of day (hr PST)
@ Davis UCD Campus Stn(DVS)
O3@DVS-SV(24,105)
Modeled O3 cleanBC
Modeled O3 baseBC
Observations
0
20
40
60
80
100
120
206
207
208
209
210
211
212
213
214
215
216
217
218
219
220
221
O3(ppb) vs Time of day (hr PST)
@ Elk Grove Stn (Bruceville Rd.)(ELK)
O3@ELK-SV(32,99)
Modeled O3 cleanBC
Modeled O3 baseBC
Observations
0
20
40
60
80
100
120
206
207
208
209
210
211
212
213
214
215
216
217
218
219
220
221

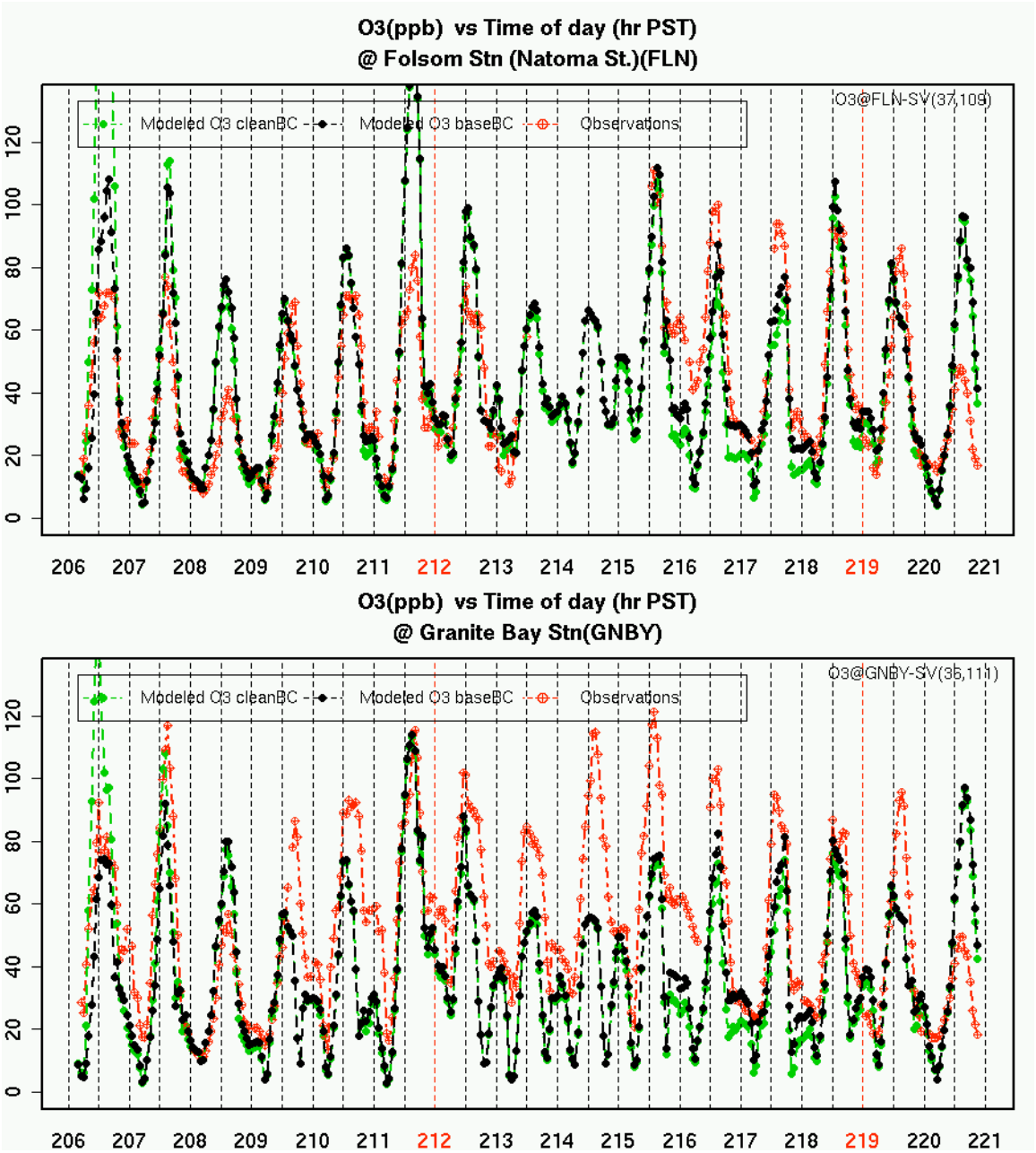
O3(ppb) vs Time of day (hr PST)
@ Folsom Stn (Natoma St.)(FLN)
O3@FLN-SV(37,109)
Modeled O3 cleanBC
Modeled O3 baseBC
Observations
0
20
40
60
80
100
120
206
207
208
209
210
211
212
213
214
215
216
217
218
219
220
221
O3(ppb) vs Time of day (hr PST)
@ Granite Bay Stn(GNBY)
O3@GNBY-SV(36,111)
Modeled O3 cleanBC
Modeled O3 baseBC
Observations
0
20
40
60
80
100
120
206
207
208
209
210
211
212
213
214
215
216
217
218
219
220
221

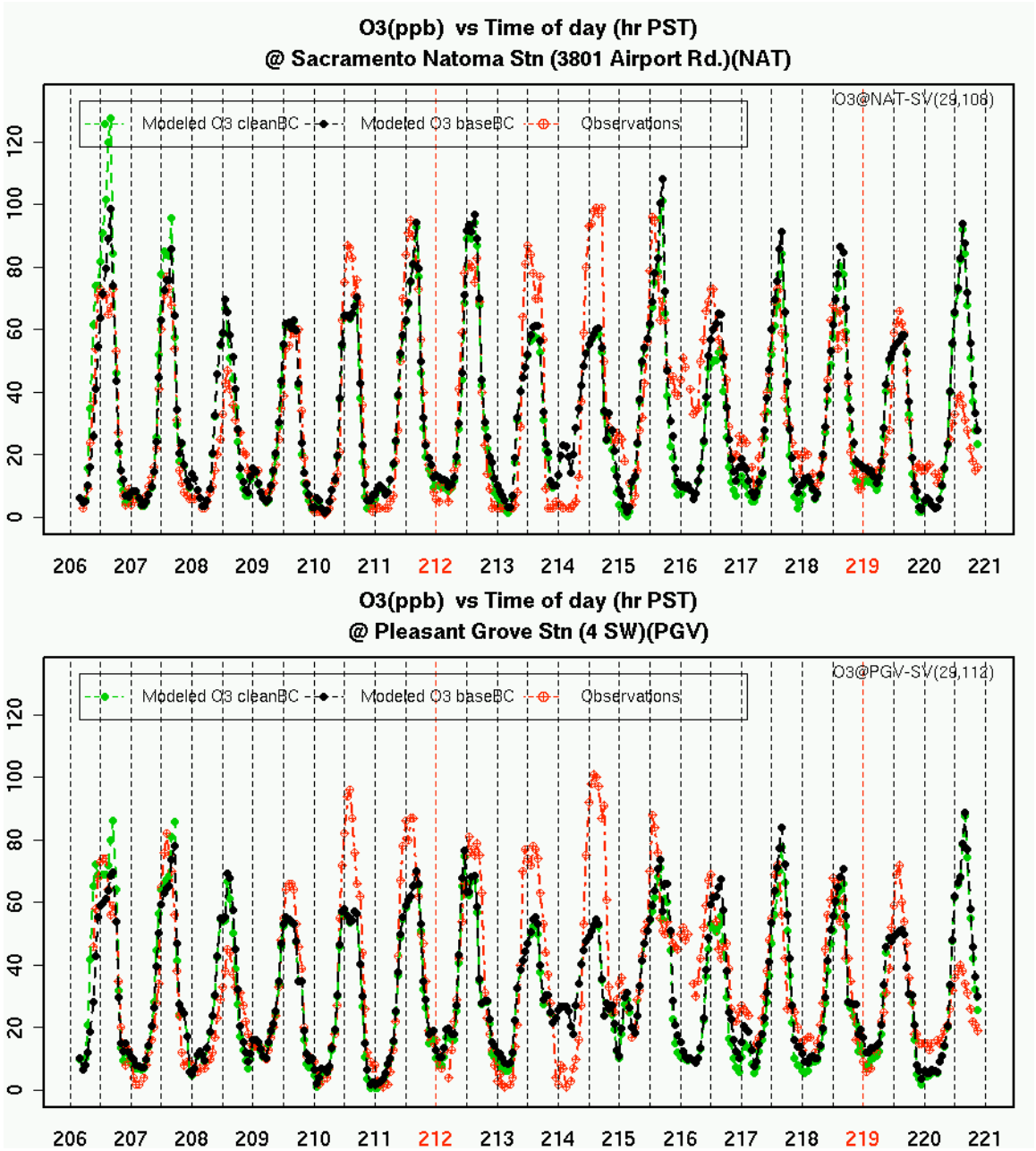
O3(ppb) vs Time of day (hr PST)
@ Sacramento Natoma Stn (3801 Airport Rd.)(NAT)
O3@NAT-SV(29,108)
Modeled O3 cleanBC
Modeled O3 baseBC
Observations
0
20
40
60
80
100
120
206
207
208
209
210
211
212
213
214
215
216
217
218
219
220
221
O3(ppb) vs Time of day (hr PST)
@ Pleasant Grove Stn (4 SW)(PGV)
O3@PGV-SV(29,112)
Modeled O3 cleanBC
Modeled O3 baseBC
Observations
0
20
40
60
80
100
120
206
207
208
209
210
211
212
213
214
215
216
217
218
219
220
221

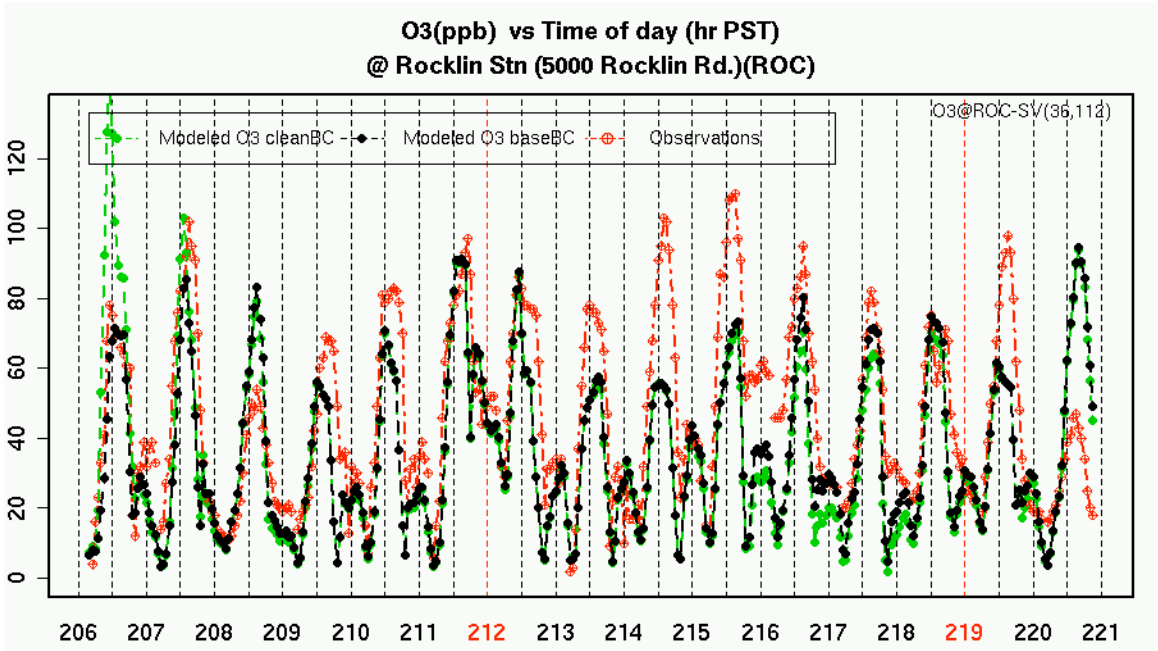
O3(ppb) vs Time of day (hr PST)
@ Rocklin Stn (5000 Rocklin Rd.)(ROC)
O3@ROC-SV(36,112)
Modeled O3 cleanBC
Modeled O3 baseBC
Observations
0
20
40
60
80
100
120
206
207
208
209
210
211
212
213
214
215
216
217
218
219
220
221

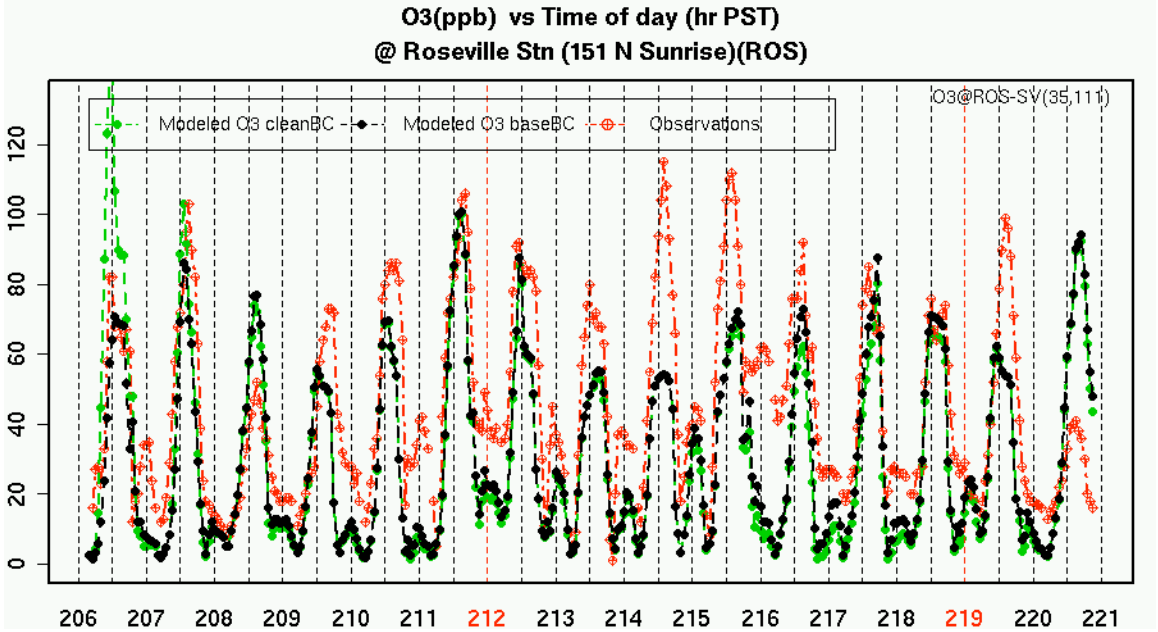
O3(ppb) vs Time of day (hr PST)
@ Roseville Stn (151 N Sunrise)(ROS)
O3@ROS-SV(35,111)
Modeled O3 cleanBC
Modeled O3 baseBC
Observations
0
20
40
60
80
100
120
206
207
208
209
210
211
212
213
214
215
216
217
218
219
220
221

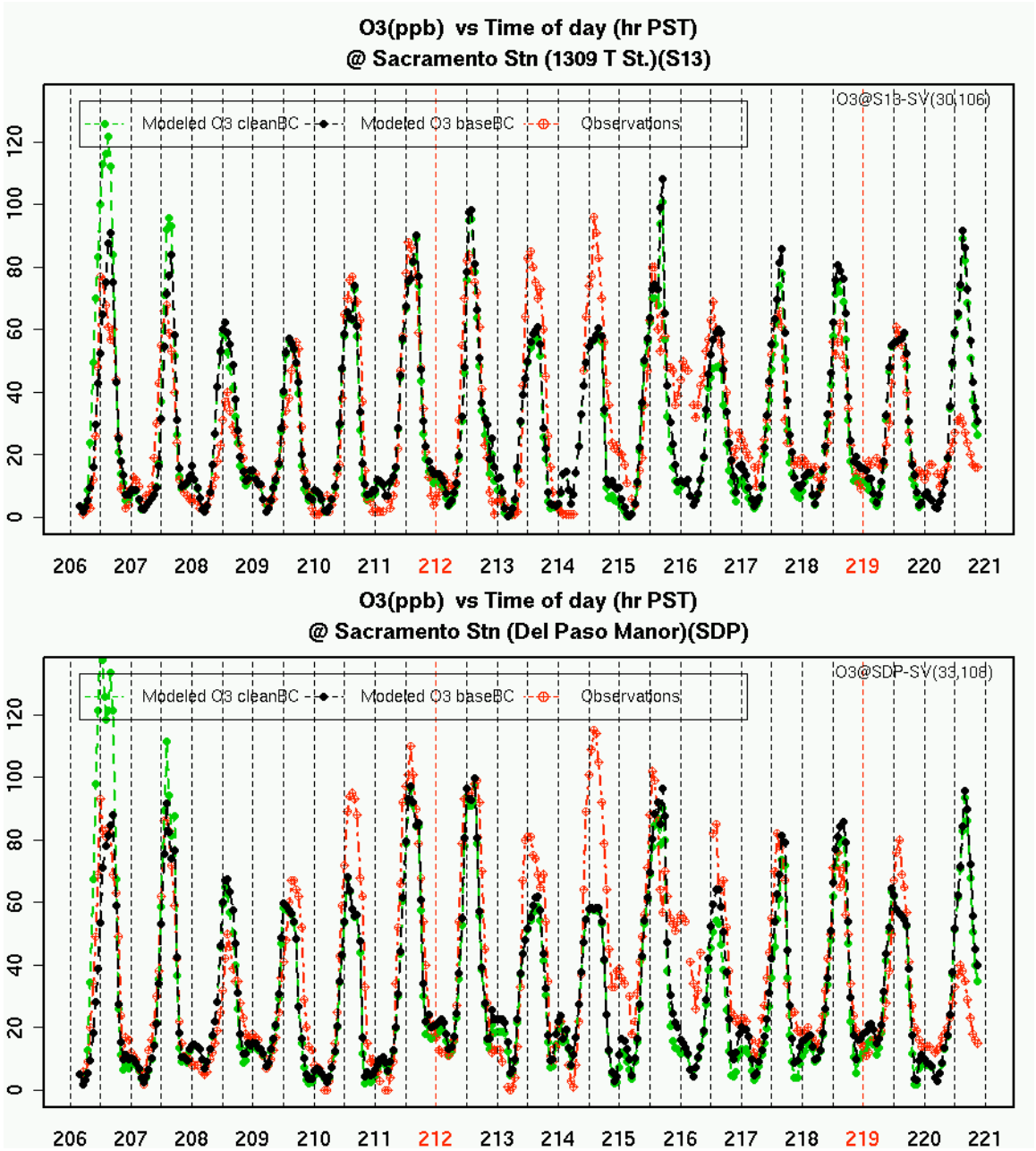
O3(ppb) vs Time of day (hr PST)
@ Sacramento Stn (1309 T St.)(S13)
O3@S13-SV(30,106)
Modeled O3 cleanBC
Modeled O3 baseBC
Observations
0
20
40
60
80
100
120
206
207
208
209
210
211
212
213
214
215
216
217
218
219
220
221
O3(ppb) vs Time of day (hr PST)
@ Sacramento Stn (Del Paso Manor)(SDP)
O3@SDP-SV(33,108)
Modeled O3 cleanBC
Modeled O3 baseBC
Observations
0
20
40
60
80
100
120
206
207
208
209
210
211
212
213
214
215
216
217
218
219
220
221

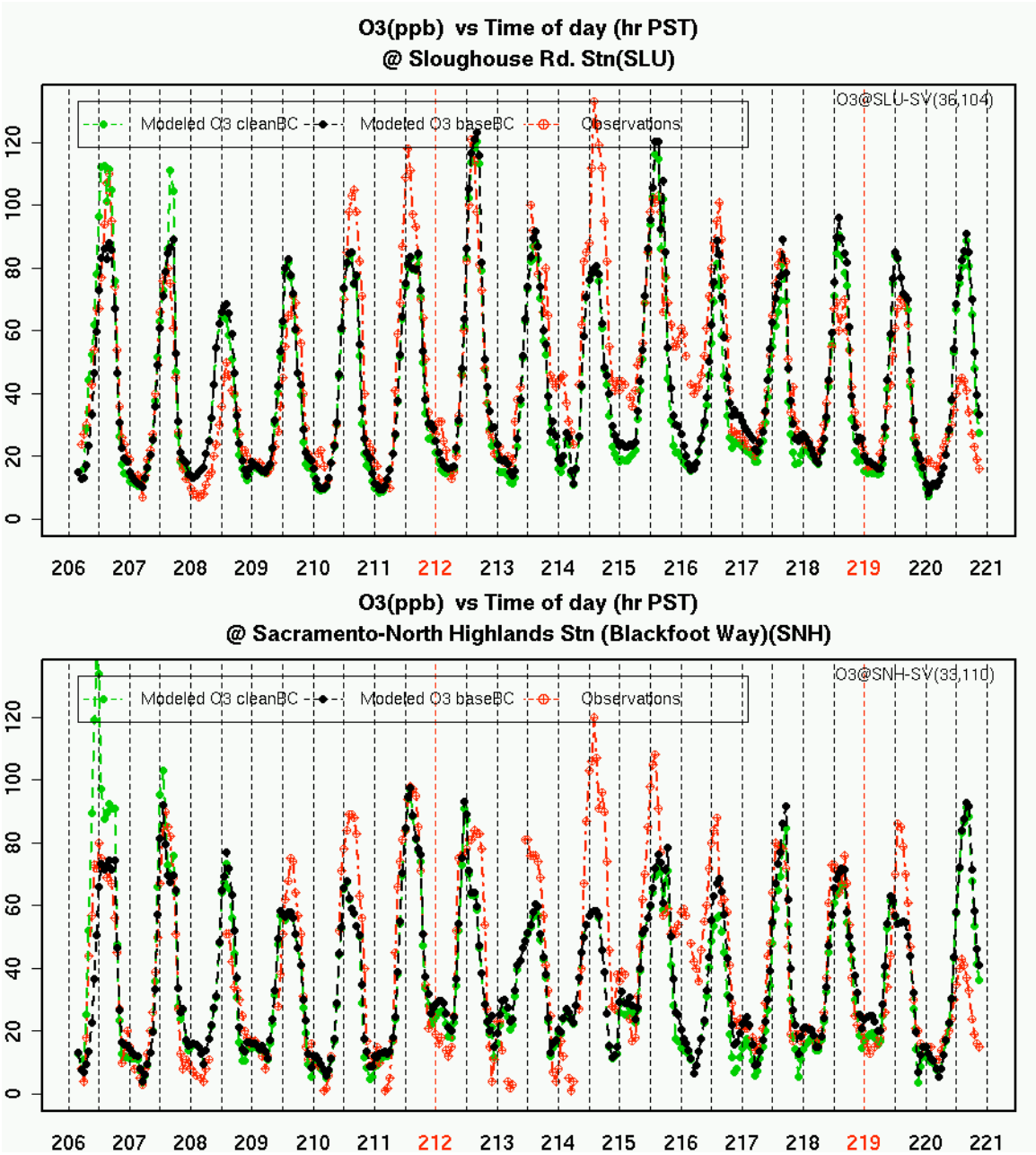
O3(ppb) vs Time of day (hr PST)
@ Sloughouse Rd. Stn(SLU)
O3@SLU-SV(36,104)
Modeled O3 cleanBC
Modeled O3 baseBC
Observations
0
20
40
60
80
100
120
206
207
208
209
210
211
212
213
214
215
216
217
218
219
220
221
O3(ppb) vs Time of day (hr PST)
@ Sacramento-North Highlands Stn (Blackfoot Way)(SNH)
O3@SNH-SV(33,110)
Modeled O3 cleanBC
Modeled O3 baseBC
Observations
0
20
40
60
80
100
120
206
207
208
209
210
211
212
213
214
215
216
217
218
219
220
221

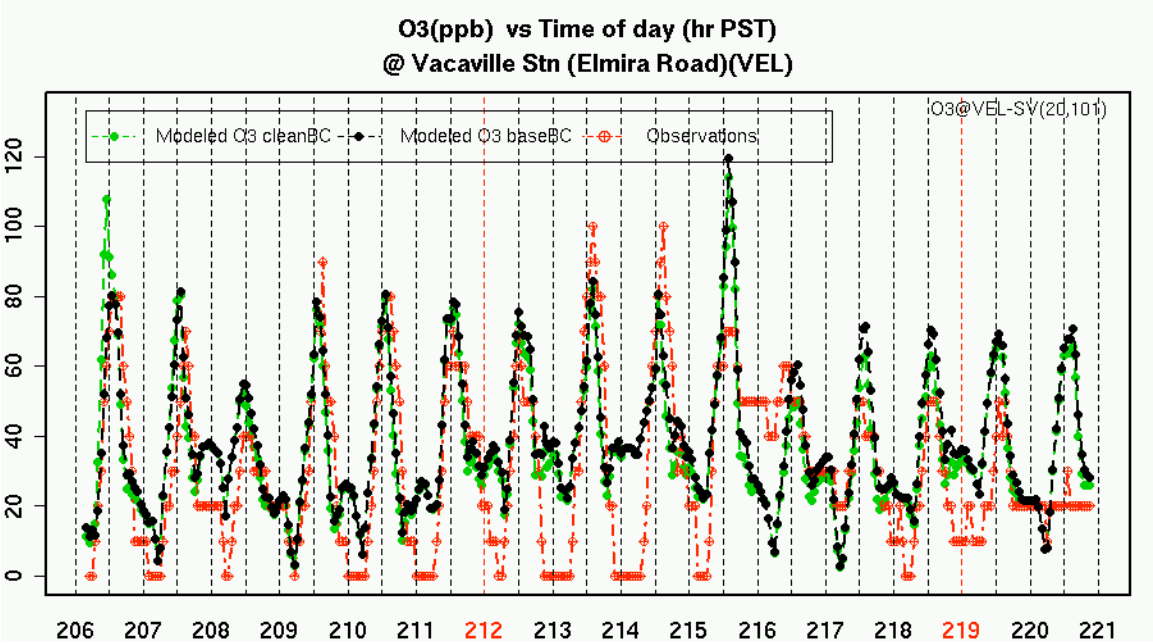
O3(ppb) vs Time of day (hr PST)
@ Vacaville Stn (Elmira Road)(VEL)
O3@VEL-SV(20,101)
Modeled O3 cleanBC
Modeled O3 baseBC
Observations
0
20
40
60
80
100
120
206
207
208
209
210
211
212
213
214
215
216
217
218
219
220
221

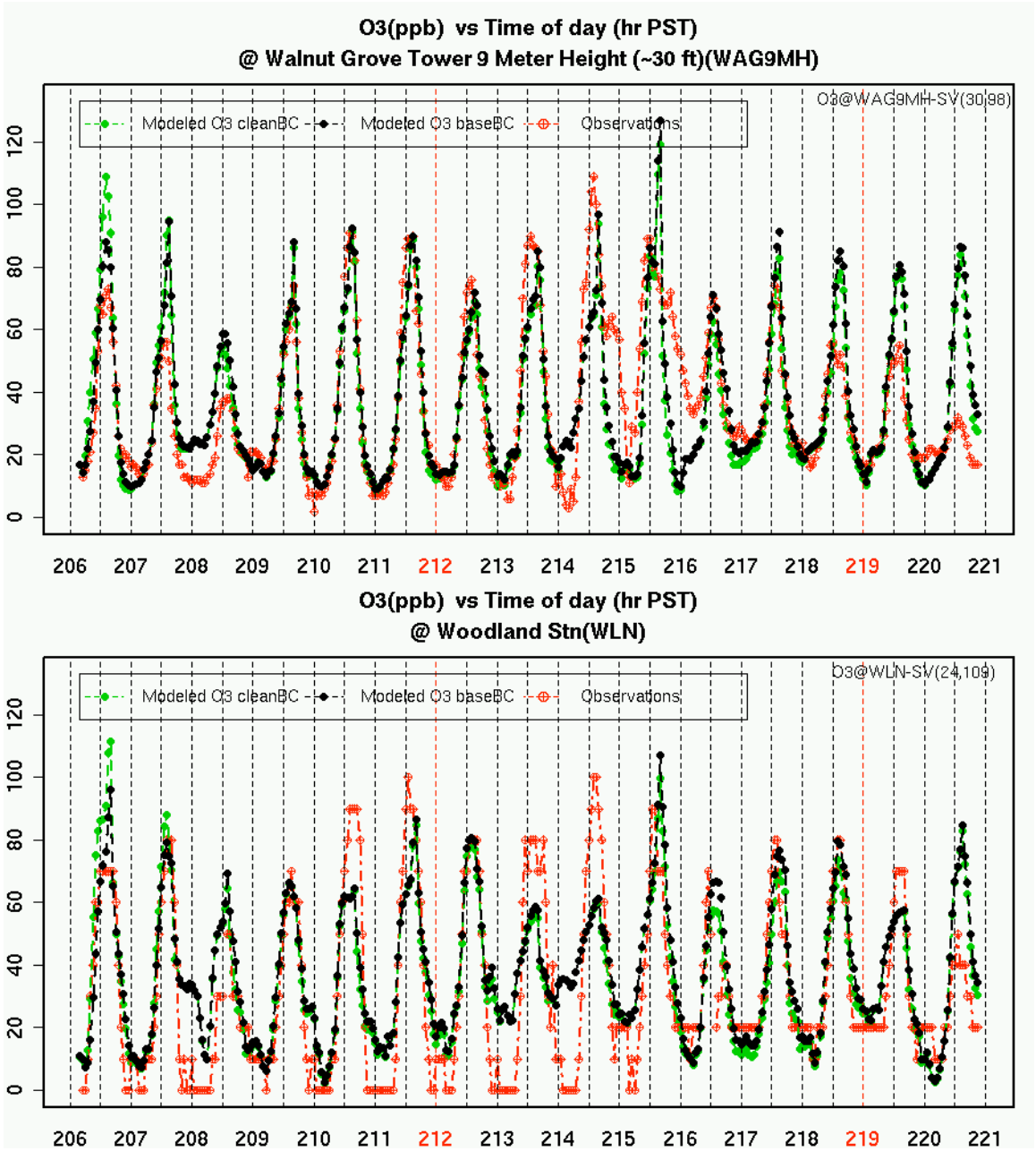
O3(ppb) vs Time of day (hr PST)
@ Walnut Grove Tower 9 Meter Height (~30 ft)(WAG9MH)
O3@WAG9MH-SV(30,98)
Modeled O3 cleanBC
Modeled O3 baseBC
Observations
0
20
40
60
80
100
120
206
207
208
209
210
211
212
213
214
215
216
217
218
219
220
221
O3(ppb) vs Time of day (hr PST)
@ Woodland Stn(WLN)
O3@WLN-SV(24,109)
Modeled O3 cleanBC
Modeled O3 baseBC
Observations
0
20
40
60
80
100
120
206
207
208
209
210
211
212
213
214
215
216
217
218
219
220
221